

**HYDROGEN PRODUCTION FROM
METHANOL-STEAM REFORMING REACTION**

BY

CHAICHAN SIRIRUANG

**A DISSERTATION SUBMITTED IN PARTIAL FULFILLMENT OF
THE REQUIREMENTS FOR THE DEGREE OF DOCTOR OF
PHILOSOPHY (ENGINEERING)
SIRINDHORN INTERNATIONAL INSTITUTE OF TECHNOLOGY
THAMMASAT UNIVERSITY
ACADEMIC YEAR 2015**

**HYDROGEN PRODUCTION FROM
METHANOL-STEAM REFORMING REACTION**

BY

CHAICHAN SIRIRUANG

**A DISSERTATION SUBMITTED IN PARTIAL FULFILLMENT OF
THE REQUIREMENTS FOR THE DEGREE OF DOCTOR OF
PHILOSOPHY (ENGINEERING)
SIRINDHORN INTERNATIONAL INSTITUTE OF TECHNOLOGY
THAMMASAT UNIVERSITY
ACADEMIC YEAR 2015**



HYDROGEN PRODUCTION FROM METHANOL-STEAM REFORMING
REACTION

A Dissertation Presented

By

CHAICHAN SIRIRUANG

Submitted to

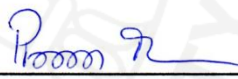
Sirindhorn International Institute of Technology

Thammasat University

In partial fulfillment of the requirements for the degree of
DOCTOR OF PHILOSOPHY (ENGINEERING)

Approved as to style and content by

Advisor and Chairperson of Thesis Committee



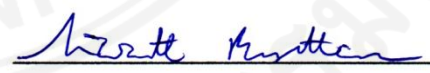
(Asst. Prof. Pisanu Toochinda, Ph.D.)

Co-Advisor



(Sumittra Charojrochkul, Ph.D.)

Committee Member and
Chairperson of Examination Committee



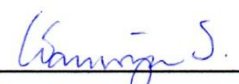
(Asst. Prof. Siwarutt Boonyarattanakalin, Ph.D.)

Committee Member



(Assoc. Prof. Luckhana Lawtrakul, Dr.rer.nat.)

Committee Member



(Asst. Prof. Wanwipa Siriwatwechakul, Ph.D.)

External Examiner: Prof. Suttichai Assabumrungrat, Ph.D.

April 2016

Acknowledgements

Firstly, I would like to express my sincere gratitude to my advisor Asst. Prof. Dr. Pisanu Toochinda for the continuous support of my Ph.D. study and related research, for his patiently corrected my writing and financially supported. His guidance helped me in all the time of research and writing of this thesis. I could not have imagined having a better advisor and mentor for my Ph.D. study.

I am deeply grateful to my co-advisor, Dr. Sumittra Charojrochkul, for providing me an opportunity to access to the laboratory and research facilities at MTEC. I am also thankful to her for carefully reading and commenting on countless revisions of the journal's manuscript. Without her precious support it would not be possible to conduct this research. I would like to thank the rest of my thesis committee, Assoc. Prof. Dr. Luckhana Lawtrakul, Asst. Prof. Dr. Siwarutt Boonyarattanakalin, and Asst. Prof. Dr. Wanwipa Siriwatwechakul, for their insightful comments and encouragement, but also for the hard questions which incited me to widen my research from various perspectives. In addition, I would like to thank Dr. Pongsak Choktaweekarn and Dr. Parnthep Julnipitawong for their supports to conduct this research in part of construction materials. A deep gratitude is also conveyed to Prof. Dr. Suttichai Assabumrungrat for serving as an external examiner.

I also thank to Thailand Graduate Institute of Science and Technology scholarship (TGIST, TG-33-13-53-022D) of National Science and Technology Development Agency (NSTDA) and Sirindhorn International Institute of Technology (SIIT) to provide the Ph.D. scholarship. I also thank to Electricity Generating Authority of Thailand for providing research support and material for this research and Synchrotron Light Research Institute (Public Organization) for XAS analysis facilities. Finally, I must express my very profound gratitude to my colleges and staffs at the School of Bio-Chemical Engineering and Technology of SIIT for supporting me during my PhD study. I would like to thank my family for providing me with unflinching support and continuous encouragement throughout my years of study and through the process of researching and writing this thesis. This accomplishment would not have been possible without them.

Abstract

HYDROGEN PRODUCTION FROM METHANOL-STEAM REFORMING

by

CHAICHAN SIRIRUANG

Bachelor degree in engineering (Major in Chemical Engineering), King Mongkut's University of Technology North Bangkok, 2006

Master degree in chemical engineering, Sirindhorn International Institute of Technology, 2010

Doctor of Philosophy (Engineering), Sirindhorn International Institute of Technology, 2016

The activities of new Cu-Zn based catalysts over Al_2O_3 based supports were evaluated in a tubular reactor at the temperature range of 200-300°C and 1 atm in a continuous mode. The physical and chemical properties of catalysts were characterized using XRD, TPR, BET surface area, SEM-EDS and XAS. At 200°C, Cu-Zn over ZrO_2 doped Al_2O_3 prepared by impregnation with an addition of urea can exhibit the hydrogen yield up to 90.3% while the yield of impregnated Cu-Zn over γ - Al_2O_3 is only 28.2%. The study of support effect indicates that ZrO_2 doped Al_2O_3 support can increase the specific copper surface area and boost the activity of the catalyst. The catalyst development from this study can lead to a novel catalyst for low temperature methanol-steam reforming to prevent the catalyst sintering. Although the hydrogen fuel cell is an alternative energy for the future, the hydrogen applications depend on the availability of low hydrogen production cost and environmental friendliness of hydrogen sources without carbon dioxide emissions in the overall process. In order to claim that a hydrogen fuel cell is a clean energy, the CO_2 produced from this reforming process must be captured. Therefore, the development of CO_2 capture methods was also investigated in parallel with a hydrogen production.

A utilization of fly ash as a solid sorbent material for CO₂ capture via surface adsorption and carbonation reaction was evaluated as an economically feasible CO₂ reduction technique. The results show that fly ash from a coal-fired power plant can capture CO₂ up to 304.7-870.1 μmol/g fly ash without any treatment. The CO₂ adsorption conditions (temperature, pressure, and moisture) affect CO₂ capture capacity of fly ash. The carbonation of CO₂ with free CaO in fly ashes was evaluated and the results indicated that the reaction consumed most of free CaO in fly ash. The fly ash after CO₂ capture was further used for an application such as a mineral admixture for concrete. Properties such as water requirement, compressive strength, autoclave expansion, and carbonation depth of mortar and paste specimens using fly ash before and after CO₂ capture such as water requirement, compressive strength, autoclave expansion, and carbonation depth were tested and compared with material standards. The results show that an expansion of mortar specimens using fly ash after CO₂ capture is greatly reduced due to the reduction of free CaO content in the fly ash compared to an expansion of specimens using fresh fly ash. There are no significant differences in the water requirement and compressive strength of specimens using fly ash, before and after CO₂ capture. The results from this study can lead to an alternative CO₂ capture technique with doubtless utilization of fly ash after CO₂ capture as a mineral admixture for concrete.

Keywords: Hydrogen production, Cu-Zn/ZrO₂ doped Al₂O₃ catalyst, CO₂ capture, CO₂ solid sorbents, Free CaO reduction, Mineral admixture

Table of contents

Chapter	Title	Page
	Signature Page	i
	Acknowledgements	ii
	Abstract	iii
	Table of Contents	v
	List of Figures	ix
	List of Tables	xii
1	Introduction	1
	1.1 Introduction	1
	1.2 Statement of problems	4
	1.3 Objectives	5
	1.4 Scope of work	6
2	Literature Review	7
	2.1 Hydrogen production for hydrogen fuel cell	7
	2.1.1 Hydrogen fuel cell	7
	2.1.2 Hydrogen sources	8
	2.1.3 Hydrogen production from methanol	9
	2.1.3.1 Methanol decomposition	9
	2.1.3.2 Partial oxidation of methanol	9
	2.1.3.3 Methanol-steam reforming	9
	2.1.4 Catalyst for methanol-steam reforming reaction	10
	2.1.4.1 Copper-based catalyst	10
	(1) Effect of preparation methods	10
	Precipitation or coprecipitation method	12
	Impregnation method	13
	Sol-gel method	14

Chapter	Title	Page
	(2) Effect of promoter	15
	2.1.4.2 The group 8-10 metal-based catalysts	20
	2.1.5 Effect of calcination temperature for Cu-Zn based catalyst	22
	2.1.6 Activation of catalyst by reduction	25
	2.1.7 Reaction conditions for Cu-Zn based catalyst	27
	2.2 CO ₂ capture by fly ash	33
	2.2.1 Conventional CO ₂ capture and storage	33
	2.2.2 Solid sorbets for CO ₂ capture process	37
	2.2.3 Fly ash	42
3	Methodology	46
	3.1 Methanol-steam reforming	46
	3.1.1 Catalyst and support preparations	46
	3.1.1.1 Impregnation method	46
	3.1.1.2 Sol-gel method	47
	3.1.2 Preparation of ZrO ₂ doped Al ₂ O ₃ support	49
	3.1.3 Methanol-steam reforming reaction in tubular reactor	50
	3.1.4 Catalyst characterizations	51
	3.2 CO ₂ capture using fly ash	52
	3.2.1 Materials	52
	3.2.2 CO ₂ capture using fly ash as solid sorbents	52
	3.2.2.1 CO ₂ capture by adsorption	53
	3.2.2.2 CO ₂ capture by carbonation	53
	3.2.3 Material Analysis	54
	3.2.4 Property testing of mortar and cement paste using fly ash as a mineral admixture	54
	3.2.4.1 Physical properties of mortar and paste specimens	55
	3.2.4.2 Carbonation depth of mortar specimens	57

Chapter	Title	Page
4	Results and Discussion	58
	4.1 Hydrogen production from methanol-steam reforming	58
	4.1.1 Effect of urea in impregnation method	58
	4.1.2 Effect of preparation methods (impregnation with urea vs. sol-gel)	62
	4.1.3 Effect of ZrO ₂ doped Al ₂ O ₃ supports	64
	4.1.3.1 Properties of ZrO ₂ doped Al ₂ O ₃ supports	64
	4.1.4 Combination of impregnation with urea method and ZrO ₂ doped Al ₂ O ₃ as support	67
	4.1.5 Stability of Cu-Zn/ZrO ₂ doped Al ₂ O ₃ with urea	70
	4.1.6 K-edge XANES spectra of Cu and Zn	72
	4.2 CO ₂ capture using fly ash	74
	4.2.1 Compositions in fly ashes and their physical properties	74
	4.2.2 CO ₂ capture using fly ash as a solid sorbent	77
	4.2.2.1 CO ₂ capture by adsorption	78
	4.2.2.2 CO ₂ capture by carbonation reaction	82
	4.2.3 Basic properties of mixtures containing fly ash after CO ₂ capture	86
	4.2.3.1 Water requirement of mortar specimens	86
	4.2.3.2 Compressive strength and strength index of mortar specimens	87
	4.2.3.3 Autoclave expansion of paste specimens	90
	4.2.3.4 Carbonation depth	91
5	Conclusions and Recommendations	94

Chapter Title	Page
References	98
Appendices	113
Appendix A	114
Appendix B	130
Appendix C	141
Appendix D	145
Appendix E	147

List of Figures

Figures	Page
2.1 Hydrogen fuel cell (HyGen Industries, Inc., 2016)	7
2.2 Hydrogen sources and process for hydrogen production (IEA, 2006)	8
2.3 Catalyst preparations by precipitation method (Ertl et al., 1997)	12
2.4 The performance of various promoters on Cu-based catalysts using for methanol-steam reforming reaction ($T= 240^{\circ}\text{C}$, $\text{H}_2\text{O}/\text{MeOH}= 1.5$). (Papavasiliou et al., 2007)	16
2.5 The performance of Zn-promoted on Cu-based catalysts at 200°C (Wang et al., 2003)	17
2.6 The performance of Zn/Zr-promoted on Cu-based catalysts at 260°C (Jeong et al., 2006)	19
2.7 The catalytic stability of Ce-promoted on Cu-based catalysts prepared by precipitation method at 553 K (\blacktriangle) CZA2, (\blacklozenge) CZCeA2 and (\blacksquare) CZCeA3 (Patel and Pant, 2007)	20
2.8 XRD patterns of Cu-Zn-Al catalyst calcined at different temperatures (Yang et al., 2004)	23
2.9 TPR profiles of Cu-Zn-Al catalyst calcined at different temperatures (Yang et al., 2004)	25
2.10 The activity testing with and without pre-reduction by hydrogen for $\text{CuO}/\text{ZnO}/\text{ZrO}_2/\text{Al}_2\text{O}_3$ catalyst (Matter and Ozkan, 2005)	26
2.11 The temperature dependence of methanol conversion and product composition during methanol steam reforming over commercial $\text{Cu}/\text{ZnO}/\text{Al}_2\text{O}_3$ catalyst (Agrell et al., 2002)	31
2.12 The process of coal-fired power plant (Sear, 2001)	42
2.13 Proposed reactions for preparation of the amine-enriched fly ash sorbent	45
3.1 $\text{Cu-Zn}/\text{Al}_2\text{O}_3$ catalysts prepared by incipient wetness impregnation method	47
3.2 Schematic diagram of sol-gel preparation method of $\text{Cu-Zn}/\text{Al}_2\text{O}_3$ catalyst	48

Figures	Page
3.3 Sol-gel preparation methods a) before sol-gel formation, b) after sol-gel formation	49
3.4 Schematic of hydrogen production from methanol-steam reforming process	50
3.5 The schematic of CO ₂ capture by adsorption over solid sorbents	54
4.1 SEM image and EDS profiles of Cu-Zn/ α -Al ₂ O ₃ prepared by impregnation without urea	61
4.2 SEM image and EDS profiles of Cu-Zn/ α -Al ₂ O ₃ prepared by impregnation with urea	61
4.3 SEM image and EDS profiles of Cu-Zn/ α -Al ₂ O ₃ prepared by sol-gel method.	63
4.4 X-ray diffraction patterns of supports: (a) α -Al ₂ O ₃ (Riedel), (b) γ -Al ₂ O ₃ (Alfar Aesar), (c) ZrO ₂ doped Al ₂ O ₃ calcined 950°C, (d) ZrO ₂ doped Al ₂ O ₃ calcined 1100°C, (e) ZrO ₂ doped Al ₂ O ₃ calcined 1200°C (▲: α -Al ₂ O ₃ , ■: γ -Al ₂ O ₃ , ●: ZrO ₂)	66
4.5 X-ray diffraction patterns of catalysts before calcination (a) Cu-Zn/ γ -Al ₂ O ₃ , (b) Cu-Zn/ γ -Al ₂ O ₃ with urea, (c) Cu-Zn/ZrO ₂ doped Al ₂ O ₃ with urea, (▲: NH ₄ NO ₃)	68
4.6 Cu K-edge XANES spectra (a), and first derivative of Cu K-edge XANES spectra (b) of Cu-Zn based catalysts and references spectra of Cu metal, Cu ₂ O and CuO	72
4.7 Zn K-edge XANES spectra (a), and first derivative of Cu K-edge XANES spectra (b) of Cu-Zn based catalysts and references spectra of Zn metal and ZnO	73
4.8 Schematic of hydrogen productions from methanol-steam reforming over over Cu-Zn/ZrO ₂ -doped Al ₂ O ₃ catalyst	74
4.9 XRD results of high free CaO fly ash before and after capture CO ₂	82
4.10 Water requirement of mortar specimens using fly ash before and after CO ₂ capture (20 wt% and 40 wt% fly ash replacement)	86

Figures	Page
4.11 Compressive strength of mortar specimens using 20 wt% of fly ash before and after CO ₂ capture at a) 7-days, b) 28-days and c) 91-days	88
4.12 Strength index of mortar specimens using 20 wt% of fly ash before and after CO ₂ capture at a) 7-days, b) 28-days and c) 91-days	89
4.13 Autoclave expansions of paste specimens using 40 wt% of fly ash before and after CO ₂ capture	90
4.14 Carbonation depths of mortar specimens using 30 wt% of fly ash before and after CO ₂ capture	92

List of Tables

Tables	Page
2.1 Physicochemical properties of copper catalysts by different preparation method	11
2.2 Summary tables for methanol-steam reforming over various supported transition metal-based catalysts	21
2.3 The types of reactor and reaction conditions of methanol-steam reforming using Cu-Zn based catalyst	28
2.4 Advantages and disadvantages of CO ₂ capture technology	34
2.5 Summary of CO ₂ storage technology	37
2.6 Solid sorbents and chemical treatment for the CO ₂ capture	38
3.1 Mix designations	55
3.2 Mix proportion and properties of samples for basic property tests	57
4.1 Hydrogen yield of Cu-Zn catalysts over alumina supports (α -Al ₂ O ₃ or γ -Al ₂ O ₃) prepared by impregnation with and without urea	59
4.2 Hydrogen yield of Cu-Zn catalysts over alumina supports (α -Al ₂ O ₃ and γ -Al ₂ O ₃) prepared by impregnation with urea and sol-gel methods	64
4.3 Physical properties of supports	65
4.4 Hydrogen yield of impregnated Cu-Zn catalysts with urea over α -Al ₂ O ₃ , γ -Al ₂ O ₃ and ZrO ₂ doped Al ₂ O ₃ supports and Cu-Zn/ γ -Al ₂ O ₃ with ZrO ₂ as promoter	67
4.5 Properties of Cu-Zn over various catalysts determined by N ₂ O chemisorption	69
4.6 Properties of catalysts before and after the accelerated sintering of Cu	70
4.7 Hydrogen yield for Cu-Zn/ γ -Al ₂ O ₃ and Cu-Zn/ZrO ₂ doped Al ₂ O ₃ at the reaction condition of 300°C and 1 atm before and after the accelerated sintering process	71
4.8 Compositions of OPC type I and fly ashes (FA-1, FA-2 and FA-3)	75
4.9 Physical properties of ordinary Portland cement type I (OPC type I) and fly ashes (FA-1, FA-2 and FA-3)	76

Tables	Page
4.10 CO ₂ adsorption using various types of fly ash (Adsorption condition; 30°C and 1 atm)	78
4.11 CO ₂ adsorption using fly ash at different adsorption temperatures (Adsorption condition; 30-150°C and 1 atm)	79
4.12 CO ₂ adsorption using fly ash at different adsorption pressure (Adsorption condition; 30°C and 1-1.5 atm)	80
4.13 CO ₂ adsorption using fly ash at different moisture contents (Adsorption condition; 30°C and 1 atm)	81
4.14 CO ₂ adsorption using fly ash (FA-1) at various wt% of NaOH	81
4.15 CO ₂ capture by carbonation reaction in fly ash with different composition of base treatments	84
4.16 Total CO ₂ capture from adsorption and carbonation using fly ash as solid sorbents	85

Chapter 1

Introduction

1.1 Introduction

A rapidly increasing world population affects too many problems in the world, especially a higher demand in energy and environmental changing. A fossil fuel cannot serve as the main energy for a long time and the energy obtained from the fossil fuel release greenhouse gases which cause environmental problems. Therefore, a renewable energy such as wind energy, solar energy, bio-mass energy and nuclear energy have been developed to replace the use of fossil fuel in the future and to reduce carbon dioxide released from fossil fuel combustion. Hydrogen fuel cell is attractive as a source of renewable energy when no carbon dioxide produced during operation (Grove, 1845; Appleby, 1994; Velu et al., 2000). Unfortunately, an acquisition of hydrogen to feed into a fuel cell to generate energy requires huge energy consumption and produces CO₂ in the process. Most of hydrogen is produced by a reforming process of hydrocarbons such as methane, methanol and ethanol (Holladay et al., 2009; Xu et al., 2008). Among these sources, methanol is very interesting due to high hydrogen per carbon ratio and low operating temperature, which results in a lower energy consumption than the reforming of other hydrocarbons (Choi and Stenger, 2002; Huang et al., 2009).

A methanol-steam reforming is a heterogeneous reaction which uses catalyst in the process. An active catalyst for methanol-steam reforming is Cu-Zn based catalyst. The commercial catalysts prepared by co-precipitation which suffers from a high demand of Cu and Zn metal contents up to 60-90 weight percent and the sintering of metal active site at high temperature (Choi and Stenger, 2002; Sá et al., 2010; Shishido et al., 2004; Turco et al., 2007). These problems lead to high cost of the catalyst and high energy consumption in the process. An incipient wetness impregnation and sol-gel techniques are introduced for the catalyst preparations to overcome these problems. An impregnation of metal over high surface area support provides an active catalyst with low metal loading. The addition of urea could enhance homogeneity of the metal salt solution (Shishido et al., 2004). Hence, an impregnation with an addition of urea could provide a well dispersed of active metal

over support. A sol gel method is widely used to synthesize nano particle catalysts and provide uniform metal thin film coating over support materials (Shi et al., 2011; Wu et al., 2004). These methods could provide a benefit in preparation of active catalyst with low metal loading and well distributed metal dispersion at low cost.

Literature reported that a catalyst support could play an important role in the activity of Cu-Zn base catalyst for methanol-steam reforming (Sá et al., 2010). The difference in structure, phase and morphology could change the chemical and physical properties of support that might effect to the activity of the catalyst. The main purpose of supports is to accomplish a good distribution of an active metal. Most of the support used for Cu-Zn based in methanol-steam reforming is alumina including a commercial catalyst. Alumina can improve the surface area of catalyst, mechanical properties and durability of catalyst (Huang et al., 2009). Moreover, metal oxides such as ZrO_2 and CeO_2 can be used as a co-metal oxide with alumina to improve the properties of the catalysts. An addition of ZrO_2 can provide several advantages on catalyst such as easy reducibility, increase metal dispersion and prevent the sintering (Huang et al., 2009).

In order to claim that a hydrogen fuel cell is a clean energy, CO_2 produced from the reforming process must be captured or disposed. Therefore, a development of CO_2 capture method was also studied and investigated in parallel with the hydrogen production. There are many methods to capture CO_2 , such as membrane separation, cryogenics, absorption, and adsorption (Shafeeyan et al., 2010). Membrane separation requires expensive membrane material and complicated operation. Cryogenics requires high energy consumption and high CO_2 concentration. CO_2 capture by chemical absorption suffers from corrosion and high operational cost (Li et al., 2013; Wang et al., 2011; Yang et al., 2008). These drawbacks make the processes not applicable for industry. Therefore, the process of adsorption by using disposal or waste materials as CO_2 solid sorbent can be a more attractive solution for CO_2 capture in the industry (Bobicki et al., 2012; Kaithwas et al., 2012; Sayari et al., 2011). The commercial solid sorbents for CO_2 capture are made of high surface area materials such as zeolite and mesoporous materials which are commonly reusable (Hedin et al., 2013; Meléndez-Ortiz et al., 2014; Zeleňák et al., 2008). However, these sorbents are very expensive. In addition, another problem for these sorbents is that the CO_2

captured sorbent must be discharged to a reservoir to recover them. Therefore, the operational and transportation costs of sorbents from the industrial area to the reservoir are considerably high. The disposable solid sorbents with a lower cost such as agricultural wastes have been introduced to solve this problem (Bachelor and Toochinda, 2012), but the CO₂ captured solid sorbents from agricultural wastes can only be used in landfilling. Instead of leaving CO₂ captured solid sorbents as valueless landfilled materials, a new technique to produce more valuable products using solid sorbent after CO₂ capture would be more interesting. Fly ash is a by-product coming out of a coal-fired power plant which can be used in roadway or pavement utilization, dam construction and admixture in cement (Ahmaruzzaman, 2010; Garrabrants et al., 2014; Papadakis, 1999). Literature also reported that fly ash can be used as solid sorbent for CO₂ capture. Finally, it becomes a waste material after capturing CO₂ without further usage for other applications (Gray et al., 2004; Mercedes Maroto-Valer et al., 2008).

In this work, the Cu-Zn based catalysts were prepared by two methods, impregnation and sol-gel over various types of supports, α -Al₂O₃, γ -Al₂O₃ and ZrO₂ doped Al₂O₃. The hydrogen production will be conducted in a tubular reactor to determine the proper condition for methanol-steam reforming reaction. These results would be providing an effective method with a lower metal catalyst for hydrogen production by methanol-steam reforming reaction. For CO₂ capture, fly ash is used as a solid sorbent for CO₂ capture and then as an admixture in cement formulation. The mortar and paste specimens were prepared using the cement with 20-40 wt% replacement of fly ashes before and after CO₂ capture. The properties of specimens such as water requirement, compressive strength, and autoclave expansion including carbonation depth were tested and compared. In addition, the fly ash with high free CaO, which is commonly found in the fly ash from lignite combustion, was investigated after CO₂ capture process. The high free CaO can cause excessive expansion in concrete structure (Kaewmanee et al., 2013). In order to enhance the CO₂ capture capacity, fly ash treated with various compositions of NaOH was investigated in this work. The results of this study could lead to a development of a novel catalytic system/process without CO₂ emission to atmosphere.

1.2 Statement of Problems

A Cu-Zn based catalyst is generally used for the hydrogen production from methanol-steam reforming. Most of Cu-Zn based catalyst is prepared by precipitation method with using 60-90% metal loading. A high metal loading in precipitation results in an increase in catalyst cost. In addition, a sintering of Cu metal at temperature over 300°C is the main cause of the deactivation of Cu-Zn based catalyst. Therefore, a proper operating condition in a low reaction temperature could prevent the sintering of Cu metal and increase the life time of catalyst.

Moreover, CO₂ produced from methanol-steam reforming reaction is another problem which causes a global warming. CO₂ adsorption over a solid sorbent could be an interesting method for the CO₂ capture. However, the cost of solid sorbent and CO₂ disposal after capturing is still controversial problem. Most of the solid sorbents are regenerated to reuse for CO₂ capture. This process uses high energy and also results in degrading these sorbents. Therefore, fly ash which is a low cost material produced from coal-fired power plant could be an attractive solid sorbent for CO₂ capture. After CO₂ capture, fly ash could be used as a mineral admixture in cement formulation.

1.3 Objectives

The objectives of this study aim at the development of the active catalyst for methanol-steam reforming reaction with a CO₂ capture process. The catalysts for methanol-steam reforming reaction were prepared by incipient wetness impregnation and sol-gel method to achieve a high hydrogen production and high activity of catalyst with low energy consumption in the process. The CO₂ capture was studied by using fly ash as a solid sorbent material. Then, fly ash after CO₂ capture was used as an admixture in cement formulation. The objectives of this study are listed as follows:

1. To study the process of hydrogen production from methanol-steam reforming reaction and CO₂ capture process.
2. To develop Cu-Zn based catalyst for methanol-steam reforming reaction by using incipient wetness impregnation and sol-gel method for catalyst preparation.
3. To determine a proper operating condition to produce the high hydrogen yield at a low reaction temperature which can prevent the Cu sintering problem.
4. To determine the proper conditions of fly ash in CO₂ capture such as compositions, moisture content, adsorption pressure, adsorption temperature and NaOH treatments.
5. To evaluate properties of mortar and cement paste specimens using fly ash before and after CO₂ capture as an admixture for construction applications (water requirement, compressive strength, autoclave expansion and carbonation depth).

1.4 Scope of work

This study focuses on the production of hydrogen with an environmentally benign from methanol-steam reforming process. The catalyst development and the CO₂ capture were separately studied in order to determine the proper condition for each process. The scope was separated into 2 parts, hydrogen production and CO₂ capture.

For hydrogen production;

- The Cu-Zn based catalysts were prepared by incipient wetness impregnation and sol-gel method.
- The active metals loading were kept constant at 20 wt% of the total catalyst and the molar ratio of Cu and Zn is constant at 1:1.
- The catalysts were prepared over various types of supports, α -Al₂O₃, γ -Al₂O₃ and ZrO₂ doped Al₂O₃.
- The experiment was conducted in the tubular reactor by varying temperature range of 200-300°C and fixed the pressure of 1 atm for methanol-steam reforming reaction.
- The activities of catalysts were calculated in term of hydrogen yield.

For CO₂ capture;

- Fly ash from Mae Moh coal-fired power plant in Thailand was used as a solid sorbent for CO₂ capture in this work.
- 2 batches of fly ash were collected from Mae Moh coal-fired power plant at interval time period of 6 months.
- The proper conditions of CO₂ capture using fly ash were investigated by varying the adsorption conditions of moisture content (0-10 wt%), pressure (1-1.5 atm), temperature (30-150°C) and NaOH treatments (0-10 wt%).
- Fly ashes after CO₂ capture were used as a mineral admixture for the concrete. The mortar and paste specimens were prepared using cement with 20-40 wt% replacement by fly ashes, before and after CO₂ capture.
- The properties of mixtures, water requirement, compressive strength, strength index, autoclave expansion, and carbonation depth were tested and compared with material standards and reference mixture.

Chapter 2

Literature Review

2.1 Hydrogen production for hydrogen fuel cell

2.1.1 Hydrogen fuel cell

A fuel cell was first invented by Sir William Grove. In 1839, Grove was experimenting on water splitting into hydrogen and water by electrolysis process (Grove, 1845). A fuel cell consists of two electrodes (anode and cathode) and electrolytes. Hydrogen was fed at the anode and oxygen was fed into the cathode to generate electricity and water. The hydrogen fed into the anode was split into proton and electron by catalytic reaction. The proton passed through electrolytes in the fuel cell while electron can create the electricity. Finally, the hydrogen and oxygen atom is combined into water molecules, which is the byproduct of this process (Appleby, 1994). Therefore, a fuel cell is considered as a renewable energy with environmentally benign to avoid the shortage of energy and CO₂ emission problem from fossil fuel.

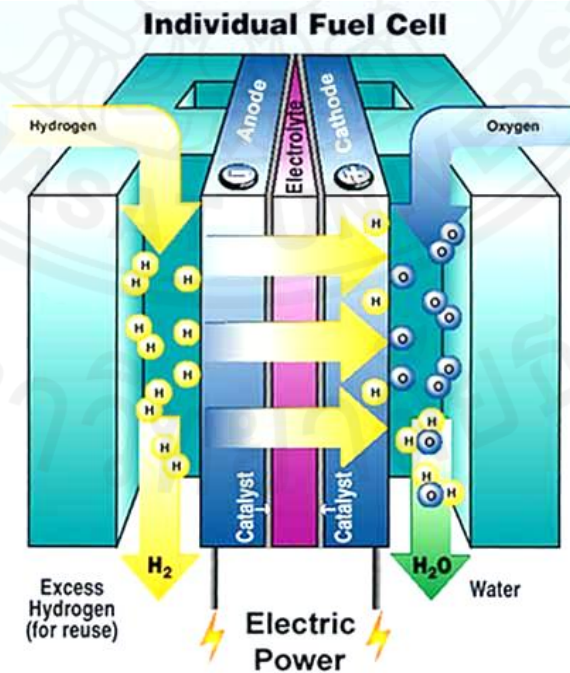


Figure 2.1 Hydrogen fuel cell (HyGen Industries, Inc., 2016)

2.1.2 Hydrogen sources

The hydrogen feed into the fuel cell is a key factor for application of fuel cell which can be produced from various sources both non-renewable sources (methane, methanol and coal) and renewable sources (biomass and water) as shown in Figure 2.2 (IEA, 2006).

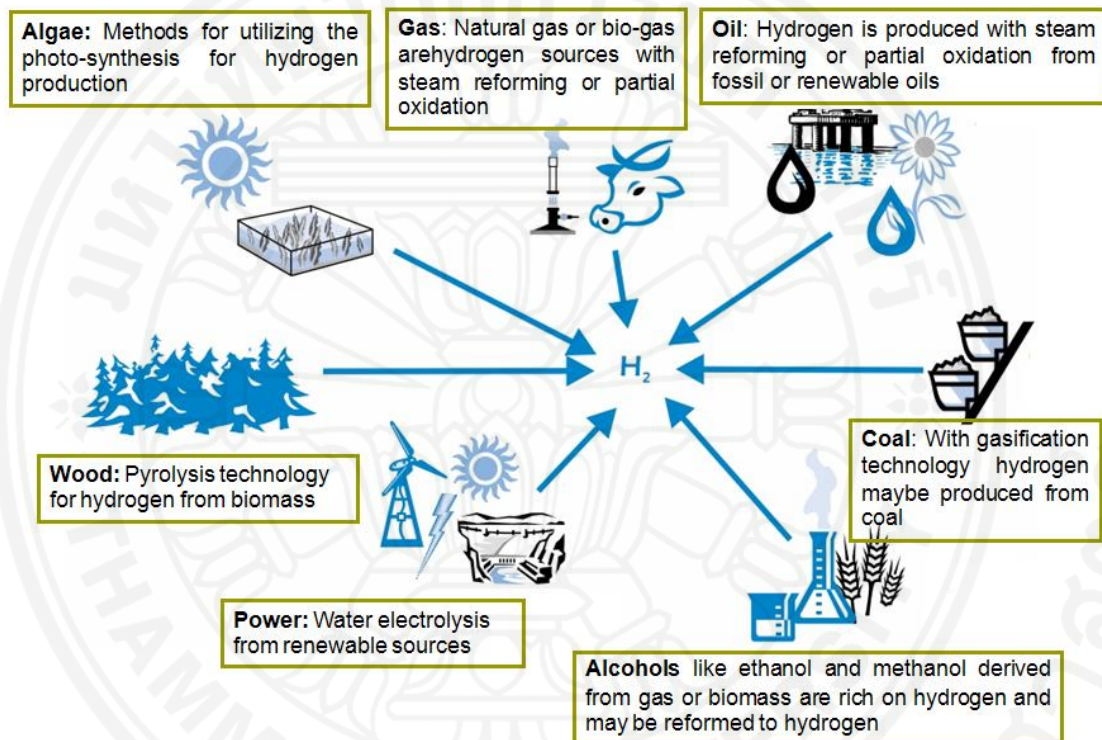


Figure 2.2 Hydrogen sources and process for hydrogen production (IEA, 2006)

There are many process technologies to produce hydrogen such as chemical, biological, electrolytic, photolytic and thermo-chemical process. Among these technologies, water electrolysis and natural gas reforming are interesting technologies of choice in the near future, while the other process technologies need a further development. The important problems of water electrolysis are cost of alkaline electrolyzers and low energy efficiency. Whereas, the hydrogen production from natural gas is non-renewable source and release CO₂ to environmental. Therefore, the development of hydrogen production process with zero emission was investigated for the long term application.

2.1.3 Hydrogen production from methanol

Methanol is an attractive source for the hydrogen production. There are three chemical reactions in conversion methanol to hydrogen, methanol decomposition, partial oxidation and methanol-steam reforming.

2.1.3.1 Methanol decomposition

The decomposition reaction is the simplest process among other reaction of hydrogen production from methanol as shown in equation 2.1. The disadvantages are that this reaction is endothermic, which requires a lot of energy for the reaction, the hydrogen yield is very small and CO is the main product of this reaction.

Decomposition reaction:



2.1.3.2 Partial oxidation of methanol

Partial oxidation is a fast and exothermic reaction as shown in equation 2.2. The drawback of partial oxidation is the heat accumulation due to its highly exothermic and fast reaction, so the catalyst might be deactivated by sintering at higher reaction temperature (Papavasiliou et al., 2004). Another limitation of this reaction is the hydrogen yield. It can produce the highest hydrogen yield of 66% when pure oxygen is fed. In case of air is used as feed into the process, the hydrogen yield is decreased (Lindström and Pettersson, 2001).

Partial oxidation reaction:



2.1.3.3 Methanol-steam reforming

The methanol-steam reforming reaction is known as a reverse reaction of methanol synthesis. Methanol-steam reforming is considered the most favorable process of hydrogen production in comparison to the decomposition and partial oxidation of methanol. This reaction could produce high hydrogen yield, high selectivity for carbon dioxide and the reaction occurs at mild reaction conditions. The

drawback of methanol-steam reforming reaction is the formation of CO as a by-product and slow response in the startup because it is an endothermic reaction (Papavasiliou et al., 2004).

Methanol-steam reforming reaction:



Therefore, Most of the hydrogen production is developed via methanol-steam reforming reaction. The process of hydrogen production from methanol-steam reforming reaction is a heterogeneous process which uses catalyst in the reaction.

2.1.4 Catalyst for methanol-steam reforming reaction

2.1.4.1 Copper-based catalyst

(1) Effect of preparation methods

The most common catalyst for methanol-steam reforming is copper-based catalyst. The copper-based catalyst can be prepared from several methods such as precipitation, impregnation, oxalate gel co-precipitation, hydrothermal synthesis and sol-gel. These methods can influence the properties of the catalyst, especially, the specific copper surface area as shown in Table 2.1 (Sá et al., 2010). The performance of copper-based catalysts depends on the status of copper. Good properties of copper for a highly active catalyst are high copper dispersion and high specific copper surface area, and small particle sizes.

Table 2.1 Physicochemical properties of copper catalysts by different preparation methods (Sá et al., 2010)

Catalysts	Preparation method	Surface area of catalyst (m^2g^{-1})	Specific copper surface area (m^2g^{-1})
Cu/ZrO ₂	Impregnation	13.1	1.0
Cu/ZrO ₂	Co-precipitation	64.2	3.5
Cu/ZrO ₂	Oxalate gel co-precipitation	71.5	18.4
Cu/ZnO	Co-precipitation	47.5	20.8
Cu/ZnO/Al ₂ O ₃	Co-precipitation	90.8	23.7
Cu/ZnO/ZrO ₂ /Al ₂ O ₃	Co-precipitation	129.7	25.9
Cu/Zn/Al	Impregnation	63.9	-
Cu/Zn/Al	Hydrothermal synthesis	84.5	-
Cu/Zn/Al	Co-precipitation	93.7	-
Cu/ZnO	Co-precipitation	40.7	16.0
Cu/ZnO	Homogeneous precipitation	76.4	41.6
Cu/ZnO/Al ₂ O ₃	Homogeneous precipitation	97.5	47.0
Cu/ZnO	Co-precipitation	48.6	20.8
Cu/ZnO/Al ₂ O ₃	Co-precipitation	91.9	22.2
Cu/ZnO/ZrO ₂	Co-precipitation	81.8	15.5
Cu/ZnO/ZrO ₂ /Al ₂ O ₃	Co-precipitation	116.2	23.3
Cu/Zn/Al	Impregnation	152.0	-
Cu/Zn/Ce/Al	Impregnation	162.0	-
Cu-Mn	Co-precipitation	9.6	-
Cu-Mn	Co-precipitation	55.2	-
Cu-Mn spinel	Soft reactive grinding technique	118.1	-
CuO/CeO ₂	Carbon template	153.0	-
CuMn ₂ O ₄	Silica template	144.0	-
CuO/ZnO/Zr ₂ O ₂	Co-precipitation	64.0	-

Precipitation or coprecipitation method

Precipitation or coprecipitation method is widely used for a synthesis of heterogeneous catalyst. These methods are promising to produce highly active catalysts. Precipitation methods occur in three main steps, supersaturation, nucleation and growth (Perego and Villa, 1997). Therefore, the precipitation method can produce catalysts or supports with high purity. The catalysts that contain more than one component can be prepared by coprecipitation method. Coprecipitation can produce a homogeneous distribution of catalyst precursors and provide a small metal cluster with uniform dispersion after calcination process. The drawbacks of this method are the high metal loading and several parameters such as pH, ageing condition and solution composition must be controlled. The commercial catalyst for methanol-steam reforming is also prepared by coprecipitation method. Figure 2.3 shows the step of catalyst preparation by precipitation method (Ertl et al., 1997)

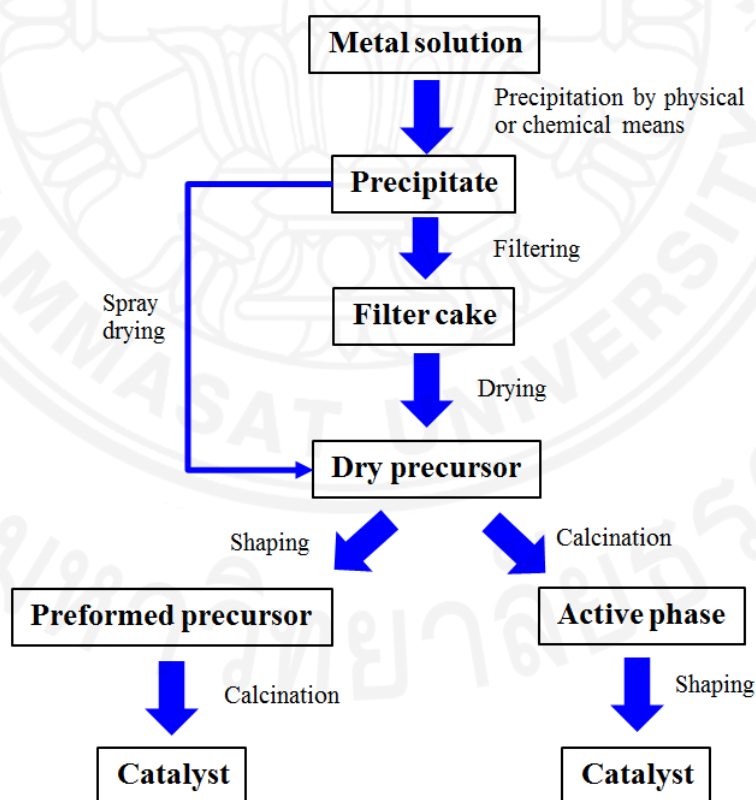


Figure 2.3 Catalyst preparations by precipitation method (Ertl et al., 1997)

Impregnation method

Impregnation method is another mean to synthesize the catalyst. This is a simple method in preparing a catalyst in which a few parameters have to be controlled during the preparation and low metal loading. There are three steps for a catalyst preparation by the impregnation method, contacting the support and the metal solution, drying the support to remove the solution and activation catalyst by calcination, reduction or treating with proper procedure. The drawback of this method is lower dispersion of metal than precipitation method (Perego and Villa, 1997). As a result, the activity of the catalyst prepared by the impregnation method is found to be lower than that prepared by the precipitation method.

Kniep et al. studied the relation between structure and the activity of the catalyst. The results shown that crystallinity, phase composition and homogeneity strongly effect to the final microstructure properties of copper catalyst. Therefore, the development of Cu catalyst should start from the proper catalyst preparation including calcination and reduction conditions in order to achieve a homogeneous microstructure of catalyst (Kniep et al., 2005).

Shen and Song reported that the preparation methods effect the performance of Cu-Zn based catalyst. In this work, impregnation, co-precipitation and hydrothermal synthesis were used as preparation method and compared the catalyst performance. The result indicated that the preparation method significantly influence the performance of Cu-Zn based catalyst, resulting in high hydrogen yield and high methanol conversion. Co-precipitation of Cu-Zn based catalyst exhibited 99-100% of methanol conversion and 71-76% of hydrogen production (Shen and Song, 2002).

Valdés-Solís et al. prepared the Cu based catalysts via a template technique using silicate-based silica xerogel as a template. The results show that increasing surface area of catalyst by nanocasting techniques results in higher initial catalytic activity in methanol-steam reforming reaction at 250°C. However, the deactivation of catalyst was not depending on the method of catalyst preparation (Valdés-Solís et al., 2006).

Sol-gel method

Sol-gel can be an alternative method for a catalyst preparation. This method is widely used to synthesize a nanoparticle or a nano-catalyst, which results in a highly active metal cluster dispersing well on the support. The advantage of sol-gel preparation are ease to control the final product, ability to produce a catalyst in different forms, ability to vary a catalyst composition at a molecular level, ability to prepare catalysts at low temperature and ability to introduce several components in a single step.

In sol-gel process, simple molecular precursors are converted into nanometer-sized particles by dissolving in an appropriate solvent. Then these particles are formed a colloidal suspension, or sol. The colloidal nano-particles are then linked together to form a network. This transformation to a gel can be initiated in several methods, but the most convenient approach is to change the pH of the reaction solution. Metal alkoxides are widely used as a precursor in a sol-gel preparation as they are highly reactive. However, the main drawbacks of the metal alkoxides are a limitation of commercial availability and high cost (Ertl et al., 1997).

Sol-gel chemistry with metal alkoxides can be described in terms of two classes of reaction:



Where X can either be H or R (an alkyl group)

Metal nitrate could be an alternative precursor as a catalyst preparation by sol-gel methods. Shi et al. studied a Cu/ZnO catalyst by using copper nitrate and zinc nitrate as a precursor in sol-gel preparation method (Shi et al., 2011). Wu et al. has synthesized NiZn ferrite over SiO₂ nanocomposite powders from nickel nitrate, zinc nitrate and iron nitrate in sol-gel method (Wu et al., 2004). Kim Woo et al. studied the physicochemical properties of Pd-alumina catalyst by using sol-gel, which results in a high dispersion of Pd and large surface area (Kim et al., 2000).

Matsumura and Ishibe prepared copper over silica support using sol-gel method. The active copper metal was varied up to 50 wt% over the silica support. The results exhibited high BET surface area of the catalysts in the range of 250-376 m²/g. The result also indicated that the crystallite size of copper is smaller than 4 nm when copper content is less than 20 wt%. However, Cu₂O was also found in this work influences to the activity of catalysts. Cu₂O can be oxidized to Cu⁺ which suppresses the formation of CO from the reverse water-gas shift reaction (Matsumura and Ishibe, 2009).

Esposito et al developed nanodispersed copper over ZrO₂ support prepared by sol-gel method. The catalysts were prepared from Zr propoxide and Cu(NO₃)₂·2.5H₂O. The result shows the high surface areas of catalysts in the range of 140-180 m²/g. (Esposito et al., 2010)

(2) Effect of promoter

In order to increase an activity of a catalyst, many researchers studied Cu-based catalysts with various types of support and promoters. The promoters used in Cu-based catalysts are Zn, Zr, Ce, Pt, Rh, Y, La, Ni, Mg, Pd, Sm, Ca, Gd, Mn, Cs, Cr, Co, Fe and Al. The supports used in Cu-based catalysts are Al₂O₃, carbon nanotube (CNT), and cordierite honeycomb. The literatures show that an addition of promoters could provide both positive and negative effects on the catalytic performance. The effect of dopants and catalyst preparations for the performance of Cu-based catalysts in methanol-steam reforming is shown in Figure 2.4.

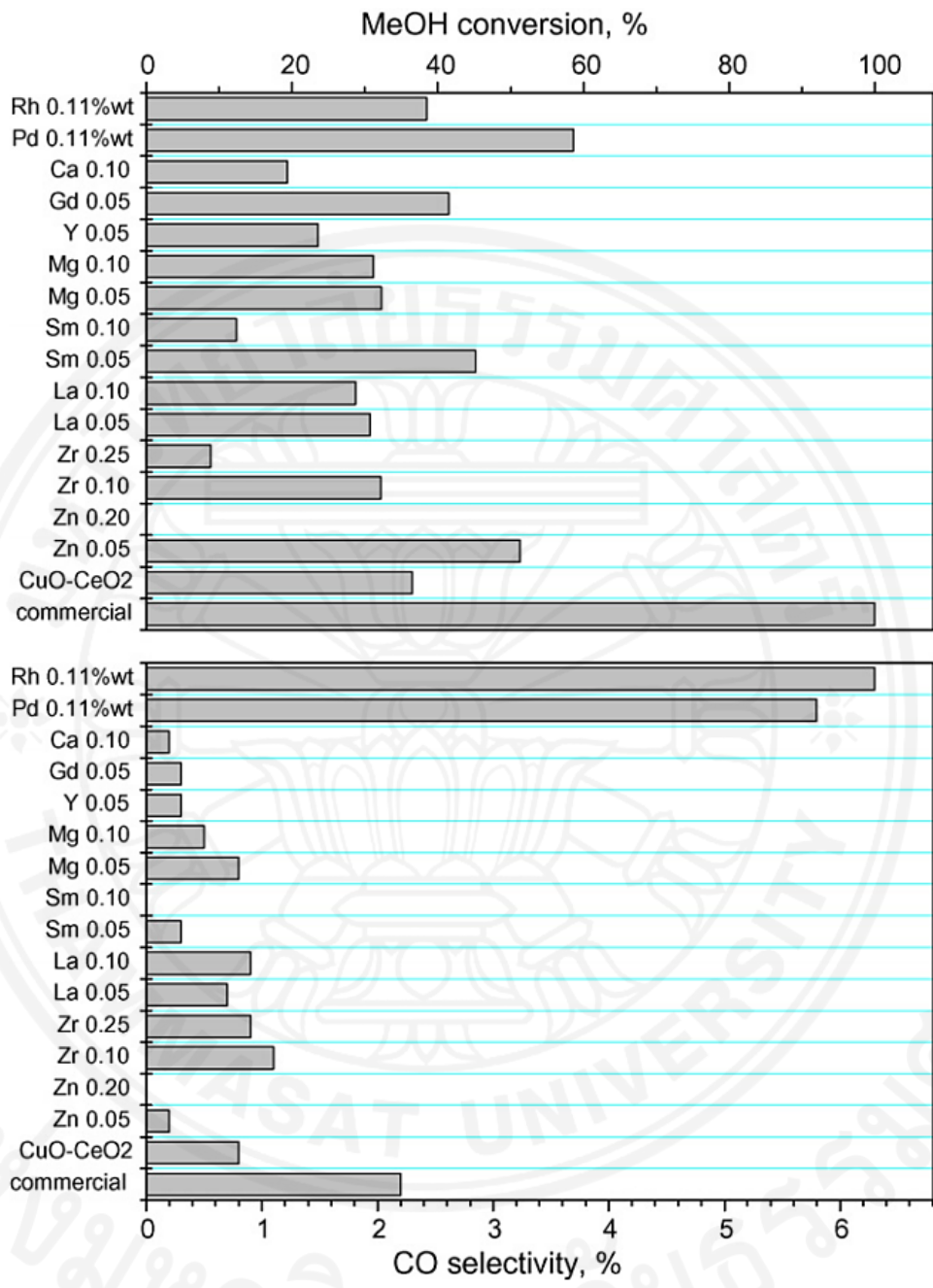


Figure 2.4 The performance of various promoters on Cu-based catalysts using for methanol-steam reforming reaction ($T= 240^{\circ}\text{C}$, $\text{H}_2\text{O}/\text{MeOH}= 1.5$). (Papavasiliou et al., 2007)

Figure 2.4 shows the methanol conversion and CO selectivity of various promoters on CuO-CeO_2 catalyst for a methanol-steam reforming reaction. The highest methanol conversion is shown in the Pd-promoted catalyst, but it provides high CO selectivity. The second one is the Zn-promoted catalyst which provides high

methanol conversion and low CO selectivity. Therefore, Zn is a proper promoter for Cu-based catalysts in methanol-steam reforming.

Most of the literature studied the steam reforming of methanol on CuO/ZnO base and CuO/ZnO/Al₂O₃ base catalyst. Fujitani and Nakamura found that an addition of Zinc oxide can improve the dispersion of Cu, reducibility of CuO and create active species on the Cu surface (Fujitani and Nakamura, 2000). The optimization of Cu/Zn ratio reaches the maximum of around one. A further increase in Zn content results in an increase in the desorption temperature where Cu⁰ surface area decreased. Actually, the rate of hydrogen production decreased over the Zn-rich catalysts (Shishido et al., 2007). Günter et al. reported that Cu and ZnO phases have a pronounced influence on the catalytic activity (Günter et al., 2001). Some researchers have proposed that the main reason for a high activity of CuO/ZnO based catalysts is the improvement in adsorption properties of catalysts (Huang et al., 2009).

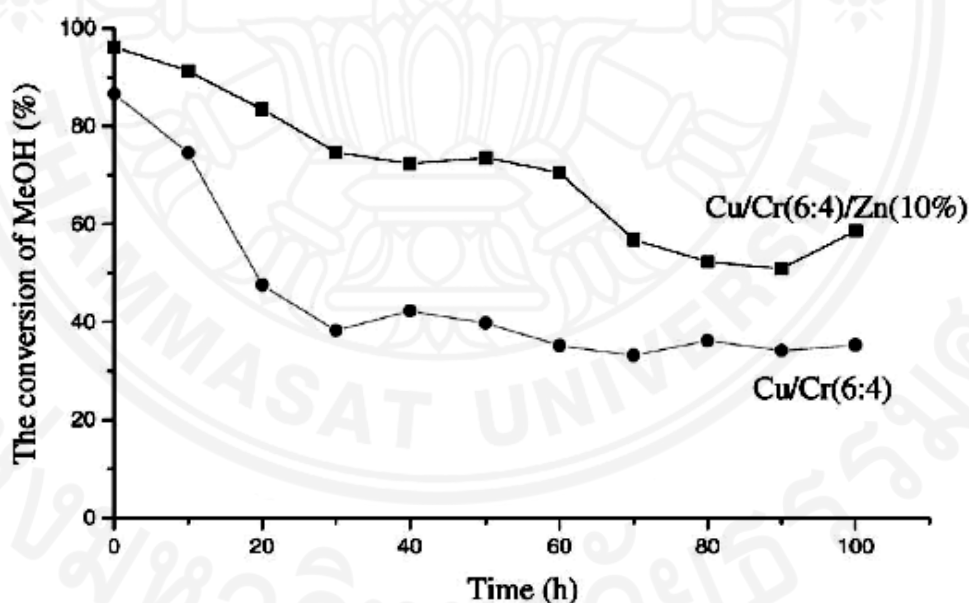


Figure 2.5 The performance of Zn-promoted on Cu-based catalysts at 200°C (Wang et al., 2003)

Figure 2.5 shows the methanol conversion over Cu/Cr and Cu/Cr/Zn catalyst. The Cu/Cr/Zn catalyst not only provides higher methanol conversion, but also improves the stability of the catalysts. Therefore, Zn could improve the methanol conversion of Cu-based catalysts.

Another method to improve the activity of catalyst is an addition of the third metal catalyst such as zirconia (ZrO_2) and ceria (CeO_2). Zirconia can be both promoter and support (Agrell et al., 2003; Breen and Ross, 1999; Jones and Hagelin-Weaver, 2009; Velu et al., 2001; Yao et al., 2006). An addition of zirconia to Cu-Zn based catalysts results in higher methanol conversions and lower CO selectivity in the methanol-steam reforming reaction (Yao et al., 2006). The promoting effect of zirconia has been attributed to the improvement in reducibility of catalysts, increases the Cu dispersion, prevents the sintering of Cu, due to its amorphous phase in catalyst, and increases the amount of Cu^+ . Thus, an addition of zirconia can improve both activity and stability of the Cu-Zn based catalysts (Huang et al., 2009; Yao et al., 2006).

Zirconia content in the catalyst is also known to possess anionic vacancies, which influence the metal dispersion and leading to a change in the morphology of the supported copper metal particle (Yao et al., 2006). ZrO_2 -promoter can lower the Al content on the surface of the catalyst and weaken the interaction between CuO and Al_2O_3 to avoid the generation of CuAl_2O_4 spinel-type compound (Yong-Feng et al., 2004).

The literature also reported that the effect of zirconia on Cu-based catalysts appear to be similar to the effects of ZnO in that zirconia improves Cu dispersion and leads to more reducible catalysts. However, it has been noted that the metal-support interaction in Cu/ ZrO_2 , which is synergy between Cu and ZrO_2 , is different from conventional Cu/ZnO catalysts. The higher activity of Cu/ ZrO_2 catalysts has also been attributed to the stabilization of Cu_2O on the surface of the reduced catalysts or during the reaction. It is believed that the formation of Cu_2O leads to both more active and more durable catalysts, since Cu_2O is less susceptible to sintering compared with Cu metal (Jones and Hagelin-Weaver, 2009).

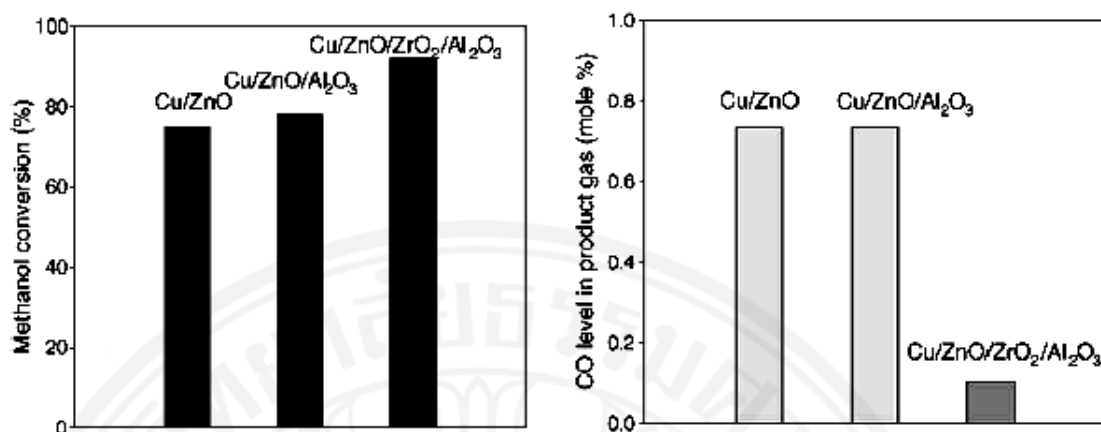


Figure 2.6 The performance of Zn/Zr-promoted on Cu-based catalysts at 260°C (Jeong et al., 2006)

Figure 2.6 shows a methanol conversion and CO selectivity over Cu/ZnO, Cu-Zn/Al₂O₃ and Cu/ZnO/ZrO₂/Al₂O₃ catalyst. The Cu/ZnO/ZrO₂/Al₂O₃ catalyst provided the highest methanol conversion and the lowest CO selectivity. Therefore, the Zn/Zr-promoted could improve the performance of Cu-based catalysts.

Ceria is another metal-promoted usually used for both support and promoter in catalyst for the methanol-steam reforming (Cheng et al., 2003; Feio et al., 2007; Gurbani et al., 2009; Liu et al., 2002; Patel and Pant, 2006, 2007, 2009; Pillai and Deevi, 2006). An addition of CeO₂ to Cu/Al₂O₃ catalysts has also shown to increase the methanol conversion, decrease CO selectivity and increase catalyst stability (Agrell et al., 2003; Breen and Ross, 1999; Huang et al., 2009; Jones and Hagelin-Weaver, 2009; Wang et al., 2003). The catalytic activity of the co-precipitation of Cu-Zn catalysts can also be improved significantly by an addition of CeO₂ during the precipitation process. It is apparent from the results that the presence of ZnO and CeO₂ help to separate the CuO to form a well-dispersed and relatively amorphous phase of CuO.

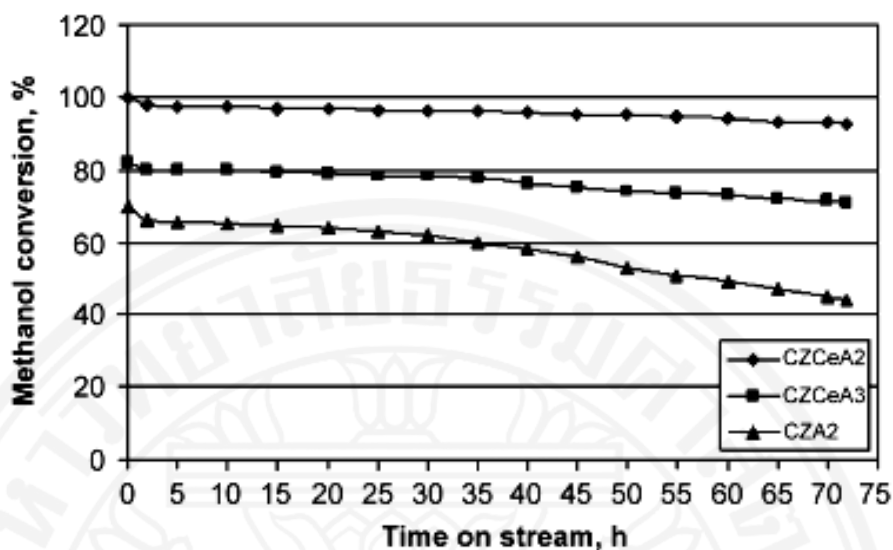


Figure 2.7 The catalytic stability of Ce-promoted on Cu-based catalysts prepared by precipitation method at 553 K (▲) CZA2, (◆) CZCeA2 and (■) CZCeA3 (Patel and Pant, 2007)

Figure 2.7 shows the catalytic stability of CZA2 (Cu-Zn/Al₂O₃: 30/20/50 wt%), CZCeA2 (Cu/Zn/Ce/Al₂O₃: 30/20/10/40 wt%) and CZCeA3 (Cu/Zn/Ce/Al₂O₃: 30/10/20/40 wt%) catalysts prepared by precipitation method. These catalysts used metal content of 50-60 wt% in the precipitation method to obtain a high methanol conversion. The highest methanol conversion is presented using the Cu/Zn/Ce/Al₂O₃ catalyst. Figure 2.7 also shows that the use of Ce in Cu-Zn/Al₂O₃ catalyst could improve the stability of a catalyst which is evidenced by slightly decrease in the activity of Cu/Zn/Ce/Al₂O₃ over 72 h.

2.1.4.2 The transition metal-based catalysts

The transition metal groups 8-10 such as Pd, Pt, Fe, Co, Ni, Ru and Ir including their compounds are generally used as a heterogeneous catalyst. The transition metal ions can change their oxidation states and become more effective as active catalysts for the methanol-steam reforming reaction. Table 2.2 shows the performance of transition metal-based catalysts over various types of support in the methanol-steam reforming reaction. However, the drawbacks of the transition metal-

based catalysts are the cost of transition metals and the high selectivity of CO. Therefore, in order to reduce the cost of hydrogen production the transition metal-based is not much attractive to use as catalysts compared to Cu-based catalyst.

Table 2.2 Summary of methanol-steam reforming over various supported transition metal-based catalysts (Sá et al., 2010)

Catalysts	Reaction temperature (°C)	Activity ($\mu\text{mol H}_2 \text{ g}_{\text{cat}}^{-1} \text{ s}^{-1}$)	CO selectivity (%)	Methanol conversion (%)
10 wt % Pd	220	-	100	10.9
1 wt % Pd	200	2	99.9	-
1 wt % Pd/SiO ₂	200	0.13	100	-
10 wt % Pd/SiO ₂	220	0.37	100	-
1 wt % Pd/Al ₂ O ₃	200	1.9	98.6	-
1 wt % Pd/La ₂ O ₃	200	3.1	92	-
1 wt % Pd/Nd ₂ O ₃	200	3.7	93	-
1 wt % Pd/Nb ₂ O ₅	200	1.5	95.8	-
10 wt % Pd/MgO	220	-	93.4	41
10 wt % Pd/In ₂ O ₃	220	-	4.5	28.3
10 wt % Pd/Ga ₂ O ₃	220	-	5.4	21.2
10 wt % Pd/CeO ₂	220	-	77.3	62.4
10 wt % Pd/Activated carbon	220	-	100	2.3
10 wt % Pd/HfO ₂	220	-	100	13.6
10 wt % Pd/Ta ₂ O ₅	220	-	100	6
1 wt % Pd/ZrO ₂	200	4	80	-
10 wt % Pd/ZrO ₂	220	-	81.6	64.3
10 wt % Pt	220	-	43.3	3
10 wt % Pt/Ga ₂ O ₃	220	-	24.5	5.4
10 wt % Pt/In ₂ O ₃	220	-	1.7	30.6

Catalysts	Reaction temperature (°C)	Activity ($\mu\text{mol H}_2 \text{ g}_{\text{cat}}^{-1} \text{ s}^{-1}$)	CO selectivity (%)	Methanol conversion (%)
10 wt % Pt/ZnO	220	-	4.6	27.6
10 wt % Pt/SiO ₂	220	-	74.4	0.3
10 wt % Ni/ZnO	220	-	95.3	15.7
10 wt % Ni/SiO ₂	220	-	98.9	7.3
10 wt % Co/ZnO	220	-	91.1	20.3
10 wt % Ru/ZnO	220	-	96.2	9.5
10 wt % Ir/ZnO	220	-	79.6	2.6

2.1.5 Effect of calcination temperature for Cu-Zn based catalyst

Calcination temperature is one of an important factor to make a highly active catalyst for methanol-steam reforming. The proper calcination can influence the surface morphology of the activated catalyst because of the surface reconstruction during the calcination process. J. Yang et al. studied Cu-Zn-Al catalyst prepared by co-precipitation method, then calcined at different temperature ranges of 300-750°C for 4 h in atmosphere as shown in Figure 2.8 (Yang et al., 2004)

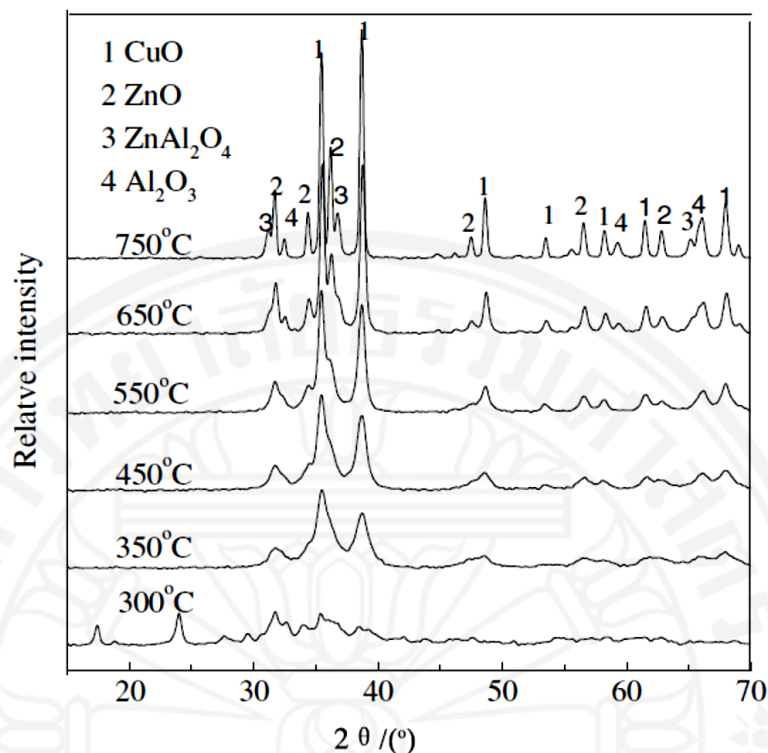


Figure 2.8 XRD patterns of Cu-Zn-Al catalyst calcined at different temperatures (Yang et al., 2004)

As the calcination temperature increases the peaks of CuO, ZnO and Al₂O₃ are clearly observed. The intensities of XRD peaks of CuO, ZnO and Al₂O₃ are increased with the increase of calcination temperature. A further increase of calcination temperature results in dramatic sharpening of the XRD peaks of CuO and ZnO. The peaks of ZnAl₂O₄ at 31.3°, 36.9° and 65.2° are observed when calcined at 750 °C. Since the width of an XRD peak is related to the size of the crystallites, it is concluded that the sharper the CuO diffraction peaks, the bigger the CuO average size of the particle distribution. The XRD results show that the increase of calcination temperature, CuO, ZnO and Al₂O₃ are formed with evident crystallization, and a spinel structure of ZnAl₂O₄ can be formed by the reaction of ZnO and Al₂O₃ at a calcination temperature of 650°C and above.

S.W. Oh et al. studied crystallite size variation with the final calcination temperature. The observations reveal that the calcination temperature strongly influences the morphology of the prepared metal oxides. In case of CuO, the

crystallite size increases until the calcination temperature reaches 500°C, which results in a lower specific surface area of copper (Oh et al., 2007).

A temperature-programmed reduction (TPR) is a commonly used for characterization of metal oxides, mixed metal oxides, and metal oxides dispersed on a support. The TPR method yields quantitative information of the reducibility of the oxide's surface, as well as a heterogeneity of the reducible surface. TPR is a method in which a reducing gas mixture flows over the sample. A thermal conductivity detector (TCD) is used to measure changes in the thermal conductivity of the gas stream. The TCD signal is then converted to concentration of active gas using a level calibration. Integrating the area under the concentration vs. time (or temperature) yields the total gas consumed.

Yang, Zheng et al. also studied the temperature program reduction of Cu-Zn-Al catalyst calcined at different temperature as shown in Figure 2.9. It can be clearly seen that the increase of the calcinations temperature causes the reduction peak shift to higher temperature which indicates that the catalysts calcined at higher temperature are more difficult to reduce than that calcined at lower temperature. The TPR profiles of the catalysts calcined at different temperatures show only one reduction peak, which was assigned to the reduction of the CuO to Cu⁰. The reduction temperature shifts to higher temperature with the increasing of the calcination temperature due to a stronger interaction between CuO and Al₂O₃, or the larger crystal of the precursor (Yang et al., 2004).

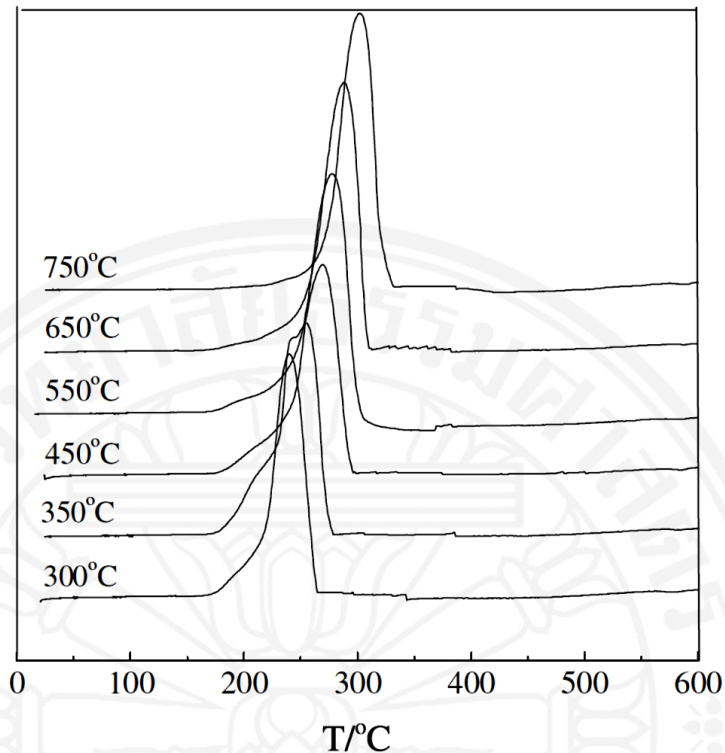


Figure 2.9 TPR profiles of Cu–Zn–Al catalyst calcined at different temperatures (Yang et al., 2004)

The calcination temperature of Cu-based catalyst affects the final form and the performance of catalysts. The increase of calcination temperature may cause undesirable compound that decreases an active metal of the catalyst. Moreover, the metal-support interaction and the crystallite size of metal will be increased and lost their active sites when calcination temperature is increased. Therefore, the calcination temperature of Cu-based catalyst should be kept at low temperature to achieve a small crystallite size and highly active Cu sites for the methanol-steam reforming reaction.

2.1.6 Activation of catalyst by reduction

Prior to the reaction, a catalyst reduction is required to convert the surface copper oxide into metallic copper-active phase. A temperature programmed reduction (TPR) technique is widely used to determine the temperature at which each catalyst is reduced. A high dispersion and large surface area of the catalyst could result in a lower temperature reduction, which means the easier reducibility could provide higher activity of the catalyst.

P.H. Matter et al. reported that the hydrogen production used CuO/ZnO/ZrO₂/Al₂O₃ catalyst in a methanol-steam reforming reaction. Figure 2.10 shows a comparison of activity of CuO/ZnO/ZrO₂/Al₂O₃ catalyst with and without reduction process. The catalyst with reduction process exhibits a higher hydrogen yield than those of the catalyst without a reduction process. Therefore, the catalyst reduction process can effect to the overall activity of catalyst (Matter and Ozkan, 2005).

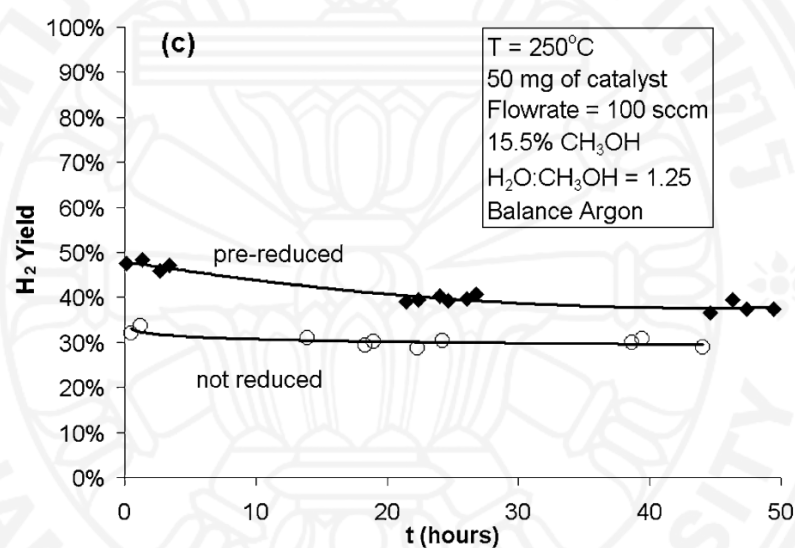


Figure 2.10 The activity testing with and without pre-reduction by hydrogen for CuO/ZnO/ZrO₂/Al₂O₃ catalyst (Matter and Ozkan, 2005)

For the Cu-Zn based catalysts, the reduction process is necessary before starting the reaction. After calcination process, Cu is in the form of copper oxide, which is not active species for the methanol-steam reforming reaction. Therefore, copper oxide will be reduced by hydrogen to form active copper metal before the reaction (Matter and Ozkan, 2005; Turco et al., 2007).

The catalyst development involves several steps such as catalyst preparation, active metal, support, calcination and reduction. These processes influence performance of catalyst.

2.1.7. Reaction conditions for Cu-Zn based catalyst

The proper reaction condition for methanol-steam reforming is very important to achieve a high hydrogen yield. The different reaction conditions can change the reaction pathway and produce undesirable product. Table 2.3 lists a vital reaction conditions (temperature, pressure and water/methanol molar ratio) of methanol-steam reforming (SRM) and autothermal reaction (ATR) using Cu-Zn based catalyst.

Table 2.3 The types of reactor and reaction conditions of methanol-steam reforming using Cu-Zn based catalyst

Ref	Reactor	Catalyst	Reaction	Conditions		
				T. (°C)	P. (atm)	H ₂ O/MeOH Molar ratio
(Peppley et al., 1999b)	Fixed-bed tubular reactor	Cu-Zn/Al ₂ O ₃	SRM	240-280	1-16	1.36
(Peppley et al., 1999a)	Fixed-bed reactor	Cu-Zn/Al ₂ O ₃	SRM	240-280	1	1
(Agrell et al., 2002)	Fixed-bed tubular reactor (quartz)	Cu-Zn/Al ₂ O ₃	SRM, ATR	175-320	1	1.3
(Agrell et al., 2003)	Packed-bed micro reactor	Cu-Zn/Al ₂ O ₃	SRM	170-320	1	1.3
(Shishido et al., 2004)	Fixed-bed flow reactor	Cu-Zn/Al ₂ O ₃	SRM	200-300	1	1.2
(Karim et al., 2005b)	Packed-bed and wall-coated reactors	Cu-Zn/Al ₂ O ₃	SRM	200	1	1.1
(Karim et al., 2005a)	Packed-bed reactor	Cu-Zn/Al ₂ O ₃	SRM	230	0.87	1.1

Ref	Reactor	Catalyst	Reaction	Conditions		
				T. (°C)	P. (atm)	H ₂ O/MeOH Molar ratio
(Choi and Stenger, 2005)	Fixed-bed tubular reactor	Cu-Zn/Al ₂ O ₃	SRM	120-325	1	1
(Jeong et al., 2006)	Fixed-bed quartz reactor	Cu-Zn/Al ₂ O ₃	SRM	180-270	1	0.6-1.5
(Larrubia Vargas et al., 2007)	Fixed-bed tubular reactor	Cu-Zn/Al ₂ O ₃	ATR	200-400	1	1.1
(Shishido et al., 2007)	Fixed-bed reactor	Cu-Zn/Al ₂ O ₃	SRM	150-300	1	1.2
(Turco et al., 2007)	Fixed-bed reactor	Cu-Zn/Al ₂ O ₃	ATR	200-400	1	1.1
(Lattner and Harold, 2007)	Fixed-bed reactor	Cu-Zn/Al ₂ O ₃	ATR	280	1.8-4.9	1
(Lee et al., 2007)	Packed-bed and wall-coated reactor	Cu-Zn/Al ₂ O ₃	SRM	200-258	1	1.1
(Yoon et al., 2007)	Fixed-bed tubular reactor	Cu-Zn/Al ₂ O ₃	SRM	260	1	1.5
(Jones et al., 2008)	Fixed-bed tubular reactor	Cu-Zn/Al ₂ O ₃	SRM	200-460	1	3.1

Ref	Reactor	Catalyst	Reaction	Conditions		
				T. (°C)	P. (atm)	H ₂ O/MeOH Molar ratio
(Lorenzut et al., 2011)	U-shaped micro reactor	Cu-Zn/Al ₂ O ₃	SRM	150-450	1	1.0
(Mrad et al., 2011)	Quartz tubular fixed bed reactor	Cu-Zn/Al ₂ O ₃	SRM	350	1	2.0
(Shi et al., 2013)	Fluidized bed reactor	Cu-Zn/Al ₂ O ₃	SRM	260-330	1	0.5-4.0
(Hammoud et al., 2015)	Fixed-bed tubular reactor	Cu-Zn/Al ₂ O ₃	SRM	200-350	1	2.0

The literature tries to determine the appropriate reaction conditions to produce the highest hydrogen yield. The temperatures of the reaction vary in an extensive range of 120-450°C to achieve a complete methanol conversion. The pressure of reaction is mostly operated at atmospheric pressure. The molar ratio of water to methanol feed varies in the range of 0.6-1.5. Most of the literature fixed the molar ratio of water to methanol at 1:1 following the stoichiometry of the methanol-steam reforming reaction.

Agrell et al. studied a temperature dependence of methanol conversion and product composition during methanol-steam reforming using a commercial catalyst (Sud-Chemie G-66 MR, 66 wt% of Cu) as shown in Figure 2.11. The result shows that the methanol conversion is increased when the reaction temperature is increased. The methanol is completely converted at temperature of 320°C (Agrell et al., 2002).

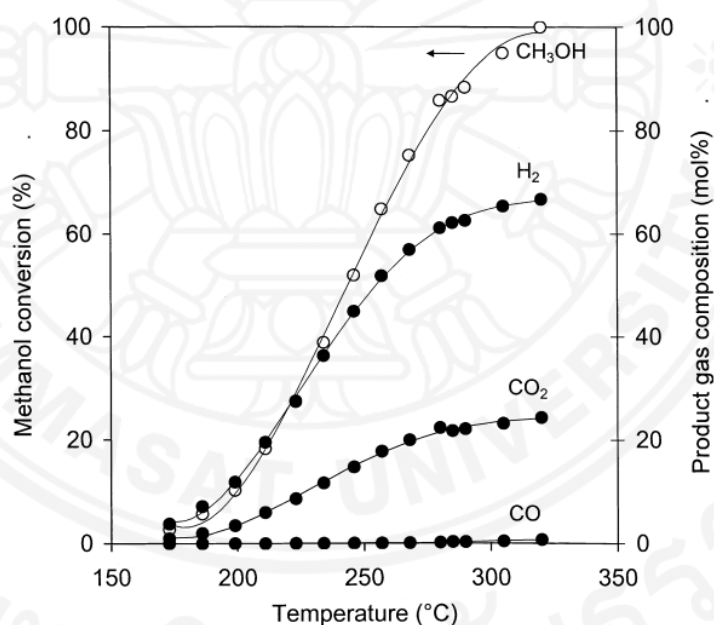


Figure 2.11 The temperature dependence of methanol conversion and product composition during methanol steam reforming over commercial Cu/ZnO/Al₂O₃ catalyst (Agrell et al., 2002)

Lorenzut et al. has also investigated Cu/ZnO/Al₂O₃ (45 wt% of Cu) in the wide range of reaction temperature of 150-450°C for the methanol-steam reforming reaction. The result shows that methanol-steam reforming can occur at the low temperature of 150°C but the methanol conversion is less than 10%. The complete

methanol conversion can exist at temperature above 275°C. However, the result also shows that the reverse water gas shift reaction can occur at the temperature higher than 300°C and produced CO which is an unwanted by-product for this reaction. (Lorenzut et al., 2011)

To develop a Cu-Zn based catalyst for production of low hydrogen cost from methanol-steam reforming reaction, the operation in a low reaction temperature could benefit to Cu-Zn based catalyst due to low energy consumption in the process and slower the sintering rate.

2.2 CO₂ capture by fly ash

2.2.1 Conventional CO₂ capture and storage

Carbon dioxide (CO₂) is one of the greenhouse gases. An increase of CO₂ can affect the climate change and global warming. CO₂ capture and sequestration involves capturing of man-made CO₂ at its source and storing before releasing to the atmosphere. The process of CO₂ capture and sequestration include three main steps; (1) capturing CO₂ and separating it from other gases; (2) purifying, compressing, and transporting the captured CO₂ to the sequestration site; and (3) injecting the CO₂ in subsurface geological reservoirs or storing it in the oceans (Perter folger, 2013).

There are many methods to capture CO₂, such as membrane separation, absorption, and adsorption (Shafeeyan et al., 2010). Membrane separation requires expensive membrane material and complicated operation. CO₂ capture by chemical absorption suffers from corrosion and high operational cost (Li et al., 2013; Wang et al., 2011; Yang et al., 2008). Adsorption process is the CO₂ capture by the intermolecular force between CO₂ and surface of solid sorbent. There are commonly three types of the adsorption process, Pressure swing adsorption (PSA), Temperature swing adsorption (TSA) and Electrical swing adsorption (ESA) (Mondal et al., 2012). Most of solid sorbents used in these processes are high cost material such as activated carbon or molecular sieves (Yang et al., 2008). Table 2.4 lists the advantages and disadvantages of CO₂ capture technologies (Li et al., 2013).

Table 2.4 Advantages and disadvantages of CO₂ capture technology

CO₂ capture technology	Advantages	Disadvantages
Chemical absorption	<ul style="list-style-type: none"> ● High selectivity so that it can capture CO₂ at low concentration in a gas stream ● Wet-scrubbing allows good heat integration and ease of heat management 	<ul style="list-style-type: none"> ● Tradeoff between heat of reaction and kinetics. Current solvents require a significant amount of steam to reverse chemical reactions and regenerate the solvent ● High energy required to heat, cool, and pump nonreactive carrier liquid (usually water) ● Vacuum stripping can reduce regeneration steam requirements, but expensive
Solid sorbent	<ul style="list-style-type: none"> ● Chemical sites provide large capacities and fast kinetics, enabling capture CO₂ at low concentration in a gas stream ● High capacities per unit mass or volume compared to chemical absorption ● Lower heating requirements than chemical absorption 	<ul style="list-style-type: none"> ● Heat required to reverse chemical reaction (even though generally less than in chemical absorption) ● Heat management in solid sorbent systems is difficult. Therefore, it can limit CO₂ capture capacity and produce undesirable issues when the absorption reaction is exothermic ● High pressure drop, especially for flue gas applications ● Solid sorbent can degrade after regeneration process
Membrane	<ul style="list-style-type: none"> ● No steam load ● No chemicals 	<ul style="list-style-type: none"> ● Membranes tend to be more suitable for high-pressure

CO₂ capture technology	Advantages	Disadvantages
	<ul style="list-style-type: none"> ● Simple and modular designs 	<p style="text-align: center;">processes</p> <ul style="list-style-type: none"> ● Tradeoff between recovery rate and product purity (difficult to meet both high recovery rate and high purity) ● Requires high selectivity (due to CO₂ concentration and low pressure ratio) ● Poor economy of scale ● Multiple stages and recycle streams may be required

For CO₂ capture by solid sorbent, a number of solids can be used to capture CO₂ to form stable compounds at the adsorption condition. After CO₂ capture, the all of a solid sorbent was be regenerated to release the CO₂ at the desorption condition. The solid sorbent will be reused for CO₂ capture process. However, solids are inherently more difficult to work with than liquids, and no solid sorbent system for large scale recovery of CO₂ from flue gas has yet been commercialized, although molecular sieve systems are used to remove impurities from a number of streams. Scientists have developed an amine-enriched solid sorbent that has been investigated with flue gas streams at temperatures similar to those found after lime/limestone desulfurization scrubbing. The CO₂ capture sorbents are prepared by treating high surface area substrates with various amine compounds. The immobilization of amine groups on the high surface area material significantly increases the contact area between CO₂ and amine. This advantage has the potential to improve the energy efficiency of the process compared to MEA scrubbing (Figueroa et al., 2008).

After CO₂ capture process, CO₂ can be stored underground, used for enhancing oil recovery, mineral sequestration, and as carbon resources to be converted into other useful compounds (Bobicki et al., 2012; Li et al., 2013). In case of CO₂ storing underground, CO₂ would be injected in a supercritical state into a porous rock formation. When CO₂ is injected at depths greater than 800 meters in a typical reservoir, the pressure keeps the injected CO₂ in a supercritical state (dense like liquid) and thus it is less likely to migrate out of the geological formation. Injecting CO₂ into deep geological formation uses existing technologies that have been primarily developed and used by the oil and gas industry. This method could potentially be adapted for long-term storage and monitoring of CO₂ (Peter folger 2013). CO₂ can be kept in the ocean storage. The potential for ocean storage of captured CO₂ is huge, but environmental impacts on marine ecosystems and other issues may determine whether large quantities of captured CO₂ will ultimately be stored in the ocean.

Another option for sequestering CO₂ produced by fossil fuel combustion involves converting CO₂ to solid inorganic carbonates, such as CaCO₃ (limestone), using chemical reactions. When this process occurs naturally, it is known as “weathering” and takes place over thousands or millions of years. The process can be accelerated by reacting a high concentration of CO₂ with minerals found in large quantities on the Earth’s surface, such as olivine (Mg, Fe)₂SiO₄ or serpentine ((Mg, Fe)₃Si₂O₅(OH)₄). Mineral carbonation has the advantage of sequestering carbon in solid, stable minerals that can be stored without risk of releasing carbon into the atmosphere over geologic time scales. The advantages and disadvantages of these processes are provided as in Table 2.5 (Bobicki et al., 2012).

Table 2.5 Summary of CO₂ storage technology

CO₂ storage technology	Advantages	Disadvantages
Geological sequestration	<ul style="list-style-type: none"> ● Feasible on a large scale ● Substantial storage capacity known ● Extensive experience ● Low cost 	<ul style="list-style-type: none"> ● Monitoring necessary ● Leakage possible
Ocean carbon sequestration	<ul style="list-style-type: none"> ● Large storage capacity 	<ul style="list-style-type: none"> ● Temporary storage ● Potential harmful effects on aquatic microbes
Industrial use	<ul style="list-style-type: none"> ● CO₂ incorporated into valuable products 	<ul style="list-style-type: none"> ● Limited storage capacity ● Short storage time
Mineral carbon sequestration	<ul style="list-style-type: none"> ● Only known form of permanent storage ● Minerals required available in quantities capable of binding all fossil-fuel bound carbon ● Carbonation products environmentally benign 	<ul style="list-style-type: none"> ● Energy intensive ● High cost

2.2.2 Solid sorbents for CO₂ capture process

The adsorption process by solid sorbents can be an alternative for CO₂ capture. However, the development of solid sorbent to increase the CO₂ capture capacity and stability for repeatability is necessary. Most of the solid sorbents made from porous materials such as MCM-41, SBA-12, SBA-15, zeolite or activated carbon. These materials require some of the chemical treatment to enhance the CO₂ capture capacity as shown in Table 2.6.

Table 2.6 Solid sorbents and chemical treatment for the CO₂ capture

Ref	Solid sorbents	Chemical treatment	CO ₂ Capture capacity	Conditions
(Gray et al., 2005)	SBA-15	<ul style="list-style-type: none"> ●Ethyleneamine ●γ-inopropyltriethoxysilane (APTS) 	SBA-15-fresh 2011.4 $\mu\text{mol CO}_2/\text{g sorbent}$	●Adsorption at 25°C
	Reformulated immobilized amine sorbent (R-IAS)	<ul style="list-style-type: none"> ●Ethyleneamine ●γ-inopropyltriethoxysilane (APTS) 	R-IAS-fresh 4188.1 $\mu\text{mol CO}_2/\text{g sorbent}$	
	Immobilized amine sorbent (IAS)	<ul style="list-style-type: none"> ●Ethyleneamine ●γ-inopropyltriethoxysilane (APTS) 	IAS-fresh 1603.9 $\mu\text{mol CO}_2/\text{g sorbent}$	
(Zhao et al., 2007a)	MCM-41	γ -(aminopropyl) triethoxysilane (APTS)	1.16 mmol/g on APTS-MCM-41	●Room temperature and various pressures
		N- β -(aminoethyl)- γ -aminopropyl dimethoxy methylsilane (AEAPMDS)	2.20 mmol/g on AEAPMDS-MCM-41	
	SBA-15	γ -(aminopropyl) triethoxysilane (APTS)	0.96 mmol/g on APTS-SBA-15	
		N- β -(aminoethyl)- γ -aminopropyl dimethoxy methylsilane (AEAPMDS)	1.27 mmol/g on AEAPMDS-SBA-15	

Ref	Solid sorbents	Chemical treatment	CO ₂ Capture capacity	Conditions
(Wang et al., 2007)	SBA-15	3-aminopropyl-triethoxysilane (APTES)	34.2 mg/g on APTES-SBA-15	<ul style="list-style-type: none"> ●Room temperature ●Partial pressure of CO₂ is 0.005 MPa
(Zhao et al., 2007b)	Zeolite 13X	Sodiumhydroxide solution of 1.0-1.2mol/L	<ul style="list-style-type: none"> ●13X-N (120 g of CO₂/mL) at 25°C ●13X-N (140 g of CO₂/mL) at 0°C 	<ul style="list-style-type: none"> ●Temperature 25°C and 0°C ●Pressure range 0-1.0 atm
	Modified zeolite 13X with kaolin binder		<ul style="list-style-type: none"> ●13X-K(100 g of CO₂/mL) at 25°C ●13X-K(100 g of CO₂/mL) at 0°C 	
(Zelenak et al., 2008)	SBA-12 mesoporous silica	3-aminopropyl (AP)	SBA-12/AP, 1.04 mmol/g	<ul style="list-style-type: none"> ●Adsorption temperature 25°C
		3-(methylamino)propyl (MAP)	SBA-12/MAP, 0.98 mmol/g	
		3-(phenylamino)propyl (PAP)	SBA-12/PAP, 0.68 mmol/g	

Ref	Solid sorbents	Chemical treatment	CO ₂ Capture capacity	Conditions
(Pevida et al., 2008)	Activated carbons	Ammonia (NH ₃)	8.4 wt.% for CN800	● Adsorption temperature 25°C
(Yue et al., 2008)	SBA-15	Tetraethylenepentamine (TEPA) Diethanolamine (DEA) Glycerol	144 mg CO ₂ /g TEPA 20.8 mg CO ₂ /g DEA 163 mg CO ₂ /g Mixed amine-modified SP	● 5% CO ₂ concentration ● 100°C desorption
(Zhang et al., 2008)	Chabazite zeolites	Alkali series (Li, Na, K) Alkaline-earth (Ca, Mg, Ba)	LiCHA 5 gmol/kg adsorbent) BaCHA 3 gmol/kg adsorbent	● Adsorption temperature below 120°C Pressure range 0-1.18atm
(Pires et al., 2008)	Tetraethoxysilane (TEOS) Phenyltriethoxysilane (PhOS)	Octylamine		
(Mercedes Maroto-Valer et al., 2008)	High carbon fly ashes (FA)	Monoethanolamine (MEA) Diethanolamine (DEA) Methyldiethanolamine (MDEA)	FA adsorbs 17.5 mg CO ₂ /g FA-DEM adsorbs 43.5 mg CO ₂ /g AC-MEA adsorbs 68.6 mg CO ₂ /g	● Adsorption temperature : 30, 70, 100 and 120°C

Ref	Solid sorbents	Chemical treatment	CO ₂ Capture capacity	Conditions
(Díaz et al., 2008)	X-zeolites	Treated with deferent sodium and cesium aqueous solutions	<ul style="list-style-type: none"> •Capacities at 100°C (10 mg/g) •Capacities at 200°C (3 mg/g) 	<ul style="list-style-type: none"> •Temperature 50, 100 or 200°C
(Yang et al., 2008)	Aminated mesoporous silica	MCM-41 impregnated with polyethylenimine (PEI)	0.45-0.6 mol CO ₂ /mol amine	
	Aminated SBA-15	MCM-41 impregnated with polyethylenimine (PEI)	1528-4188 μmol CO ₂ /g sorbent	
	PEI-impregnated MCM-41	MCM-41 impregnated with polyethylenimine (PEI)	246 mg CO ₂ /g PEI or 82 mg CO ₂ /g sorbent	
	Anthracite activated carbon	MCM-41 impregnated with polyethylenimine (PEI)	65.7 mg CO ₂ /g sorbent	
	Lithium silicate	MCM-41 impregnated with polyethylenimine (PEI)	360 mg CO ₂ /g sorbent	
(Lee et al., 2009)	Potassium-based dry sorbent (KZrI)	Anhydrous alkali metal carbonate (K ₂ CO ₃)	91.6mg CO ₂ /g sorbent	<ul style="list-style-type: none"> •Temperature 50-100°C •Pressure 1 atm.
(Ribeiro et al., 2013)	Activated carbon honeycomb monolith with zeolite 13X particles	-	81.4% of the fed CO ₂	Flue gas (8% of CO ₂ balanced by N ₂)

2.2.3 Fly ash

Fly ash is one of the residues generated by coal combustion. Fly ash composes of fine particles that are driven out of the furnace with the flue gases. Ash that falls to the bottom of the boiler is called bottom ash. Fly ash is generally captured by electrostatic precipitators or other particle filtration equipment before the flue gases reach the chimney of a coal-fired power plant as shown in Figure 2.12. Since the particles solidify rapidly while suspended in the exhaust gases, fly ash particles are generally spherical in shape and range in size from 0.5 μm to 300 μm . The major consequence of the rapid cooling is that few minerals have time to crystallize, and that mainly amorphous, quenched glass remains. Nevertheless, some refractory phases in the pulverized coal do not melt (entirely), and remain crystalline. Consequently, fly ash is a heterogeneous material. SiO_2 , Al_2O_3 , Fe_2O_3 and occasionally CaO are the main chemical components present in fly ashes (Fly ash, 2014). The mineralogy of fly ashes depends on type of coal and combustion condition in furnace. The main phases encountered are quartz (SiO_2), kaolinite ($\text{Al}_2\text{Si}_2\text{O}_5(\text{OH})_4$), siderite (FeCO_3), and illite ($(\text{K},\text{H}_3\text{O}) (\text{Al},\text{Mg},\text{Fe})_2(\text{Si},\text{Al})_4\text{O}_{10}[(\text{OH})_2,(\text{H}_2\text{O})]$). The less predominant minerals in the unreacted coals include calcite (CaCO_3), pyrite (FeS_2) and hematite (Fe_2O_3) (Ahmaruzzaman, 2010).

Production of Fly Ash

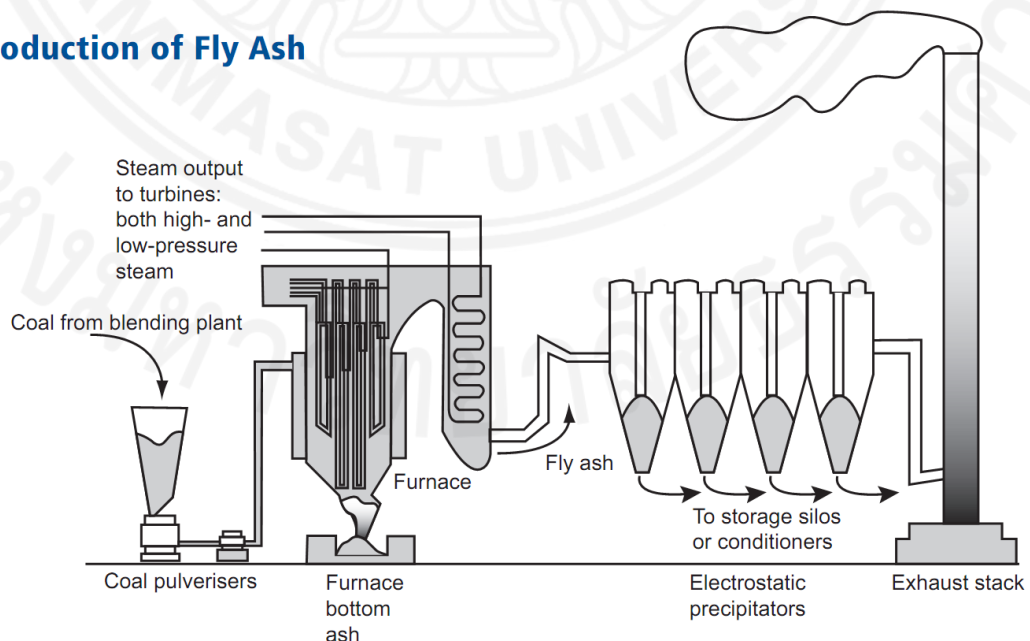


Figure 2.12 The process of coal-fired power plant (Sear, 2001)

The current annual production of coal ash world-wide is estimated around 600 million tones, with fly ash constituting about 500 million tones at 75-80% of the total ash produced. The amount of coal waste (fly ash) was released by factories and thermal power plants have been increasing throughout the world. The disposal of the large amount of fly ash has become a serious environmental problem. The present day utilization of ash on a worldwide basis varied widely from a minimum of 3% to a maximum of 57%, yet the world average only amounts to 16% of the total ash. A substantial amount of ash is still disposed of in landfills and/or lagoons at a significant cost to the utilizing companies and thus to the consumers (Ahmaruzzaman, 2010).

Fly ash can be used in several purposes which depend on its quality. According to ASTM C618, fly ash can classify into class F and class C for using as a mineral admixture in concrete (ASTM C618, 2003). Literature report that fly ash can be used in roadway or pavement utilization, dam construction and admixture in cement (Ahmaruzzaman, 2010; Garrabrants et al., 2014; Papadakis, 1999). Fly ash improves the performance and quality of fresh concrete and hardened concrete. For fresh concrete, fly ash affects the plastic properties of concrete by improving workability, reducing water demand, reducing segregation and bleeding, and lowering heat of hydration. For hardened concrete, fly ash increases strength, reduces permeability, reduces corrosion of reinforcing steel, increases sulphate resistance, and reduces alkali-aggregate reaction (Metha and Monteiro, 2006).

When fly ash is incorporated in concrete, two possible reasons may be adopted to explain the changes in the reaction mechanisms. One is the pozzolanic reaction of amorphous phases in fly ash, and the other is the influence of fly ash on the hydration of cement (Wang, 2014). As fly ash is blended with Portland cement, it contributes to the consumption of Ca(OH)_2 and the formation of cementitious products, like C-S-H gel which are formed during the cement hydration process. The compressive strength development at early ages is affected negatively with an addition of fly ash in cement. However, at 90 days, fly ash blended mortars were developed more than 80–97% of the Portland cement mortar's compressive strength (Kocak and Nas, 2014). However, high free lime content fly ash may affect both mechanical properties and durability of concrete. K. Kaewmanee et al. reported that a high free lime content of fly ash tends to cause higher autoclave expansion and alkali-aggregate reaction (Kaewmanee et al.,

2013). The autoclave expansion is an undesirable property of concrete because it results in the cracking of concrete.

In case of CO₂ capture using fly ash, it can be used as a solid sorbent for CO₂ capture or as a mineral carbonation with alkaline components in fly ash. One of the advantages of fly ash used for CO₂ capture is its on-site application. This is very effective to minimize the CO₂ capture and storage cost and reduces the treatment and disposal cost of fly ash. In addition, the final products of fly ash after CO₂ capture process have the potential to use as mixture in concrete. Fly ash is also directly used to support the sorbent on which CO₂ capture components such as amine can be impregnated. In addition, fly ash can be a raw material of meso-porous substances, zeolite and SiO₂, which can be the sorbent supports for CO₂ capture. Therefore, the dry process can be effectively used for CO₂ capture rather than storage because the sorbents should be regenerated. However, fly ash may be used as a CO₂ capture component for direct contact with the flue gas of the coal-fired power plant in the fluidized reactor. The storage capacity in the process was reported to be 0.207 g CO₂/g fly ash (Wee, 2013).

M. Mercedes Maroto-Valer et al used high fly ash to derive the activated carbon as a solid sorbent for CO₂ capture. The samples were steam activated at 850°C, resulting in a significant increase of the surface area (1075 m²/g). The activated samples were impregnated with different amine compounds (Monoethanolamine, Diethanolamine and Methyldiethanolamine). The results show that Amine (MDEA, DEA, MEA, and MDEA + MEA) impregnation can improve significantly the CO₂ adsorption of the samples. The MEA impregnated over activated carbons can achieve the highest CO₂ capture capacity of 68.6 mg CO₂/g sorbent (Mercedes Maroto-Valer et al., 2008).

M.L. Gray et al have studied the CO₂ capture using fly ash. Fly ash containing 9.5% of unburned carbon was used as a solid sorbent and 3-chloropropylamine-hydrochloride (CPAHCL) and the potassium hydroxide were used as chemical treatment as shown in Figure 2.13. The highest CO₂ capture on this work was 174.6 μmol/g samples for CPAHCL treated over the fly ash carbon sample. The low CO₂ capture capacity was caused by the low surface area of the solid sorbent in this study.

However, The CO₂ capture after regeneration of this solid sorbent is very low (Gray et al., 2004).

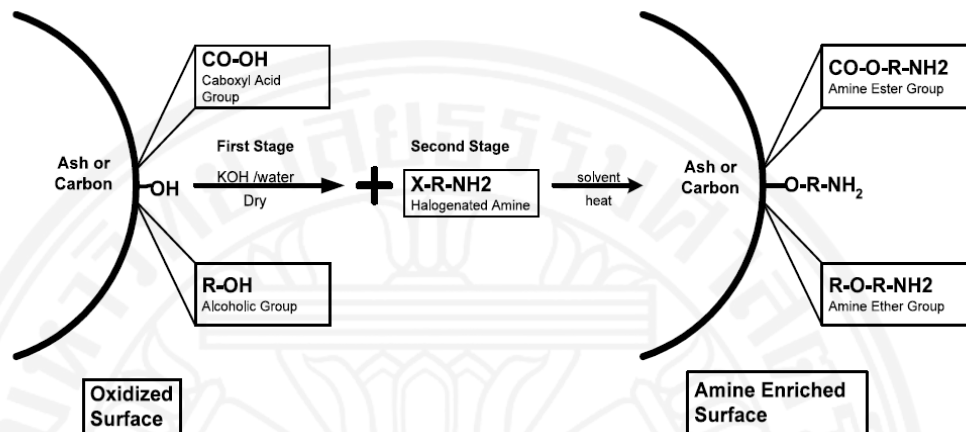


Figure 2.13 Proposed reactions for preparation of the amine-enriched fly ash sorbent

The interesting property of fly ash as a solid sorbent for CO₂ is the high stability and its free CaO which can react with CO₂. The drawback in using fly ash as a solid sorbent is low CO₂ capture capacity. In case of chemical treatment, the cost of preparation is increased and the regeneration is not satisfied with industry application. Finally, it becomes a waste material after capturing CO₂ without further usage for other applications (Gray et al., 2004; Mercedes Maroto-Valer et al., 2008).

Chapter 3

Methodology

3.1 Methanol-steam reforming

3.1.1 Catalyst and support preparations

3.1.1.1 Impregnation method

20wt% of Cu-Zn over various supports was prepared using an incipient wetness impregnation. $\text{Cu}(\text{NO}_3)_2 \cdot 3\text{H}_2\text{O}$ ($\geq 99\%$, Fluka) and $\text{Zn}(\text{NO}_3)_2 \cdot 6\text{H}_2\text{O}$ ($\geq 99\%$, Fluka) were dissolved in DI water separately to obtain the solution concentration of 1.25 M. Cu-Zn salt solution mixture was prepared by combining Cu and Zn solutions with the molar ratio of 1:1. The Cu-Zn solution was dropped into the supports drop by drop to impregnate the active metals on supports. For the impregnation with additional of urea, two moles of urea ($\geq 99\%$, Carlo Erba) were added into Cu-Zn solution and then impregnated over the supports. The concentration of urea is 2.5 M. In case of the direct addition of ZrO_2 in Cu-Zn over $\gamma\text{-Al}_2\text{O}_3$, the catalyst was prepared by impregnation by dissolving of $\text{ZrO}(\text{NO}_3)_2 \cdot 6\text{H}_2\text{O}$ ($\geq 99.5\%$, Fluka Analytical) of 0.125 M into Cu-Zn salt solution. The mixed solution was added drop by drop over $\gamma\text{-Al}_2\text{O}_3$ support. The additional amount of $\text{ZrO}(\text{NO}_3)_2 \cdot 6\text{H}_2\text{O}$ was calculated and results in 10wt% ZrO_2 in total catalyst weight after calcination. All impregnated catalysts were dried at room temperature for 24 h and at 105°C for 6 h and then calcined at 300°C for 3 h. Figure 3.1 shows the incipient impregnation method of Cu-Zn over Al_2O_3 with urea 2 mole in preparation method.

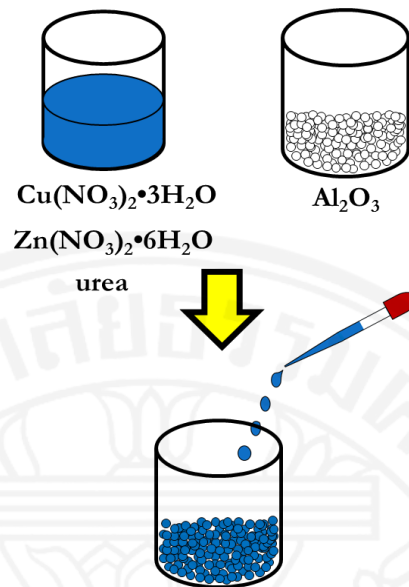


Figure 3.1 Cu-Zn/ Al_2O_3 catalysts prepared by incipient wetness impregnation method

3.1.1.2 Sol-gel method

Sol-gel catalysts: 20wt% Cu-Zn of sol-gel catalysts were prepared by dissolving Cu $(\text{NO}_3)_2 \cdot 3\text{H}_2\text{O}$ ($\geq 99\%$, Fluka), Zn $(\text{NO}_3)_2 \cdot 6\text{H}_2\text{O}$ ($\geq 99\%$, Fluka), citric acid ($\text{C}_6\text{H}_8\text{O}_7 \cdot \text{H}_2\text{O}$) ($\geq 99\%$, Ajax Finechem) in DI water. The mixture was heated to 70°C with constant stirring. 25 wt% ammonia was dropped into the solution to adjust pH at 7. Then the support was added into the solution. The mixture was further stirred at 70°C for 4 h to ensure the sol-gel was completely formed. The sol-gel catalysts were evaporated at 105°C for 4 h. Then the viscous gel was dried at 130°C for 6 h to remove ammonia and water. Dry gels were calcined at 300°C for 3 h. Figure 3.2 shows the sol-gel preparation method of Cu-Zn/ Al_2O_3 catalyst used in this work.

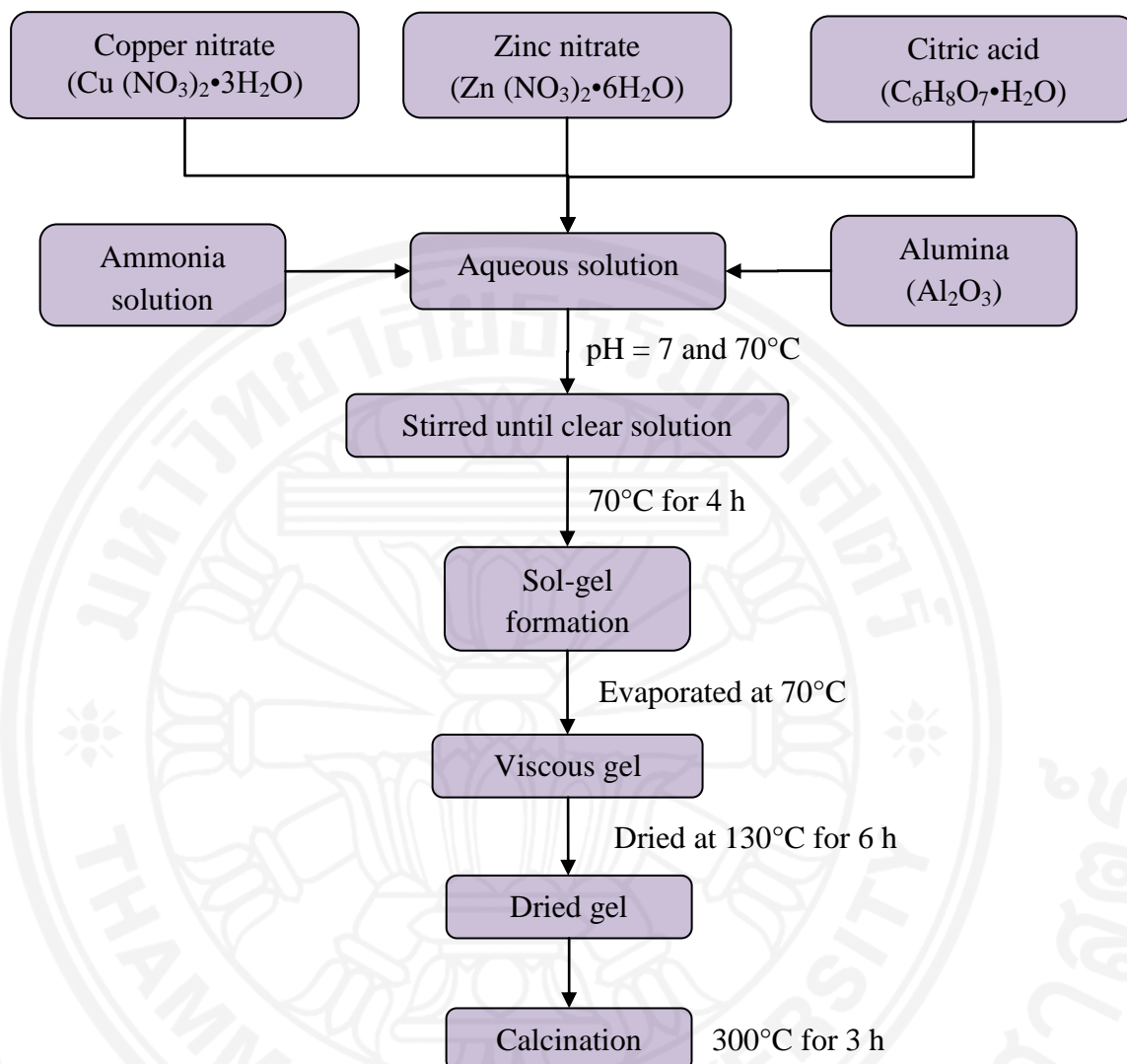


Figure 3.2 Schematic diagram of sol-gel preparation method of Cu-Zn/Al₂O₃ catalyst

Figure 3.3 shows the different colour of solution before and after sol-gel formation. The colour of metal salt solution was changed to dark blue when the ammonia solution was added into the solution to adjust pH to 7. Then the solution gradually becomes light blue when ammonia was evaporated out of the solution as shown in Figure 3.3 b.



Figure 3.3 Sol-gel preparation methods a) before sol-gel formation, b) after sol-gel formation

3.1.2 Preparation of ZrO_2 doped Al_2O_3 support

ZrO_2 doped Al_2O_3 support was prepared by the following steps. $\text{ZrO}(\text{NO}_3)_2 \cdot 6\text{H}_2\text{O}$ ($\geq 99.5\%$, Fluka Analytical) and $\text{Al}(\text{NO}_3)_3 \cdot 9\text{H}_2\text{O}$ ($\geq 98.5\%$, Sigma-Aldrich) were dissolved in DI water separately to obtain the solution concentration of 0.5 M. Metal salt solution mixture was prepared by combining 0.5 M Zr salt solution and 0.5 M Al salt solution with the ZrO_2 to Al_2O_3 weight ratio of 1 to 9. The 25wt% ammonia in aqueous solution (Merck) was added into the metal salt solution drop by drop to adjust pH to be 9 to form gel. The gel formation of ZrO_2 - Al_2O_3 was performed at room temperature for 48 h. After that, the gel was filtered and dried at 105°C in an oven (Binder) for 12 h to obtain the solid support. The solid support was then calcined at different temperatures i.e. 950, 1100 and 1200°C for 4 h to obtain ZrO_2 doped Al_2O_3 support.

All the catalysts in this study contain 20 wt% of metal loading with a molar ratio of Cu and Zn at 1:1. The supports of catalysts were α - Al_2O_3 (Riedel), γ - Al_2O_3 (Alfar Aesar) and ZrO_2 doped Al_2O_3 .

3.1.3 Methanol-steam reforming reaction in tubular reactor

The hydrogen production from methanol-steam reforming over various catalysts was investigated using a stainless steel tubular reactor. Two grams of catalyst were packed between quartz wool in the reactor. The reduction of catalysts was conducted inside the reactor with 20 ml/min of 10% H₂ balanced in N₂ at 300 °C for 1 h. The reactor was flushed with 20 mL/min N₂ at 300°C for 30 min to get rid of hydrogen in the reactor. The liquid mixture of methanol and water at 1:1 molar ratio was loaded into a syringe pump. The reactant flow rate of syringe pump was set at 1 mL/h. The inlet line was heated using a heating tape to convert liquid mixture to vapor prior to flowing into the reactor. The vapor of methanol and water was carried by 20 ml/min N₂, and introduced into the reactor in a continuous mode at various reaction temperatures. The outlet gas was collected and analyzed via a Gas Chromatography (Perkin Elmer, Autosystem XL) with Porapak Q column (Supelco) coupled with a thermal conductivity detector (TCD). Schematic of hydrogen production from methanol-steam reforming process is shown in Figure 3.4.

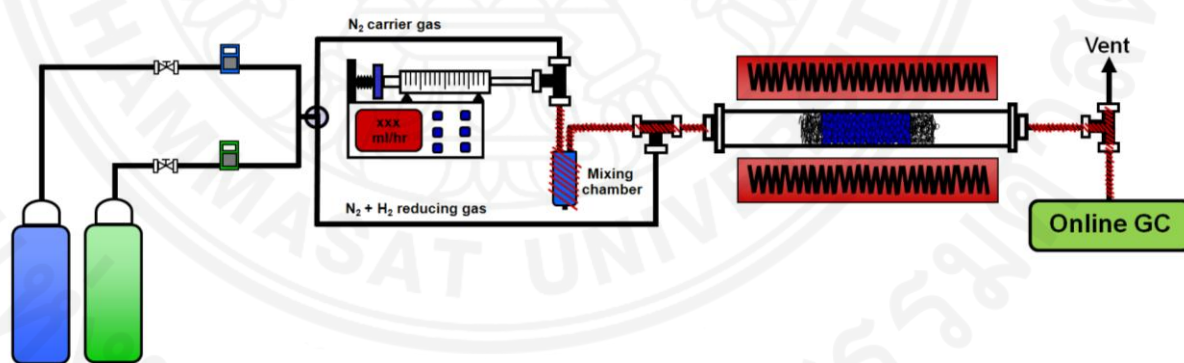


Figure 3.4 Schematic of hydrogen production from methanol-steam reforming process

3.1.4 Catalyst characterizations

The morphology and elemental composition of catalysts were inspected using a Scanning Electron Microscope (SEM, JEOL JSM-5410) coupled with an Energy Dispersive Spectrometry (EDS, Oxford, Oxford Instrument).

The surface areas of the catalyst supports were determined by using a BET surface area (Autosorb-1C, Quantachrome Instruments).

The catalysts were characterized using an X-ray diffraction (X'Pert PRO diffractometer, Panalytical, Almelo,) using Cu $K\alpha_1$ radiation, 2θ between 20° - 75° , 0.02° step size, and 0.5 sec step time.

The N_2O chemisorption by pulse injection technique (BELCAT-B, BEL Japan Inc.) was used to determine the specific areas of copper in the catalysts. The pretreatment of catalyst surface was performed in the temperature of 300°C in helium stream of 50 sccm to clean the surface of catalysts. After that the catalysts were oxidized with oxygen (50 sccm) and reduced with hydrogen (50 sccm) at temperature of 300°C to achieve the copper metal. After pretreatment process the catalysts were cooled down to 50°C then the N_2O (10% N_2O/He) was introduced into the system by pulse injection. Thermal conductivity detector (TCD) was used to analyze the outlet gases. The volume of chemisorbed gas was determined by the different volume of gases remain in the system and the volume of initial gases in each injection until it was unchanged. The specific surface area, metal dispersion and average particle size of copper were calculated by ChemMaster Data Analysis Software.

X-ray Absorption Spectroscopy (XAS) was used to investigate the oxidation state of Cu and Zn in the catalysts. The transmission-mode XAS spectra were measured at beamline BL-8 of Synchrotron Light Research Institute (Public Organization), Nakhon Ratchasima, Thailand. The first derivative of Cu K-edge normalized XANES spectra of Cu^0 (8979.1 eV), Cu^{1+} (8980.2 eV) and Cu^{2+} (8982.9 eV) were used as standard references for the oxidation state of Cu in catalysts. The first derivative of Zn K-edge normalized XANES spectra of Zn^0 (9659.2 eV) and Zn^{2+} (9661.5 eV) were used as a standard reference for the oxidation state of Zn in catalysts.

3.2 CO₂ capture using fly ash

3.2.1 Materials

Three types of fly ash were considered in this study named as FA-1, FA-2 and FA-3. FA-1 and FA-2 were collected at interval time period of 6 months in order to obtain fly ash with variation of composition. FA-3 was prepared by adding free CaO to FA-1 to obtain the total free CaO content of 5 wt%. Therefore, FA-3 represented a high free CaO fly ash. All fly ashes were dried at room temperature for 48 h and in an oven at 110°C for 8 h to get rid of all moisture. In case of base treatment, fly ashes were treated by the aqueous solution of NaOH ($\geq 99\%$, Fluka) with the various compositions of 0, 5 and 10 wt% NaOH. Then the fly ashes treated with NaOH were dried at room temperature for 48 h and in an oven 110°C for 8 h. The ordinary Portland cement type I was used for the entire work. River sand conforming to ASTM C33-92a (ASTM C33, 2003) was used as fine aggregate and its specific gravity was 2.60.

3.2.2 CO₂ capture using fly ash as solid sorbents

CO₂ capture was conducted in a tubular reactor as shown in Figure 3.5. The CO₂ stream (Praxair, >99.8%) was flowed into the reactor by using a regulator and needle valve to control the gauge pressure at 1 atm. The adsorption temperature of CO₂ was performed at room temperature for 1 h in a batch mode. After that, nitrogen gas (Praxair, >99.995%) was flowed into the reactor with a flow rate of 30 mL/min for 30 min to flush the system to remove gaseous CO₂ and any weak interaction of CO₂ on fly ash surface. After the nitrogen flush, the gas samples were collected from the reactor and injected to Gas Chromatography (GC) to ensure there is no gaseous CO₂ left in the reactor. The fly ash was further heated to 150°C to desorb and release all CO₂ capture by adsorption which will be explained in the next section.

3.2.2.1 CO₂ capture by adsorption

To determine the amount of CO₂ capture by adsorption over the fly ash surface, the desorption process was carried out at 150°C to desorb all adsorbed CO₂ on fly ash. The temperature was maintained at 150°C for 1 h in a batch mode using furnace (model TF150) with PID controller. The gas samples were collected and injected into Perkin Elmer (Waltham, Mass., USA) Autosystem XL Gas Chromatograph (GC) with Porapak Q column (Supelco, Bellefonte, PA, USA) coupled with a thermal conductivity detector (TCD) to determine the amount of CO₂ which is the total CO₂ capture by adsorption on the fly ash.

3.2.2.2 CO₂ capture by carbonation

The solid fly ash after desorption were collected and analyzed using ethylene diamine tetra acetic acid (EDTA) titration to determine an amount of CO₂ captured from carbonation reaction. The solid fly ash after desorption was stirred in 50 ml of deionized water for 12 h to dissolve any remaining free CaO into Ca²⁺ ion. EDTA titration is used to determine an amount of Ca²⁺ in the sample. The amount of free CaO reacted with CO₂ in the capture process by carbonation can be determined through a comparison of Ca²⁺ ions in aqueous solution of fresh fly ash and in the fly ash after CO₂ capture. The EDTA titration was done by using EDTA (≥99%, Ajax Finechem Pty Ltd.) 0.025M as the standard solution. Ammonium chloride (≥99.5%, Sigma Aldrich) and ammonium hydroxide (28%, Sigma Aldrich) were used as the buffer solution. Eriochrome Black T (Panreac) was used as an indicator.

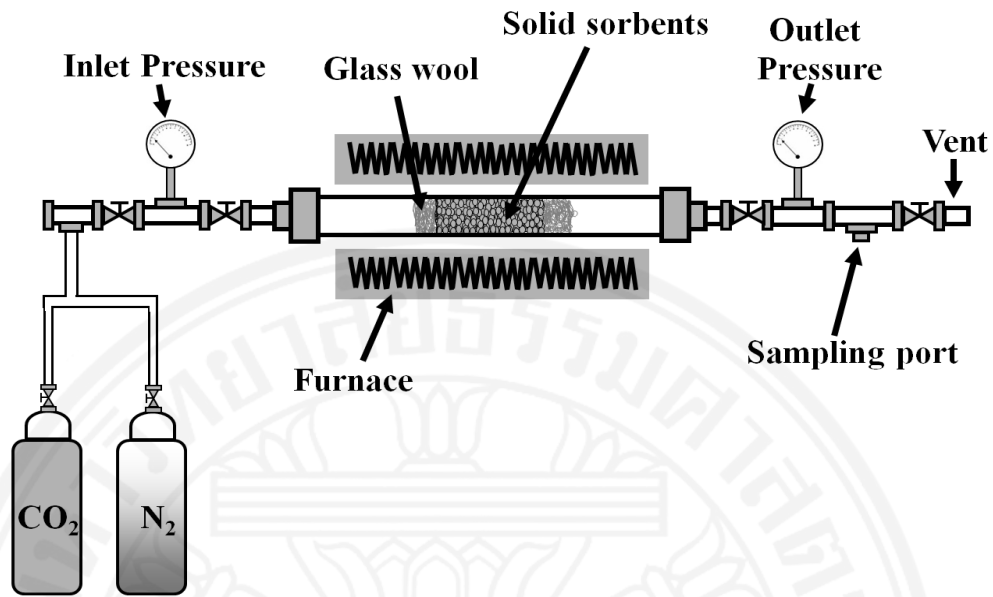


Figure 3.5 The schematic of CO₂ capture by adsorption over solid sorbents

3.2.3 Material Analysis

The chemical compositions in fly ash were analyzed using an X-ray fluorescence spectrometer, PANalytical PW-2404. The crystal structures of chemical compositions in the fly ash such as free CaO, Ca(OH)₂ and CaCO₃ were analyzed using X-ray diffraction technique (X'Pert PRO diffractometer, Panalytical, Almelo, the Netherlands) using Cu K α_1 radiation, 10°-80° 2-theta, 0.02° step size, 0.5 sec step time. XRD technique is used to evaluate the consumption of free CaO and Ca(OH)₂ as well as the formation of CaCO₃ after CO₂ capture.

3.2.4 Property testing of mortar and cement paste using fly ash as a mineral admixture

The mortar and cement paste specimens were prepared and tested for physical property to compare with the material standards and reference mixture. The mix designation and compositions of mortar and paste specimens were listed in Table 3.1. The specimen using pure ordinary Portland cement type I (C100) is the reference mixture in this study. For the specimens containing fly ash, the number in front of FA represents the weight percentage of fly ash in the total binder. FA-1, FA-2 and FA-3 are types of fly ash. Physical properties of mortar and paste containing fly ash were

determined by using the replacement ratios of fly ash of 0.2 and 0.4 in the mix proportions. For the carbonation depth, the specimens were prepared by using the replacement ratio of fly ash of 0.3 in the mix proportions.

Table 3.1 Mix designations

Mix designation	OPC Type I (wt %)	Fly ash (wt %)			Fly ash replacement ratio
		FA-1	FA-2	FA-3	
C100	100	-	-	-	0.0
20FA-1	80	20	-	-	0.2
20FA-2	80	-	20	-	0.2
20FA-3	80	-	-	20	0.2
30FA-1	70	30	-	-	0.3
30FA-2	70	-	30	-	0.3
30FA-3	70	-	-	30	0.3
40FA-1	60	40	-	-	0.4
40FA-2	60	-	40	-	0.4
40FA-3	60	-	-	40	0.4

3.2.4.1 Physical properties of mortar and paste specimens

The significant basic property tests of all specimens using fly ash as a mineral admixture were tested. Water requirement was tested according to ASTM C1437 standard (ASTM C1437.,1999). This method is used to determine the flow of mortars containing cementitious materials other than hydraulic cements. The flow of mortar specimens can obtain by using the flow table apparatus by place the mold over the flow table then fill the mold with mortar. Cut off the mortar to a plane surface flush with the top of the mold. Lift the mold away from the mortar 1 min after that immediately drop the flow table through a height of 12.7 ± 0.13 mm 25 times in 15 s. The flow is the resulting increase in average base diameter of the mortar mass, expressed as a percentage of the original base diameter. Water requirement is

calculated from the ratio of required water to obtain 110 ± 5 flow degree of test mortar mixture to that of cement-only mortar mixture.

Compressive strength was tested according to ASTM C109 standard (ASTM C109/C109M.,1999). This test method was used to determine the compressive strength of hydraulic cement mortars, using 2-in. or [50-mm] cube specimens. The proportions of materials for the standard mortar shall be one part of cement to 2.75 parts of graded standard sand by weight. Compressive strength of mortar specimens can be determined by using testing machine.

The autoclave expansion according to ASTM C151 standard was used to identify the expansion effect from free CaO content in fly ash (ASTM C151., 2000). The autoclave expansion was tested in the high pressure steam vessel with the condition at pressure of 2 ± 0.07 MPa and temperature of $216\pm 2^{\circ}\text{C}$ for 3 h. The autoclave expansion of specimens is calculated by comparing the length of the specimens before autoclaving and that after autoclaving.

The replacement ratios of fly ash to cement were 0.2 and 0.4 in the mix proportions. The mortar samples were cast with a sand/binder ratio of 2.75 by weight. The mix proportions of samples for the basic property tests are shown in Table 3.2.

Table 3.2 Mix proportion and properties of samples for basic property tests

Testing items	Paste/mortar	Dimension (cm×cm×cm)	Fly ash replacement ratio	Sand to binder ratio	ASTM standards
Water requirement	Mortar	Fresh mixture	0, 0.2, 0.4	2.75	C1437
Autoclave expansion	Paste	2.5x2.5x28.5	0, 0.2, 0.4	-	C151
Compressive strength	Mortar	5x5x5	0, 0.2, 0.4	2.75	C109

*Remarks: Autoclave expansion condition: Temperature = $216\pm 2^{\circ}\text{C}$, Pressure = $2\pm 0.07\text{ MPa}$,
Time = 3 h

3.2.4.2 Carbonation depth of mortar specimens

In order to study the carbonation depth on mortar specimens, the accelerated carbonation was done by exposing the mortar specimens under a CO_2 enriched chamber. The mortar specimens were prepared by using fly ash, both before and after CO_2 capture, with the cement replacement ratio of 0.3 by weight. The water to binder ratio of 0.55 and the sand to binder ratio of 2.75 were used for all mix proportions. All mortar specimens were cast in cube with the dimension of 5 cm x 5 cm x 5 cm. The mortar specimens were cured in water for 28 days prior to the carbonation depth testing. The mortar samples were carbonated under a condition of 4% CO_2 concentration (40,000 ppm) in an accelerated carbonation chamber for a period of 28 days. The temperature and relative humidity in the carbonation chamber were controlled at 40°C and $50\pm 5\%$ RH, respectively.

Chapter 4

Results and discussion

4.1 Hydrogen production from methanol-steam reforming

The active catalyst for methanol-steam reforming can be developed by different approaches such as modification of novel metal active sites, addition of promoter, changing the supports, and the development of catalyst preparation method (Sá et al., 2010). This study focuses on the approach of developing a new catalyst preparation method and using the new support to increase the hydrogen production activity of the catalyst. The new preparation of impregnation with urea can increase the dispersion and reduce the metal cluster to provide more active sites on the catalyst. Moreover, the new ZrO₂ doped Al₂O₃ support can enhance the activity of the Cu-Zn-based catalyst at low operational temperature.

In order to evaluate the catalyst activity, the methanol-steam reforming was conducted in a tubular reactor and analyzed for the product gas compositions using a GC. The activity of catalysts is measured in term of hydrogen yield. Hydrogen yields are calculated using equation 4.1 derived from stoichiometric coefficients of methanol and hydrogen from the balanced chemical reaction;

$$\text{Hydrogen yield (\%)} = \frac{1}{3} \frac{\text{mol of H}_2}{\text{mole of CH}_3\text{OH fed}} \times 100\% \quad (4.1)$$

4.1.1 Effect of urea in impregnation method

The first approach to enhance the catalytic activity of Cu-Zn-based catalyst for methanol-steam reforming is an evaluation of catalyst preparation method. Impregnation is a conventional method for a catalyst preparation because the process is low cost, simple, and requires low metal loading. However, the main disadvantage of this method is uneven dispersion of metal over the support. Literature reports that an addition of urea can provide homogeneity of metal salt solution, especially in bi-metallic salt solution. The homogeneity of solution can benefit the better dispersion of metal cluster for impregnating the salt solution on the support (Shishido et al., 2007).

The development of impregnation method using urea has been investigated to improve the metal dispersion over the catalyst support. The good dispersion of metal can reduce a required metal loading on the catalyst. Table 4.1 lists the hydrogen yields of the methanol-steam reforming using an impregnated Cu-Zn over α -Al₂O₃ and γ -Al₂O₃ with and without urea at reaction temperature range of 200-300°C and 1 atm. The maximum reaction temperature was kept at 300°C to prevent the sintering of metal cluster.

Table 4.1 Hydrogen yield of Cu-Zn catalysts over alumina supports (α -Al₂O₃ or γ -Al₂O₃) prepared by impregnation with and without urea

T(°C)	Hydrogen yield (%)			
	Cu-Zn/ α -Al ₂ O ₃	Cu-Zn/ α -Al ₂ O ₃	Cu-Zn/ γ -Al ₂ O ₃	Cu-Zn/ γ -Al ₂ O ₃
	Without urea	With urea	Without urea	With urea
200	15.0±0.01	31.4±0.28	28.2±0.51	35.9±0.35
250	37.7±0.40	68.3±1.54	75.2±0.55	93.7±2.62
300	58.7±1.39	91.6±1.47	84.1±0.85	99.8±0.54

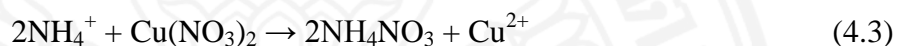
According to the results in Table 4.1, the hydrogen yield of all catalysts considered in this study increases with the reaction temperature. An addition of urea during impregnation can increase the hydrogen yield of Cu-Zn/ α -Al₂O₃ and Cu-Zn/ γ -Al₂O₃ at all reaction temperatures. With an addition of urea, the hydrogen yield of Cu-Zn catalyst over α -Al₂O₃ can increase from 58.7% to 91.6% at 300°C. For high surface area γ -Al₂O₃ support, the Cu-Zn catalysts with an addition of urea can increase the hydrogen yield up to 99.8% at 300°C. The results also show that the types of alumina support affect the yield of hydrogen. The impregnation of Cu-Zn without urea over γ -Al₂O₃ produces higher hydrogen product than Cu-Zn without urea over α -Al₂O₃ support. An addition of urea can increase the metal dispersion and the effect can be clearly pointed out in high surface area γ -Al₂O₃ support. At 250°C, Cu-Zn/ γ -Al₂O₃ with urea achieves a hydrogen yield of 93.7% while the Cu-Zn/ α -Al₂O₃ without urea exhibits a yield of 68.3% only.

A well dispersed metal is caused by homogeneity of metal salt solution from urea addition (Shishido et al., 2007). Moreover, the metal clusters are also suppressed from the self-explosion of ammonium nitrate. The dissociation of urea produces ammonium ions in a salt solution followed by a reaction between ammonium ion and metal nitrate to form ammonium nitrate as indicated in reactions 4.2 and 4.3.

Dissociation of urea



Formation of ammonium nitrate



A presence of ammonium nitrate in the catalysts induces a vigorous combustion during the calcination process, which results in a better metal cluster dispersion over the support and smaller metal cluster size. The effect of urea can be confirmed using SEM images as depicted in Figure 4.1 and Figure 4.2. Therefore, a catalyst preparation by an impregnation method with urea can provide smaller Cu-Zn clusters and uniform dispersion over support than the normal impregnated catalyst without urea.

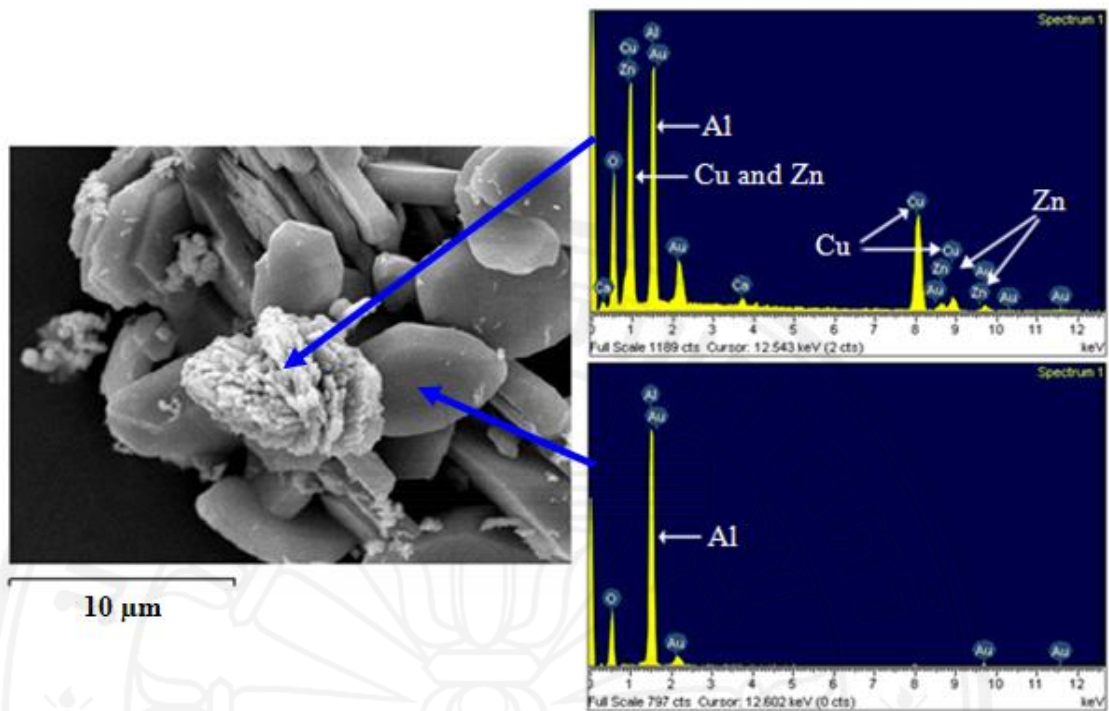


Figure 4.1 SEM image and EDS profiles of Cu-Zn/ α - Al_2O_3 prepared by impregnation without urea

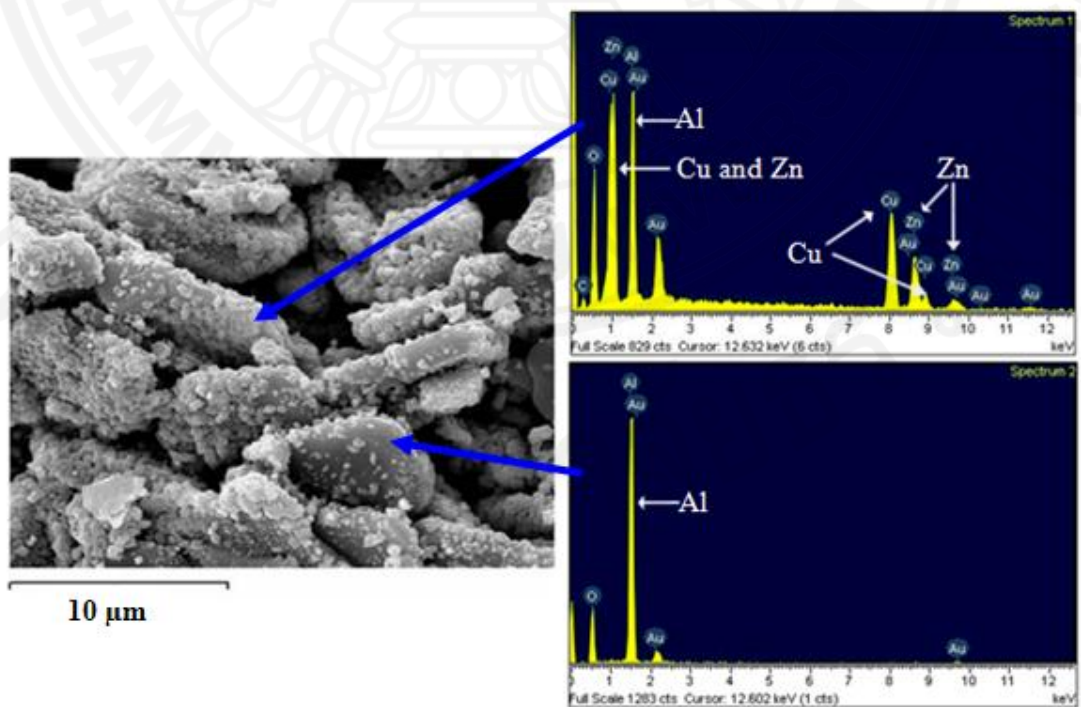


Figure 4.2 SEM image and EDS profiles of Cu-Zn/ α - Al_2O_3 prepared by impregnation with urea

Figure 4.1 shows the SEM-EDS results of Cu-Zn over α -Al₂O₃ support prepared by an impregnation method without urea. The shape of α -Al₂O₃ is like flat plates and non-porous. Therefore, the distribution of Cu-Zn clusters is easily observed over the α -Al₂O₃. The image of Cu-Zn over α -Al₂O₃ without urea shows large metal clusters deposited over α -Al₂O₃ plates. Cu-Zn clusters in Cu-Zn over α -Al₂O₃ without urea were estimated about 1-6 μ m in size. Figure 4.1 also shows larger available areas of α -Al₂O₃, which were not occupied by metals. The EDS result confirmed that the metal clusters were Cu and Zn while the flat plates were alumina.

For the impregnation of Cu-Zn with urea, Cu-Zn clusters disperse well over the α -Al₂O₃ support as shown in Figure 4.2. Cu-Zn clusters in Cu-Zn over α -Al₂O₃ with urea were estimated about 0.2-1 μ m in size, which are apparently smaller than those of Cu-Zn over α -Al₂O₃ without urea catalyst. The small Cu-Zn clusters are also uniformly dispersed to cover all the surface of alumina supports. A well dispersed tiny metal clusters are desirable for catalysts that lead to have more available active sites in them. Therefore, a higher hydrogen yield could be expected from Cu-Zn over α -Al₂O₃ with urea catalyst than that of Cu-Zn over α -Al₂O₃ without urea catalyst due to a better dispersion of Cu-Zn catalyst.

4.1.2 Effect of preparation methods (impregnation with urea vs. sol-gel)

An addition of urea in the catalyst preparation by impregnation method provides a better dispersion of Cu-Zn over the catalyst support from the previous section. Sol-gel method is generally used to produce a catalyst with high metal dispersion and surface area. Therefore, a hydrogen production activity of the catalyst prepared by the method of impregnation with urea should be compared with the activity of the catalyst prepared by sol-gel. Figure 4.3 shows an SEM image and EDS profiles of Cu-Zn/ α -Al₂O₃ prepared by sol-gel method. The method also provides small Cu-Zn clusters and better dispersion over α -Al₂O₃ support.

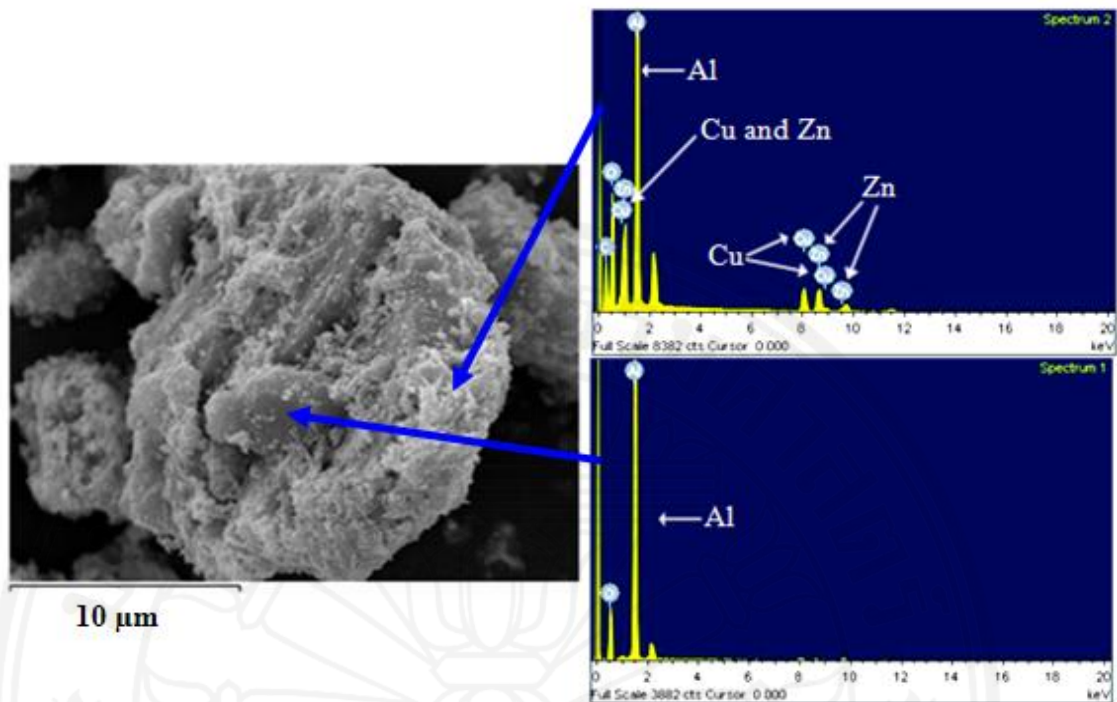


Figure 4.3 SEM image and EDS profiles of Cu-Zn/ α -Al₂O₃ prepared by sol-gel method.

Table 4.2 Hydrogen yield of Cu-Zn catalysts over alumina supports (α -Al₂O₃ and γ -Al₂O₃) prepared by impregnation with urea and sol-gel methods

T (°C)	Hydrogen yield (%)			
	Impregnation	Sol-gel	Impregnation	Sol-gel
	Cu-Zn/ α -Al ₂ O ₃	Cu-Zn/ α -Al ₂ O ₃	Cu-Zn/ γ -Al ₂ O ₃	Cu-Zn/ γ -Al ₂ O ₃
200	31.4±0.28	37.1±0.48	35.9±0.35	36.7±0.40
250	68.3±1.54	71.4±1.52	93.7±2.62	72.2±1.01
300	91.6±1.47	95.1±1.73	99.8±0.54	95.6±1.53

Table 4.2 lists the hydrogen yield of Cu-Zn catalysts prepared by impregnation with urea and sol-gel method. For the α -Al₂O₃ support, the Cu-Zn catalyst prepared by sol-gel method can produce slightly higher hydrogen than those from an impregnation with urea at a temperature range of 200-300°C. The differences in hydrogen yield are about 3.1-5.7%. In contrast, the hydrogen production of the Cu-Zn catalyst over γ -Al₂O₃ support prepared by impregnation with urea exhibited higher hydrogen yield than the catalyst prepared by sol-gel method at 250-300°C. The hydrogen yield of impregnated catalyst with urea is higher than the yield of sol-gel catalyst about 4.2-21.5%. At 250°C, the hydrogen yield of Cu-Zn/ γ -Al₂O₃ prepared by impregnation can achieve the yield of 93.7% while the Cu-Zn/ γ -Al₂O₃ prepared by sol-gel exhibits the yield of 72.2% only. The effect of impregnation method with urea can be observed clearly in high surface area of γ -Al₂O₃ support which agrees well with results in the previous section. To maximize the hydrogen yield, a preparation of Cu-Zn catalyst over γ -Al₂O₃ support by impregnation with urea is recommended due to advantages in metal dispersion, low requirement of metal loading, and low cost.

4.1.3 Effect of ZrO₂ doped Al₂O₃ supports

4.1.3.1 Properties of ZrO₂ doped Al₂O₃ supports

The new support, ZrO₂ doped Al₂O₃, was prepared and calcined at different temperatures to study the relationship between calcination temperatures and the physical properties of supports. The BET surface area and XRD techniques were used to investigate the phases and total surface areas of the new supports compared to those

of α -Al₂O₃ (Riedel) and γ -Al₂O₃ (Alfar Aesar). Table 4.3 exhibits the physical properties of α -Al₂O₃, γ -Al₂O₃ and ZrO₂ doped Al₂O₃ supports. The α -Al₂O₃ possesses a low surface area of 3.25 m²/g while γ -Al₂O₃ possesses a rather high surface area of 175.6 m²/g.

For our ZrO₂ doped Al₂O₃ supports the result shows that an increase of calcination temperature decreases the surface area of ZrO₂ doped Al₂O₃ supports. The ZrO₂ doped Al₂O₃ support calcined at 950°C has a high surface area of 116.3 m²/g which is in the same range as the surface area of γ -Al₂O₃ (175.6 m²/g). ZrO₂ doped Al₂O₃ support being heat treated at 1100°C and 1200°C have low surface areas of 44.2 m²/g and 15.4 m²/g, respectively. The low surface area of these supports is closer to that of α -Al₂O₃ (3.25 m²/g).

Table 4.3 Physical properties of supports

Supports	Surface area ^a (m ² /g)	Pore volume (cm ³ /g)	Average pore diameter (Å)
α -Al ₂ O ₃ (Riedel)	3.25	0.0035	43.3
γ -Al ₂ O ₃ (Alfar Aesar)	175.6	0.29	66.7
ZrO ₂ doped Al ₂ O ₃ (calcined 950°C)	116.3	0.32	111.2
ZrO ₂ doped Al ₂ O ₃ (calcined 1100°C)	44.2	0.22	195.9
ZrO ₂ doped Al ₂ O ₃ (calcined 1200°C)	15.4	0.07	183.1

^aDetermined by multipoint BET method

Phase identifications of supports were analyzed using an XRD technique. Figure 4.4 shows the XRD patterns of α -Al₂O₃ (JCPDS NO.: 46-1212), γ -Al₂O₃ (JCPDS No.: 04-0880) and ZrO₂ doped Al₂O₃ supports calcined at different temperatures. Two alumina supports showed different XRD patterns. The α -Al₂O₃ support shows the main peak at 25.6°, 35.1°, 43.5°, 57.5° and 66.5°. These sharp peaks are the most stable form of alumina and they are formed as a perfect crystalline. Whereas, the γ -Al₂O₃ shows the characteristic peaks at 37.5°, 45.7° and 67.3°.

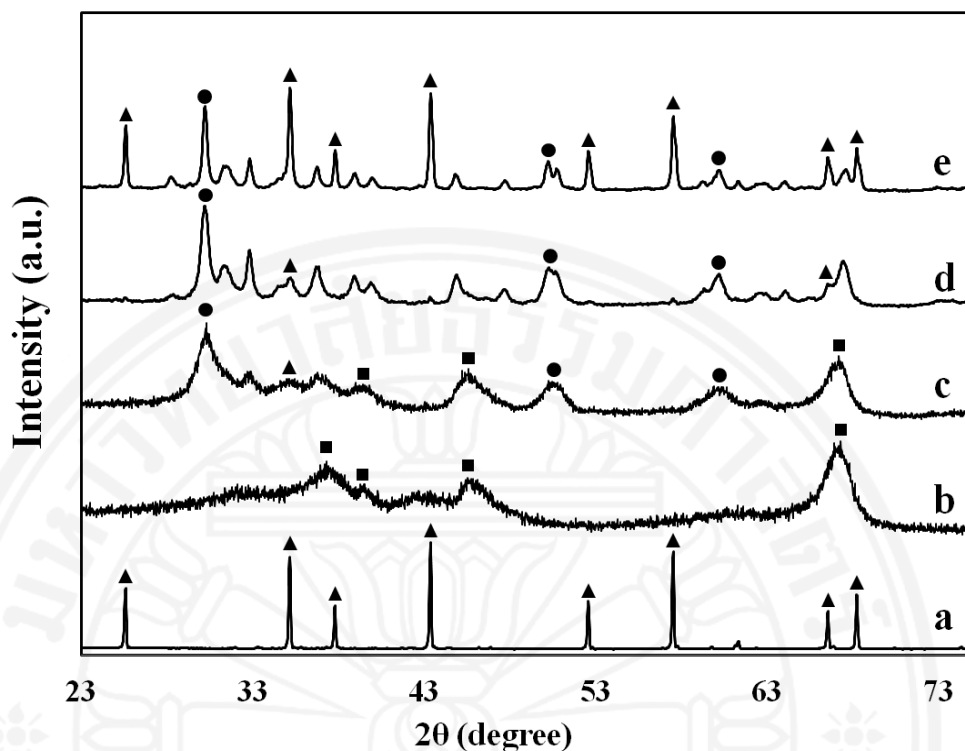


Figure 4.4 X-ray diffraction patterns of supports: (a) α - Al_2O_3 (Riedel), (b) γ - Al_2O_3 (Alfar Aesar), (c) ZrO_2 doped Al_2O_3 calcined 950°C , (d) ZrO_2 doped Al_2O_3 calcined 1100°C , (e) ZrO_2 doped Al_2O_3 calcined 1200°C (\blacktriangle : α - Al_2O_3 , \blacksquare : γ - Al_2O_3 , \bullet : ZrO_2)

ZrO_2 doped Al_2O_3 calcined at 950°C displays the main peaks of ZrO_2 (JCPDS No.: 50-1089) at 30.3° , 50.3° and 59.8° and the main peaks of Al_2O_3 at 37.5° , 45.7° and 67.3° . The XRD pattern of Al_2O_3 peak in ZrO_2 doped Al_2O_3 support (Fig. 2c) is similar to the pattern of γ - Al_2O_3 (Fig. 2b). These results can confirm that ZrO_2 doped Al_2O_3 calcined at 950°C can produce a mixed oxide support in a form of ZrO_2 and γ - Al_2O_3 .

ZrO_2 doped Al_2O_3 calcined at 1200°C shows the peaks of ZrO_2 (JCPDS No.: 50-1089) at 30.3° , 50.3° and 59.8° and the peaks of Al_2O_3 at 25.6° , 35.1° , 43.5° , 57.5° and 66.5° . The XRD pattern of Al_2O_3 peak in the support (Fig. 2e) is similar to the pattern of α - Al_2O_3 (Fig. 2a). The pattern also indicates the perfect crystalline like α - Al_2O_3 . These results indicate that ZrO_2 doped Al_2O_3 calcined at 1200°C produces a mixed oxide support in a form of ZrO_2 and α - Al_2O_3 . The ZrO_2 doped Al_2O_3 calcined at 1100°C shows a similar XRD pattern. However, the characteristic peak of α - Al_2O_3 and crystalline pattern are not as clear as the same support calcined at 1200°C .

The different calcination temperatures results in a phase transformation of alumina and a decrease of surface area of the ZrO₂ doped Al₂O₃ support. The results agree with the BET surface areas of ZrO₂ doped Al₂O₃ at different calcination temperatures. Therefore, the ZrO₂ doped Al₂O₃ support calcined at 950°C was selected as the catalyst support to compare with γ -Al₂O₃.

4.1.4 Combination of impregnation with urea method and ZrO₂ doped Al₂O₃ as support

Table 4.4 shows the hydrogen yields from methanol-steam reforming over Cu-Zn based catalysts over different supports (α -Al₂O₃, γ -Al₂O₃ and ZrO₂ doped Al₂O₃). In order to determine the effective use of ZrO₂ in the Cu-Zn based catalysts for methanol-steam reforming, a direct addition of ZrO₂ in Cu-Zn over γ -Al₂O₃ was utilized as a promoter and compared to the hydrogen production with others.

Table 4.4 Hydrogen yield of impregnated Cu-Zn catalysts with urea over α -Al₂O₃, γ -Al₂O₃ and ZrO₂ doped Al₂O₃ supports and Cu-Zn/ γ -Al₂O₃ with ZrO₂ as promoter

T (°C)	Hydrogen yield (%)			
	Cu-Zn/ α -Al ₂ O ₃	Cu-Zn/ γ -Al ₂ O ₃	Cu-Zn/ γ -Al ₂ O ₃ ZrO ₂ as promoter	Cu-Zn/ZrO ₂ doped Al ₂ O ₃
200	31.4±0.28	35.9±0.35	40.5±0.58	90.3±1.15
250	68.3±1.54	93.7±2.62	95.0±2.31	95.6±1.27
300	91.6±1.47	99.8±0.54	86.2±1.44	89.6±2.87

From Table 4.4, Cu-Zn/ZrO₂ doped Al₂O₃ catalyst exhibited the highest hydrogen yield among these catalysts at low temperatures (200-250°C). At 200°C, the hydrogen yield of Cu-Zn/ZrO₂ doped Al₂O₃ can achieve 90.3 %, which is higher than that of Cu-Zn/ α -Al₂O₃ and Cu-Zn/ γ -Al₂O₃ for 31.4% and 35.9%, respectively. The hydrogen yield of Cu-Zn/ZrO₂ doped Al₂O₃ reached the highest yield of 95.6 at 250°C. The result also shows that an addition of ZrO₂ as a promoter into Cu-Zn/ γ -Al₂O₃ can slightly increase the hydrogen yield about 1.3-4.6% at a temperature range

of 200-250°C. For Cu-Zn catalyst, an introduction of ZrO₂ as a mixed oxide support with Al₂O₃ yields higher activity in methanol steam reforming than being used as promoter. At 300°C, the catalysts with ZrO₂ showed a decrease in hydrogen yield while the hydrogen yield of non ZrO₂ catalysts increased. Therefore, the reaction temperature of Cu-Zn/ZrO₂ doped Al₂O₃ catalysts is recommended at the range of 200-250°C. A hydrogen production from methanol-steam reforming at low temperature as 200°C can provide the benefits to the process operation in terms of low energy consumption and prevention of the catalyst sintering.

The effect of zirconia on the Cu-Zn catalyst with the urea addition was also investigated to enhance the activity of the catalyst. Figure 4.5 illustrates the XRD patterns of the Cu-Zn based catalysts before calcination.

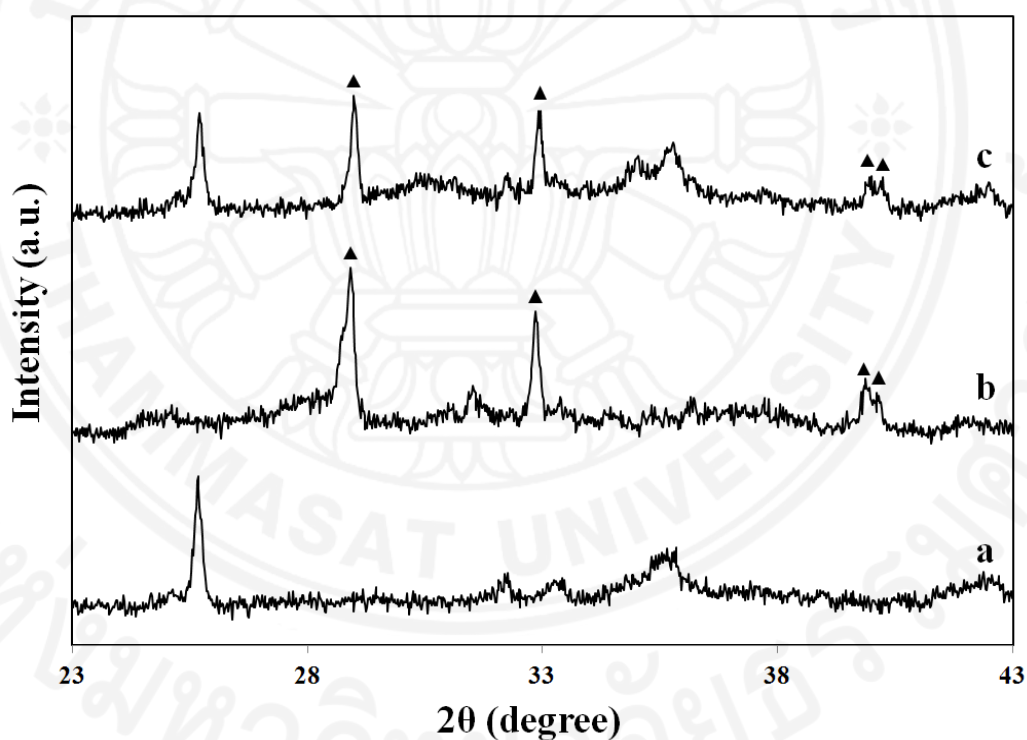


Figure 4.5 X-ray diffraction patterns of catalysts before calcination (a) Cu-Zn/ γ -Al₂O₃, (b) Cu-Zn/ γ -Al₂O₃ with urea, (c) Cu-Zn/ZrO₂ doped Al₂O₃ with urea, (▲:NH₄NO₃)

Cu-Zn/ γ -Al₂O₃ and Cu-Zn/ZrO₂ doped Al₂O₃, which are prepared by impregnation method with urea, show the main peak of ammonium nitrate at 28.9° and 32.9° (JCPDS NO.: 08-0452). In contrast, there is no peak representing ammonium nitrate in the Cu-Zn/ γ -Al₂O₃ catalyst prepared by impregnation method

without urea. A presence of ammonium nitrate provides a better dispersion during the calcination of catalysts (Shen and Song, 2002). Therefore, an addition of urea in the impregnation method of Cu-Zn/ZrO₂ doped Al₂O₃ could provide a high metal dispersion and high specific copper surface area.

Table 4.5 Properties of Cu-Zn over various catalysts determined by N₂O chemisorption

Catalysts	Metal dispersion (%)	S _{Cu} surface area (m ² /g catalyst)	Average particle size (nm)
Cu-Zn/γ-Al ₂ O ₃	0.8733	0.56276	119.5266
Cu-Zn/γ-Al ₂ O ₃ with Urea	2.6652	1.71746	39.1653
Cu-Zn/ZrO ₂ doped Al ₂ O ₃ with urea	5.0629	3.26255	20.6172

Table 4.5 lists the properties of copper active sites over various catalysts. An addition of urea in the impregnation method of the Cu-Zn catalyst has increased the metal dispersion and the specific copper surface area. Moreover, an addition of ZrO₂ in Al₂O₃ as a co-support can further improve the copper dispersion. The specific copper surface area of Cu-Zn/ZrO₂ doped Al₂O₃ is higher than Cu-Zn/γ-Al₂O₃, approximately 2 times. The high copper dispersion and high copper surface area can provide more active sites for the methanol-steam reforming reaction and achieve a higher hydrogen production.

4.1.5 Stability of Cu-Zn/ZrO₂ doped Al₂O₃ with urea

The stability of catalyst is one of the desirable properties for the long term use of catalyst. The Cu-Zn based catalyst and especially copper metal are vulnerable to sintering at above 300°C which causes a long term catalytic deactivation. In order to evaluate the stability of these catalysts, the accelerated sintering of Cu was performed by methanol steam reforming at 500°C for 5 h. The catalysts after sintering of Cu were characterized and compared with fresh catalyst in Table 4.6.

Table 4.6 Properties of catalysts before and after the accelerated sintering of Cu

Catalysts	Cu dispersion (%)	S _{Cu} surface area (m ² /g catalyst)	Average particle size (nm)
Cu-Zn/γ-Al ₂ O ₃	2.6652	1.7174	39.1653
Cu-Zn/γ-Al ₂ O ₃ (after sintering of Cu)	1.6500	1.0632	63.2608
Cu-Zn/ZrO ₂ doped Al ₂ O ₃	5.0629	3.2625	20.6172
Cu-Zn/ZrO ₂ doped Al ₂ O ₃ (after sintering of Cu)	1.4352	0.9248	72.7295

Table 4.6 shows the properties of catalysts before and after the accelerated sintering of Cu. The specific copper surface area of both Cu-Zn/γ-Al₂O₃ and Cu-Zn/ZrO₂ doped Al₂O₃ are decreased after sintering process at 500°C for 5 h. The copper surface area reduced from 1.7174 m²/g to 1.0632 m²/g for Cu-Zn/γ-Al₂O₃ and reduced from 3.2625 m²/g to 0.9248 m²/g for Cu-Zn/ZrO₂ doped Al₂O₃. The results show that an addition of zirconia as a support in alumina does not help preventing the sintering of Cu.

Table 4.7 Hydrogen yield for Cu-Zn/ γ -Al₂O₃ and Cu-Zn/ZrO₂ doped Al₂O₃ at the reaction condition of 300°C and 1 atm before and after the accelerated sintering process

Catalysts	Hydrogen yield (%)	
	Before sintering of Cu	After sintering of Cu (500°C for 5 h)
Cu-Zn/ γ -Al ₂ O ₃	99.8±0.54	21.04±0.24
Cu-Zn/ZrO ₂ doped Al ₂ O ₃	89.6±2.87	80.94±0.89

Table 4.7 exhibits the hydrogen yields at the reaction temperature of 300°C for Cu-Zn/ γ -Al₂O₃ and Cu-Zn/ZrO₂ doped Al₂O₃ before and after the accelerated sintering of Cu. After the accelerated sintering process, the hydrogen yield of Cu-Zn/ γ -Al₂O₃ reduced from 99.8% to 21.04% due to a decrease of the specific copper surface area. While the hydrogen yield of Cu-Zn/ZrO₂ doped Al₂O₃ slightly decreased from 89.6% to 80.94%. The specific copper surface area of Cu-Zn/ZrO₂ doped Al₂O₃ is lower than that of Cu-Zn/ γ -Al₂O₃ but the hydrogen yield was still higher. Therefore, the specific surface area of active Cu sites may not be the only reason for the high activity of this catalyst. Literatures report that the pure zirconia support of catalyst can boost the activity of methanol-steam reforming reaction (Szizybalski et al., 2005). The Cu-Zr interaction can promote the partial oxidation of Cu to be Cu⁺ instead of full oxidation to form Cu²⁺. The partially oxidized Cu⁺ is the active species for methanol-steam reforming reaction (Jones et al., 2010). The ZrO₂ support can also assist in stabilizing the active copper catalyst which stimulates the high activity of catalyst (Szizybalski et al., 2005). For ZrO₂ doped Al₂O₃, The effect of ZrO₂ dopant to the XANES spectra of Cu and Zn in the catalyst for methanol-steam reforming reaction will be discussed in the next section.

4.1.6 K-edge XANES spectra of Cu and Zn

K-edge XANES technique with the first derivative of XANES spectrum can be used to identify the form of metal active site on supports. The edge position in XANES spectrum corresponds to the maximum peak of the first derivative which can determine the oxidation state of metal (Khemthong et al., 2013). Cu metal, Cu_2O , CuO, Zn metal, and ZnO were used as references for Cu^0 , Cu^{1+} , Cu^{2+} , Zn^0 , and Zn^{2+} , respectively.

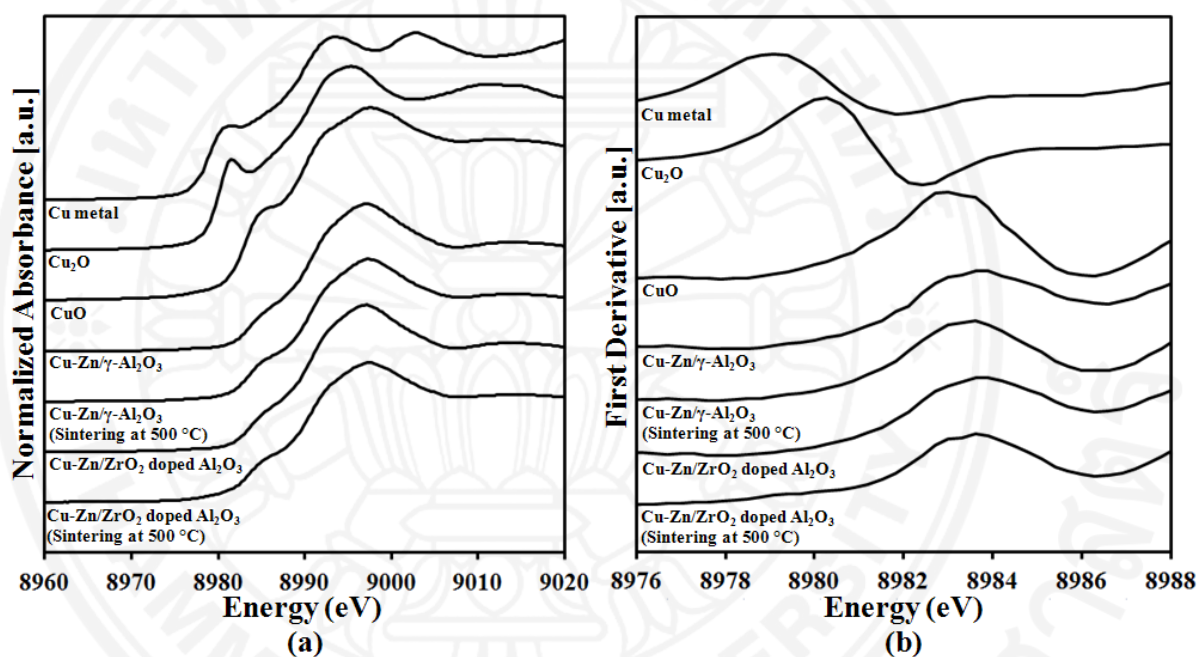


Figure 4.6 Cu K-edge XANES spectra (a), and first derivative of Cu K-edge XANES spectra (b) of Cu-Zn based catalysts and references spectra of Cu metal, Cu_2O and CuO

From Figure 4.6a, Cu-Zn/ γ - Al_2O_3 and Cu-Zn/ ZrO_2 doped Al_2O_3 show similar patterns of Cu K-edge XANES spectra to the spectrum of CuO which indicate that Cu on the catalysts is in form of Cu^{2+} . The first derivatives of XANES spectra of Cu-Zn catalysts over different supports also show the same pattern to that of CuO as shown in Figure 4.6b. Therefore, the supports do not alternate the form of Cu on the catalysts in this study. In addition, Cu-Zn/ γ - Al_2O_3 and Cu-Zn/ ZrO_2 doped Al_2O_3 show no change in edge position and maximum peak before and after sintering of Cu at 500°C.

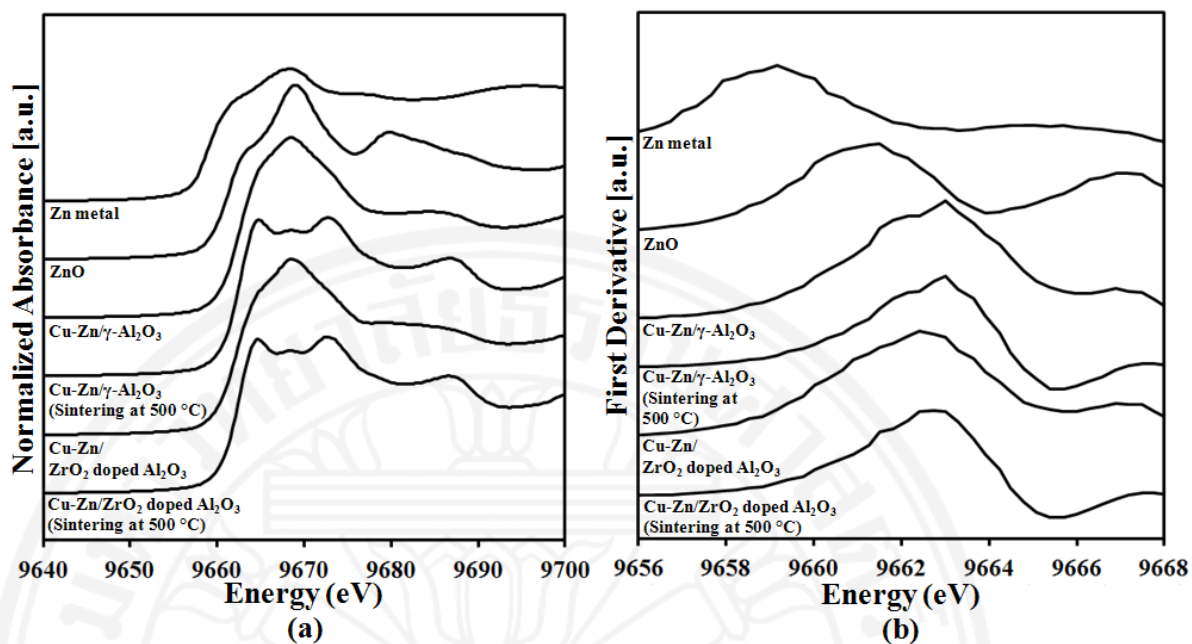


Figure 4.7 Zn K-edge XANES spectra (a), and first derivative of Cu K-edge XANES spectra (b) of Cu-Zn based catalysts and references spectra of Zn metal and ZnO

From Figure 4.7a, Cu-Zn/ γ -Al₂O₃ and Cu-Zn/ZrO₂ doped Al₂O₃ show the similar patterns of Zn K-edge XANES spectra which indicate that Zn on the catalysts are similar to Zn²⁺. The first derivatives of Zn K-edge XANES spectra of the catalysts show slightly different edge positions of Zn in Cu-Zn/ZrO₂ doped Al₂O₃ and Cu-Zn/ γ -Al₂O₃ as shown in Figure 4.7b. The Zn edge position in Cu-Zn/ZrO₂ doped Al₂O₃ is at a slightly lower energy compared to the Zn edge position in Cu-Zn/ γ -Al₂O₃. From the electrostatic model, X-ray energy required to excite electron relates to the binding energy between electron and nucleus (Joseph et al., 2012). This result indicates that the support could change the electronic property of Zn and induce a different electronic interaction between Zn and Cu, which could benefit the catalytic activity of methanol-steam reforming at low temperature.

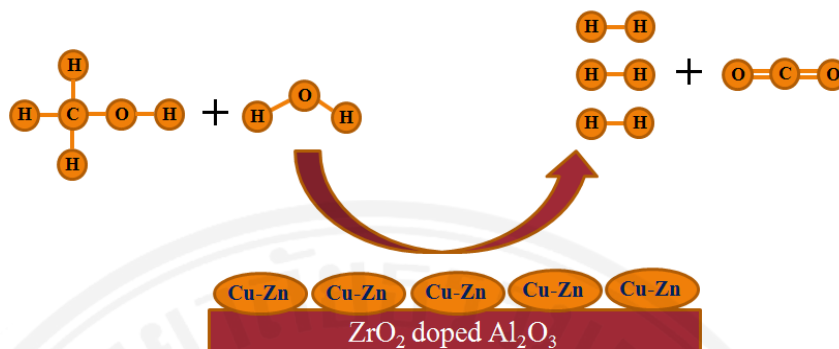


Figure 4.8 Schematic of hydrogen productions from methanol-steam reforming over Cu-Zn/ZrO₂-doped Al₂O₃ catalyst

Hydrogen production from methanol-steam reforming reaction over Cu-Zn/ZrO₂-doped Al₂O₃ can provide the high hydrogen yield (90.3%) at low temperature of 200°C. This condition can prevent the Cu from thermal sintering and loss their active site. Consequently, the life time of catalyst increases which can benefit to reduce downtime and more profitable process. The addition of urea in impregnation method and ZrO₂-doped Al₂O₃ can improve the Cu-Zn dispersion over support which results in a higher specific Cu surface area. Besides the Cu surface area, the oxidation state of Cu is a crucial factor to the methanol-steam reforming reaction. Although Cu⁰ is a main active site for this reaction, the presence of Cu¹⁺ in the catalyst can greatly boost up the reaction (Jones et al., 2010). ZrO₂-doped Al₂O₃ support can alter the electronic property of Zn which is co-active metal with Cu. Lower edge position in Zn XANES spectra can relate to a low energy consumption to excite electron in Zn atom. Therefore, the easily loss electron of Zn in Cu-Zn/ZrO₂-doped Al₂O₃ can induce CuO to be Cu⁺ which is the most active species for methanol-steam reforming reaction. As a result, Cu-Zn/ZrO₂-doped Al₂O₃ can exhibit the higher hydrogen yield at low temperature. The result also shows that ZrO₂-doped Al₂O₃ support involves in methanol-steam reforming reaction and promotes hydrogen production even the specific copper surface area is decreased from sintering.

4.2 CO₂ capture using fly ash

Fly ash is a by-product from combustion of coal in coal-fired power plants. Fly ash can be used as a solid sorbent for CO₂ capture due to its low cost. In addition, free CaO content in fly ash can capture CO₂ via a carbonation reaction. Therefore, the compositions and the properties of fly ashes were investigated to study these effects on CO₂ capture capacity. After CO₂ capture process, fly ash can be further used as a mineral admixture in cement formulation.

4.2.1 Compositions in fly ashes and their physical properties

The compositions of fly ashes mainly vary according to the compositions of coal. Table 4.8 illustrates the compositions of two types of fly ash (FA-1 and FA-2) from Mae Moh coal-fired power plants in Thailand, which were collected at different times of the year. FA-3 was prepared from the FA-1 with an addition of free CaO to obtain a total free CaO content of 5 wt%. The FA-3 was treated as a representative of fly ash with high free CaO.

Table 4.8 Compositions of OPC type I and fly ashes (FA-1, FA-2 and FA-3)

Sample	Chemical Compositions (%)									
	SiO ₂	Al ₂ O ₃	Fe ₂ O ₃	CaO	MgO	Na ₂ O	K ₂ O	SO ₃	LOI (1025°C)	Free CaO
OPC type I	18.93	5.51	3.31	65.53	1.24	0.15	0.31	2.88	trace	0.75
FA-1	35.71	20.44	15.54	16.52	2.00	1.15	2.41	4.26	0.49	1.71
FA-2	26.61	13.60	18.34	24.97	2.33	1.75	1.77	8.53	0.53	3.93
FA-3	34.51	19.75	15.01	19.32	1.93	1.11	2.33	4.12	0.47	5.00

Table 4.8 lists the composition obtained from XRF of OPC type I and fly ashes used in this study. The XRF data shows that different batches of coal after burning results in different compositions of fly ashes (compared FA-1 with FA-2). For the FA-

3, an addition of free CaO into FA-1 to obtain 5 wt% of free CaO content leads to the small changes of other compositions according to Table 4.8. Majority of compositions in fly ashes consist of SiO₂, Al₂O₃, CaO and Fe₂O₃ which are high thermal stability compounds (Boycheva et al., 2013). This property can prevent the deformation, degradation or decomposition of the composition in sorbents at high operation temperature which are the necessary properties for CO₂ capture material in the industrial process (Wee, 2013).

The main compositions of fly ash, SiO₂, Al₂O₃, and CaO, indicate that fly ashes can serve as a mineral admixture for concrete. SiO₂ and CaO, in fly ash can influence the hydration and pozzolanic reactions to develop the strength of concretes (Tangtermsirikul et al., 2004). However, the high amount of SO₃ and free CaO can cause the volume instability in forms of expansion (Kaewmanee et al., 2013; Yamei et al., 1997). According to the Thai Industrial Standard, TIS 2135 (TIS 2135, 2002), FA-1, FA-2 and FA-3 are classified as class 2b due to their high CaO content. The standard sets the fly ash with CaO content higher than 10wt% as class 2b fly ash. However, FA-2 has SO₃ content higher than 5wt% limitation as specified by TIS 2135 which does not satisfy the requirement to be used as an admixture (TIS 2135, 2002). It is noted that a large amount of SO₃ and free CaO in fly ash are undesirable for fly ash as a mineral admixture for concrete.

Table 4.9 Physical properties of ordinary Portland cement type I (OPC type I) and fly ashes (FA-1, FA-2 and FA-3)

Samples	Physical properties	
	Specific gravity	Blaine fineness (cm ² /g)
OPC type I	3.15	3100
FA-1	2.21	2867
FA-2	2.57	2820
FA-3	2.26	2884

The physical properties (specific gravity and fineness) of ordinary Portland cement type I (OPC type I) and different types of fly ash (FA-1, FA-2 and FA-3) are shown in Table 4.9. The specific gravity and the Blaine fineness were tested according to ASTM C188 and ASTM C204, respectively (ASTM C188, 2003; ASTM C204, 2007).

Blaine fineness is the specific surface area of fly ash in the unit of cm^2/g . Blaine fineness of fly ash as a mineral admixture can enhance the performance in concrete. The high fineness of fly ash can result in better dissolution and more reactive in cement mixture which results in a higher strength of the cement mixture (Chindaprasirt et al., 2004; Chindaprasirt et al., 2007). The Blaine fineness of all fly ashes in this study is classified as class 2b according to TIS 2135 standard. The standard sets the Blaine fineness of material to be more than $2,000 \text{ cm}^2/\text{g}$ for class 2b materials (TIS 2135, 2002). Both composition and Blaine fineness indicate that fly ashes in this study except FA-2 are class 2b which can be used as a mineral admixture in concrete.

4.2.2 CO₂ capture using fly ash as a solid sorbent

Fly ash can capture CO₂ by two major mechanisms, surface adsorption on solid sorbent and carbonation reaction. For adsorption, the CO₂ capture can occur from physical adsorption between CO₂ and the surface of solid sorbent. Therefore, the high surface area of solid sorbent can provide available sites for CO₂ adsorption (Ahmaruzzaman, 2010). However, this process is reversible at high temperature as CO₂ can be released back to the atmosphere when the surface of solid sorbent is activated by heating (Mercedes Maroto-Valer et al., 2008).

For carbonation reaction, the amount of free CaO in fly ash is an important composition for this reaction. CO₂ reacts with free CaO to form CaCO₃. This reaction is reversible at the temperature range of 750-950°C for the decomposition of CaCO₃ (Stanmore and Gilot, 2005). The normal operation temperature of CO₂ capture is much lower than 750°C (Sayari et al., 2011). Therefore, the carbonation reaction can capture CO₂ without easily releasing back to the atmosphere. The reaction can as well reduce the amount of free CaO in fly ash which causes an excessive expansion

problem when high free CaO fly ash is used as a mineral admixture in cement mixtures.

4.2.2.1 CO₂ capture by adsorption

The CO₂ capture by surface adsorption depends on various factors. The composition of fly ash (various batches), temperature, pressure, and moisture content may affect the performance of CO₂ adsorption. The CO₂ capture by adsorption on the fly ash is investigated by determining the concentration of CO₂ in the gas samples which were collected after the desorption process of all adsorbed CO₂ on fly ash surface done in batch mode at 150°C for 1 h and analyzed using GC. The effect of adsorption conditions are studied by the same procedure.

Effect of various batches of fly ashes; the performance of CO₂ capture by adsorption of various types of fly ash is listed in Table 4.10. The adsorption conditions were fixed at a temperature of 30°C and a pressure of 1 atm for 1 h in batch mode. After that, CO₂ desorption was done to release the amount of CO₂ capture by adsorption as described above.

Table 4.10 CO₂ adsorption using various types of fly ash (Adsorption condition; 30°C and 1 atm)

Solid sorbent material	Blaine fineness (cm ² /g)	Amount of CO ₂ Capture (μmol/g fly ash)
FA-1	2867	2.90±0.30
FA-2	2820	1.62±0.10
FA-3	2884	2.20±0.50

According to Table 4.10, FA-1 exhibited the highest CO₂ capture capacity (2.90 μmol/g fly ash). The surface area is a major factor for the CO₂ capture via adsorption which can relate to the Blaine fineness of the fly ash. The specific surface area is directly proportional to the Blaine fineness (Shirai et al., 2011). As shown in Table 4.10, the Blaine fineness of FA-1 is higher than FA-2, then it provides higher surface area that can capture more CO₂ than FA-2. An addition of free CaO to FA-1

results in a change of compositions of FA-3 as shown in Table 4.8. The CO₂ adsorption on FA-1 and FA-3 are not significantly different.

Effect of temperature; the adsorption temperature of CO₂ capture using fly ash as a solid sorbent was investigated in the temperature range of 30-150°C. In this testing, the fly ash (FA-1) with no moisture is used in CO₂ capture and the adsorption pressure is kept constant at 1 atm.

Table 4.11 CO₂ adsorption using fly ash at different adsorption temperatures (Adsorption conditions; 30-150°C and 1 atm)

Adsorption temperature (°C)	Amount of CO ₂ Capture (μmol/g fly ash)
30	2.90±0.30
60	1.57±0.10
100	0.29±0.02
150	0.00±0.00

Table 4.11 shows that fly ash can capture the highest amount of CO₂ (2.90 μmol/g fly ash) at the lowest tested temperature of 30°C. The amount of CO₂ capture by fly ash decreases 40.6 %, 90.0%, and 100% when the adsorption temperature is increased to 60°C, 100°C, and 150°C, respectively. As mentioned in the early section, CO₂ adsorption is reversible at high temperatures because the higher temperature can activate the CO₂ desorption from fly ash surface back to the atmosphere. Therefore, the proper adsorption temperature should be low to achieve a higher CO₂ capture capacity.

Effect of pressure; the CO₂ capture by adsorption was tested at the adsorption pressure of 1-1.5 atm. This pressure range is considerably selected in order to represent the pressure of CO₂ capture process continuously for industrial applications.

Table 4.12 CO₂ adsorption using fly ash at different adsorption pressure (Adsorption condition; 30°C and 1-1.5 atm)

Pressure (atm)	Amount of CO ₂ Capture (μmol/g fly ash)
1.0	2.90±0.30
1.2	3.23±0.02
1.5	4.29±0.01

Table 4.12 denotes the performance of CO₂ capture capacity by varying the adsorption pressure within the range of 1-1.5 atm while adsorption temperature was kept constant at 30°C. The results show that the performance of CO₂ capture depends on adsorption pressure. The adsorption pressure of 1.2 atm and 1.5 atm can increase the amount of CO₂ capture at 11.3% and 47.9% over the CO₂ adsorbed amount at the pressure of 1 atm, respectively. The increase of adsorption pressure can boost the gas diffusion into the pore and adsorption over the solid sorbents (Sayari et al., 2011). Even though the high pressure can increase the CO₂ adsorption but, it can be complicated for a continuous operation and costly on the facility investment.

Effect of moisture; all fly ashes were dried at 110°C for 6 h removing all moisture in the samples to study the effect of moisture content on CO₂ adsorption. Then, the DI water was added to the dry fly ash samples in a dry box to obtain the desired moisture content of 5 and 10 wt% of the samples. The fly ash samples were loaded into the tubular reactor under dry condition for CO₂ capture by adsorption. The CO₂ adsorption was conducted in the tubular reactor by engaged 99.8% CO₂ into the reactor at 1 atm and 30°C for 1 h in a batch mode.

Table 4.13 CO₂ adsorption using fly ash at different moisture contents (Adsorption condition; 30°C and 1 atm)

Moisture contents (wt%)	Amount of CO ₂ Capture (μmol/g fly ash)
0	2.90±0.30
5	3.34±0.10
10	3.75±0.30

Table 4.13 shows that the CO₂ capture performance is slightly increased along with an increase of moisture content. Without moisture in fly ash, CO₂ was adsorbed at 2.90±0.30 μmol/g fly ash. An addition of moisture at 5 wt% and 10 wt% can increase an amount of CO₂ capture by 15.2% and 29.3% in relative to completely dried fly ash, respectively.

Effect of NaOH addition in fly ash; the alkaline bases are commonly used to enhance the CO₂ capture capacity of solid sorbent (Bobicki et al., 2012; Nikulshina et al., 2008). NaOH was added to fly ash in the form of aqueous solution and the composition of NaOH in liquid solution are 0, 5 and 10 wt% in total weight solid sorbent. The sorbents were dried at 110°C for 24 h to get rid of moisture. The CO₂ adsorptions were conducted in a batch mode at 30°C and 1 atm for 1 h and followed by the desorption at 150°C to determine the CO₂ capture capacities of sorbents. Table 4.14 shows the result of CO₂ capture using fly ash with and without an addition of NaOH to evaluate the effect of NaOH to CO₂ capture performance.

Table 4.14 CO₂ adsorption using fly ash (FA-1) at various wt% of NaOH

Solid sorbent material	Amount/Type of Base	Amount of CO ₂ Capture (μmol/g sorbent)
FA-1	0% wt NaOH	2.90±0.3
	5% wt NaOH	34.80±1.4
	10% wt NaOH	72.60±2.1

The results show that NaOH addition in FA-1 can enhance the CO₂ adsorption capacity of fly ash. The performance of CO₂ capture via adsorption increases along with the increased amount of NaOH. FA-1 with 10% wt of NaOH can adsorb the highest amount of CO₂ up to 72.60±2.1 μmol/g sorbent. Although an addition of NaOH in fly ash can increase the CO₂ capture capacity, NaOH can add unwanted moisture and high content of NaOH into fly ash. Literature reports that an addition of NaOH in concrete can change the compressive strength and durability of concrete (Smaoui et al., 2005). Thus, an addition of NaOH causes an extra cost and also may harm the feasibility in using fly ash as a mineral admixture in concrete which requires more investigation to evaluate the utilization of fly ash with NaOH as admixture in concrete.

4.2.2.2 CO₂ capture by carbonation reaction

It is recognized that free CaO in fly ash can react with CO₂ to form carbonate compounds. The carbonation reaction is shown in equation 4.4 (Chowdhury et al., 2013).



The EDTA titration method was used to measure the free CaO content of fly ash before and after CO₂ capture. The ratio of the free CaO in fly ash reacted with CO₂ can be calculated by dividing the difference in content of free CaO before and after CO₂ capture. The free Ca²⁺ consumption by the carbonation reaction can be calculated by using equation 4.5.

$$\text{Free Ca}^{2+} \text{ consumption (\%)} = \frac{\text{Free Ca}_{\text{initial}}^{2+} - \text{Free Ca}_{\text{left}}^{2+}}{\text{Free Ca}_{\text{initial}}^{2+}} \times 100\% \quad (4.5)$$

The FA-1 was used to capture CO₂ and then the amount of free Ca²⁺ consumption was calculated using equation 4.5. The results show that 98.8% of free CaO in the fly ash was used in the carbonation reaction. The XRD of fly ash before and after CO₂ capture also confirms the formation of CaCO₃ from the carbonation reaction as shown in Figure 4.8.

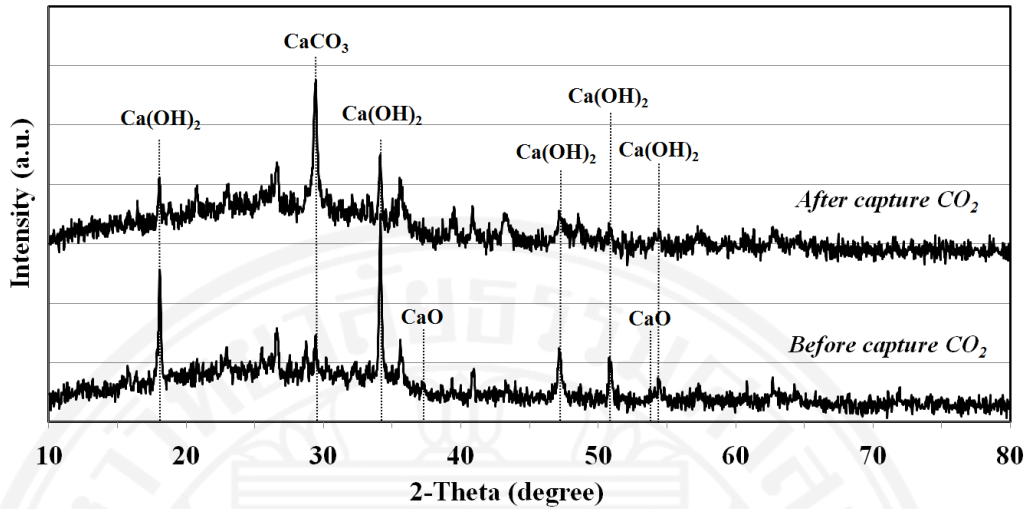


Figure 4.9 XRD results of high free CaO fly ash before and after capture CO₂

The free CaO content in fly ash can be converted into Ca(OH)₂ in the presence of low moisture content in the atmosphere (Dubina et al., 2013). According to the XRD results, there is no CaO found in the fly ash before capturing CO₂ due to storage at normal atmosphere with the presence of moisture. Ca(OH)₂ is found in fly ash instead and becomes the main component for the carbonation reaction. Figure 4.9 illustrates that, after capturing CO₂, peak of Ca(OH)₂ was decreased. Meanwhile, CaCO₃, which is the product of carbonation reaction of CO₂, emerged to be present with a higher peak on the XRD pattern. This result agreed with the literature by two steps of reaction (Montes-Hernandez et al., 2009). Firstly, the formation of calcium hydroxide from the reaction of free CaO and water is shown in the equation 4.6;



After that, calcium hydroxide can react with CO₂ to form CaCO₃ as in equation 4.7;



According to equations 4.6 and 4.7, CO₂ can be captured by free CaO in fly ash via carbonation reaction to form CaCO₃.

Table 4.15 CO₂ capture by carbonation reaction in fly ash with different composition of base treatments

Sorbent Materials	Amount/Type of Base	Amount of free CaO in Carbonation Reaction (g free lime/100 g FA)	Free Ca ²⁺ consumption by carbonation (%)
FA-1	0wt% of NaOH	1.69±0.01	98.8
FA-1	5wt% of NaOH	1.71±0.02	99.9
FA-1	10wt% of NaOH	1.71±0.01	99.9
FA-2	0wt% of NaOH	3.89±0.03	98.9
FA-3	0wt% of NaOH	4.86±0.02	97.2

Table 4.15 shows the CO₂ capture by carbonation reaction in fly ashes with and without NaOH addition. The compositions of free CaO in fly ash are in the range from 1.71 wt% to 5 wt%. The data clearly shows that carbonation reaction from CO₂ capture can consume most of the available free CaO in all fly ash samples up to 99.9%. An addition of NaOH can slightly increase the consumption of free CaO by carbonation. The data support the use of CO₂ capture via carbonation to reduce free CaO content in fly ash without any base treatment.

Table 4.16 Total CO₂ capture from adsorption and carbonation using fly ash as solid sorbents

Sorbent	Free CaO (wt%)	CO ₂ capture (adsorption) (μmol/g fly ash)	CO ₂ capture (carbonation) (μmol/g fly ash)	Total CO ₂ capture (μmol/g fly ash)
FA-1	1.71	2.9±0.3	301.8±1.8	304.7±2.1
FA-2	3.93	1.6±0.1	694.6±5.4	696.2±5.5
FA-3	5.00	2.2±0.5	867.9±3.2	870.1±3.7

Table 4.16 shows the comparison of CO₂ capture capacity of fly ash between CO₂ capture by surface adsorption and CO₂ capture by carbonation reaction. The results show that the carbonation reaction can capture the majority of CO₂ up to 99.77% of the CO₂ capture capacity (for FA-2 and FA-3) while the adsorption shares only a small portion of CO₂ capture. Therefore, the total amount of CO₂ capture is dominated by the carbonation reaction and depends on the amount of free CaO composition. Even though the adsorption shows small CO₂ capture capacity relative to carbonation, the literature reports that the CO₂ adsorption can provide the attractive interaction between CO₂ and sorbent surface which can immobilize CO₂ to stay on the surface of sorbent to aid the carbonation reaction (Burghaus, 2014). The capture capacities of fly ashes in this study are comparable to the capacity of disposal solid sorbent (351 μmol/g of amine enriched solid sorbent) which requires chemical treatment and can be further used only for land filling (Bachelor and Toochinda, 2012). For the use of fly ash as a CO₂ capture solid sorbent and a mineral admixture in cement, fly ash without NaOH treatment is recommended for effective CO₂ capture along with reduction of the free CaO content in fly ash. The properties of mortar and cement paste containing fly ash after CO₂ capture as a mineral admixture will be discussed in the next section.

4.2.3 Basic properties of mixtures containing fly ash after CO₂ capture

Further applications of fly ash after CO₂ capture as a mineral admixture was investigated by comparing the basic properties of mortar and cement paste specimens containing fly ash before and after CO₂ capture. The basic properties of all fly ash mixtures such as water requirement, compressive strength, and autoclave expansion were investigated and illustrated in Figure 4.9 to Figure 4.13, respectively.

4.2.3.1 Water requirement of mortar specimens

Figure 4.10 shows the water requirement of mortar specimens using pure cement and mortar specimens containing fly ash before and after CO₂ capture. Water requirement is calculated from the ratio of required water to obtain 110%±5 flow degree of test mortar mixture to that of cement-only mortar mixture following standard ASTM C1437 (ASTM C1437, 1999).

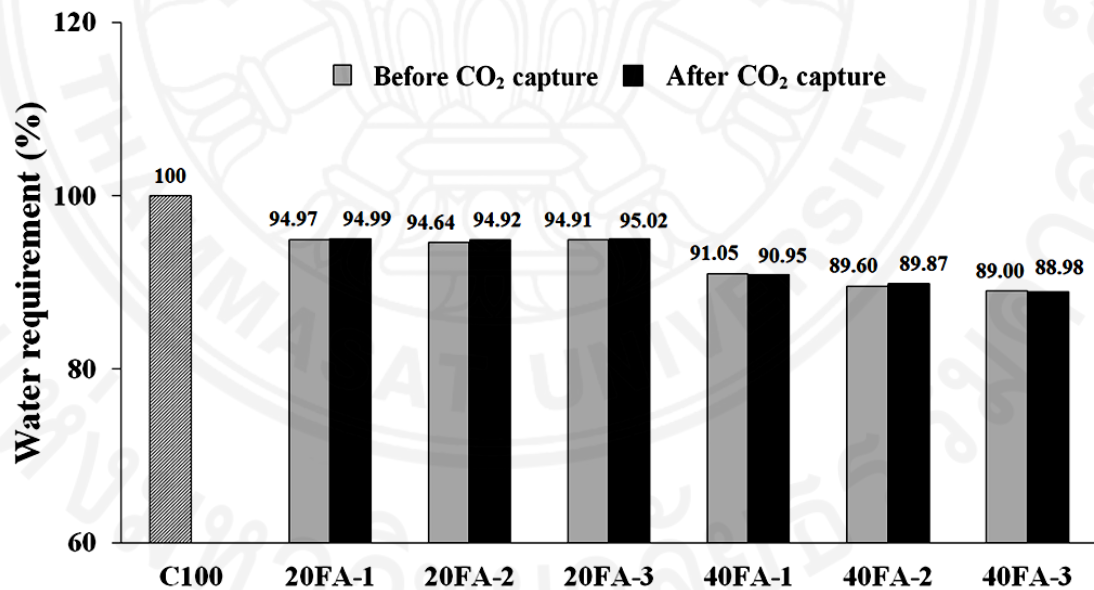


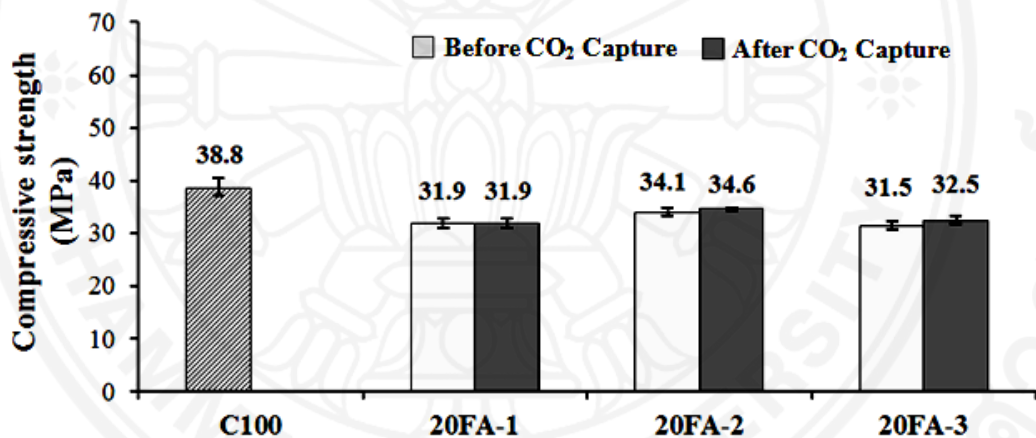
Figure 4.10 Water requirement of mortar specimens using fly ash before and after CO₂ capture (20 wt% and 40 wt% fly ash replacement)

The higher percentages of fly ash replacement can result in a decrease of water requirement. The mixtures containing fly ashes (20 wt% and 40 wt%) required less water than the cement-only mixture. There is no significant difference of water

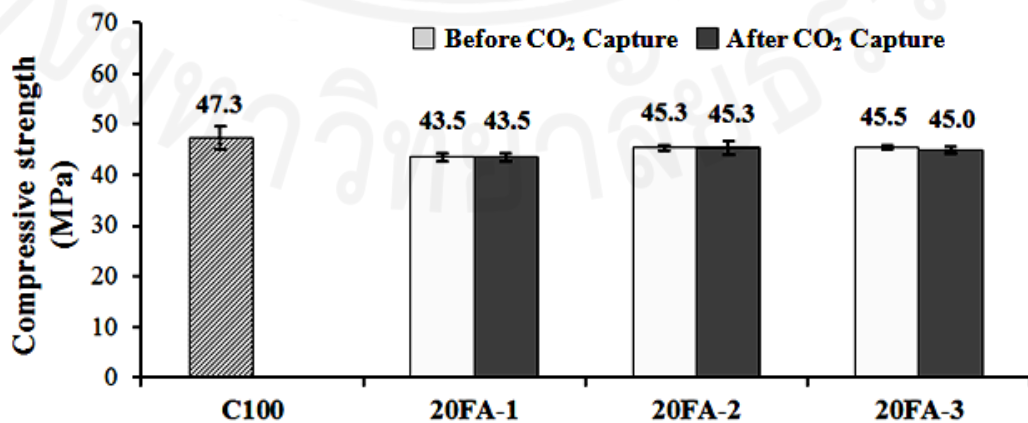
requirement among FA-1, FA-2 and FA-3. There is also no difference in the water requirement between the mortar specimens using fly ash before and after CO₂ capture.

4.2.3.2 Compressive strength and strength index of mortar specimens

Compressive strength is one of the necessary properties needed to be tested to evaluate the feasibility in using fly ash as a mineral admixture. Figure 4.11 illustrates the compressive strengths of mortar specimens using 20 wt% fly ashes before and after CO₂ capture at different ages (7, 28 and 91 days). Mixtures containing 20 wt% fly ash replacements at 7 and 28 days show lower compressive strength compared to cement-only mortars.



a) 7 days



b) 28 days

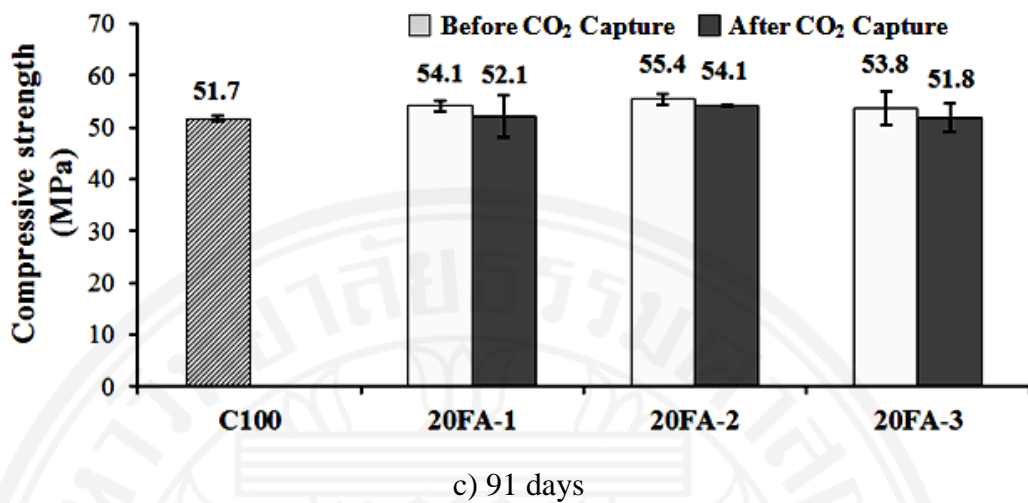


Figure 4.11 Compressive strength of mortar specimens using 20 wt% of fly ash before and after CO₂ capture at a) 7-days, b) 28-days and c) 91-days

After the curing period of 91 days, the compressive strength of mixtures containing 20 wt% fly ash replacement increases to be almost the same as that of cement-only mortar. The mortar specimens with fly ash requires a longer time than those with pure cement to develop the compressive strength. The reason is that fly ash requires more time to form calcium silicate hydrate gel relative to pure cement as reported from literature (Saeki and Monteiro, 2005; Wang, 2014). The compressive strengths of mortar specimens with 20 wt% fly ash replacement before and after CO₂ capture remain almost unchanged for all curing periods. Therefore, there is no significant changes in the compressive strength between mortar specimens using 20 wt% of fly ash before and after CO₂ capture.

Figure 4.12 demonstrates the strength index of mortar specimens in this study. The strength index can be calculated from equation 4.8.

$$\text{Strength index} = \frac{\text{Compressive strength of mortar specimens}}{\text{Compressive strength of cement – only mortar}} \times 100\% \quad (4.8)$$

The strength index of mortar must achieve the requirements of TIS 2135 standard. The standard requires strength index to be at least 75% at 7 and 28 curing days and 85% at 91 curing days (TIS 2135, 2002). The dash lines on Figure 4.11

indicate the required strength index of the mortar specimens according to TIS 2135 standard.

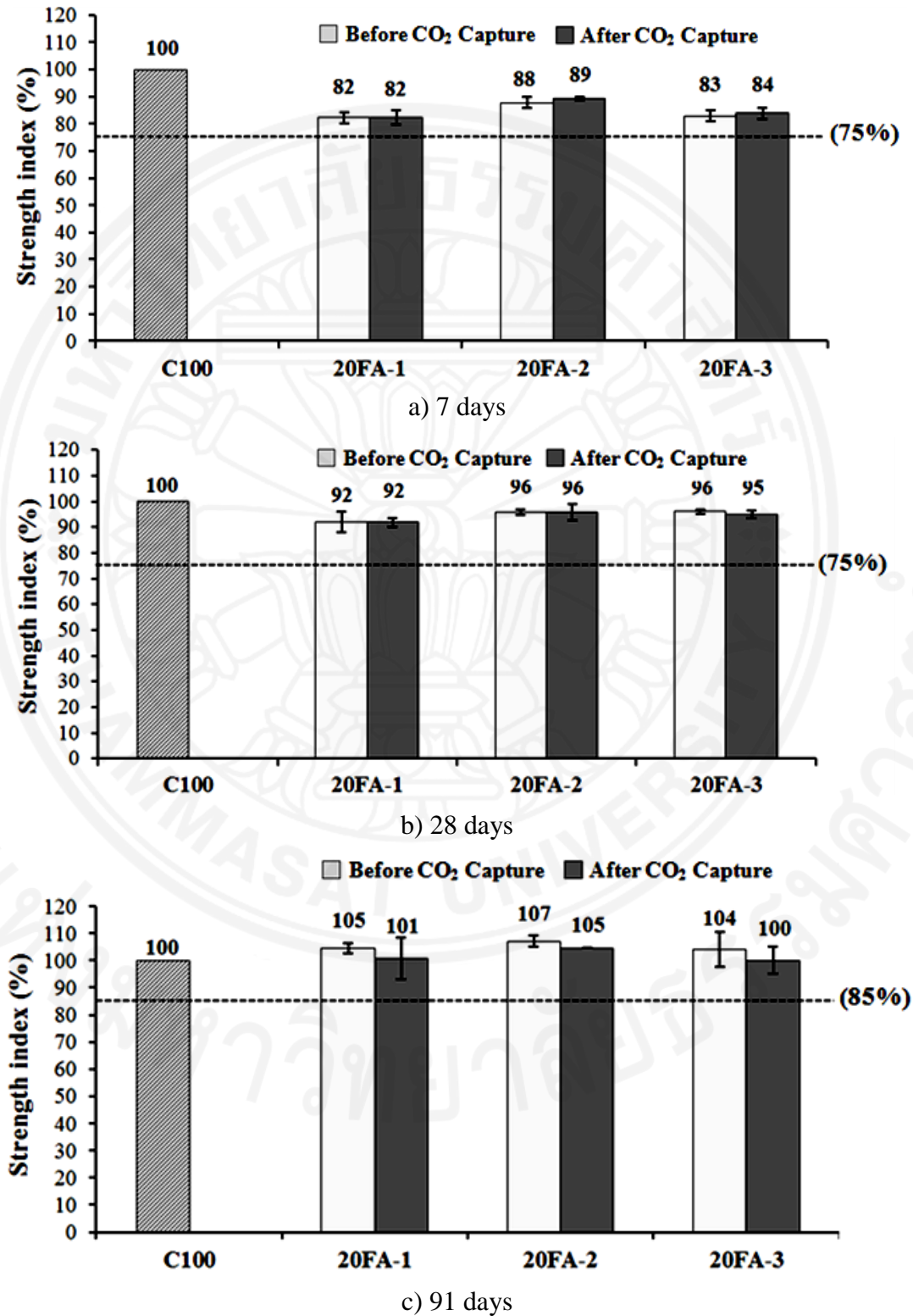


Figure 4.12 Strength index of mortar specimens using 20 wt% of fly ash before and after CO₂ capture at a) 7-days, b) 28-days and, c) 91-days

Strength index of all mortar specimens using 20 wt% of fly ash before and after CO₂ capture satisfy the TIS 2135 standard at all tested ages. The results from Figure 4.10 and Figure 4.11 confirm that fly ash after CO₂ capturing process can be used as a mineral admixture in concrete.

4.2.3.3 Autoclave expansion of paste specimens

Figure 4.13 depicts the % autoclave expansion of paste specimens using 40 wt% of fly ash before and after CO₂ capture. The autoclave expansion was tested according to ASTM C151 to evaluate the delayed expansion of paste specimens due to the hydration of some oxide compounds, especially free CaO or free MgO (ASTM C151, 2000). The positive sign indicates the expansion of specimen while the negative sign implies the contraction.

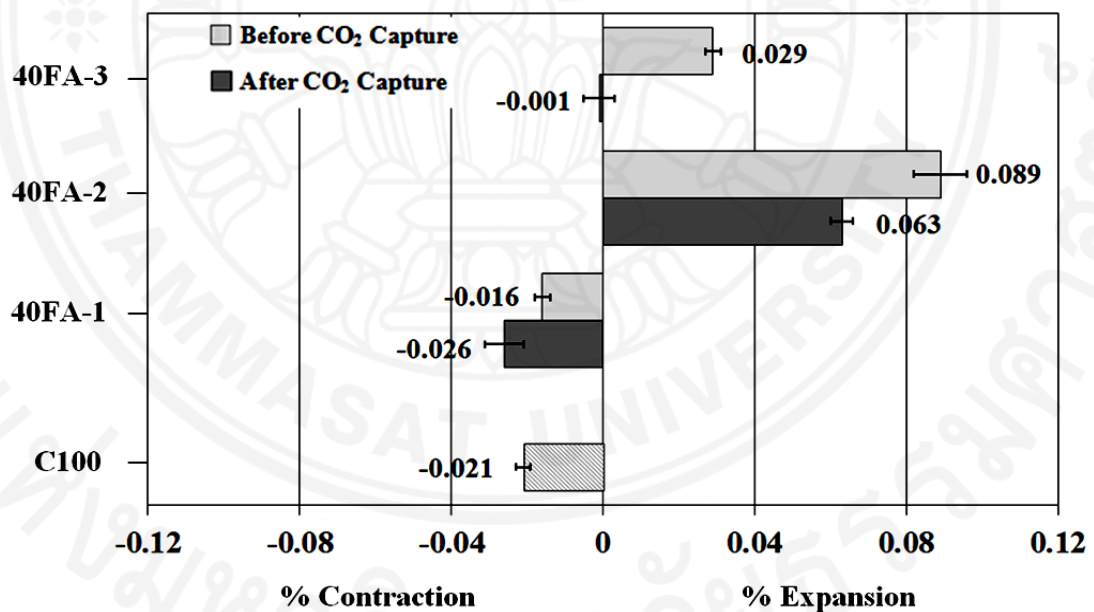


Figure 4.13 Autoclave expansions of paste specimens using 40 wt% of fly ash before and after CO₂ capture

From Figure 4.13, the cement-only mixture shows contraction after autoclave expansion test. The % expansion of 40FA-1 shows the negative sign of contraction instead of expansion. After CO₂ capture, paste specimen can contract more due to the reduction of free lime content which results in more contraction.

Mixture 40FA-3 shows an expansion up to 0.029%. The compositions of FA-3 and FA-1 are almost identical except the free CaO content, which are 5 wt% and 1.71 wt%, respectively. The results indicate that the expansion of 40FA-3 is higher than that of 40FA-1 due to higher free CaO content in the fly ash. Expansion of 40FA-3 after CO₂ capture also decreased from that before CO₂ capture because the free CaO was mostly consumed in the CO₂ capture by carbonation process.

For 40FA-2, the paste specimens expand the most among all specimens in this study. Literature reports that the compositions of fly ash can affect the autoclave expansion, especially for free CaO and SO₃ contents (Kaewmanee et al., 2013). FA-2 contains free CaO content of 3.93 wt% and SO₃ content of 8.53 wt% which are considerably high relative to those of other fly ashes in this study. 40FA-2 using fly ash after CO₂ capture shows expansion of specimen, but the expansion was reduced relative to the specimen using fresh fly ash.

The differences of expansion between paste specimen using FA before and after CO₂ capture clearly show that the CO₂ capture process can reduce expansion in the specimens by the reduction of free CaO from carbonation reaction.

4.2.3.4 Carbonation depth

The carbonation depth is an important parameter for evaluating steel corrosion resistance of reinforced concrete. Normally, corrosion of reinforcing steels is protected by high alkalinity inside the pores (Chang and Chen, 2006; Khunthongkeaw et al., 2006). Most of the Ca(OH)₂ in the concrete is derived from the hydration reaction of cement and water. The partial replacement of cement by fly ash can lower the amount of Ca(OH)₂ due to the pozzolanic reaction of fly ash, which can increase the carbonation depth of the specimens and results in a corrosion of steel.

The amount of free CaO in fly ash can affect the carbonation depth in mortar specimens. The free CaO in fly ash reacts with moisture to form Ca(OH)₂ as shown in equation 4.6. Free CaO forms Ca(OH)₂ which reacts with CO₂ and provides the carbonation resistance to the mortar specimens. The CO₂ capture process can also consume free CaO in fly ash the same way as above. This is considered as a competitive reaction with carbonation reaction. Therefore, the effect of mortar specimens using fly ash before and after CO₂ capture to the carbonation depth should

be investigated. Literature reports that the carbonation depth does not only depend on CaO content. The depth can be affected by many factors such as the CO₂ diffusivity, porosity of the specimen, etc (Khunthongkeaw et al., 2006). The comparisons of carbonation depth among each batch of fly ash are still unclear and require further investigations. Therefore, this work focuses on the comparison of carbonation depth between the mortar specimen using fly ash before and after CO₂ capture.

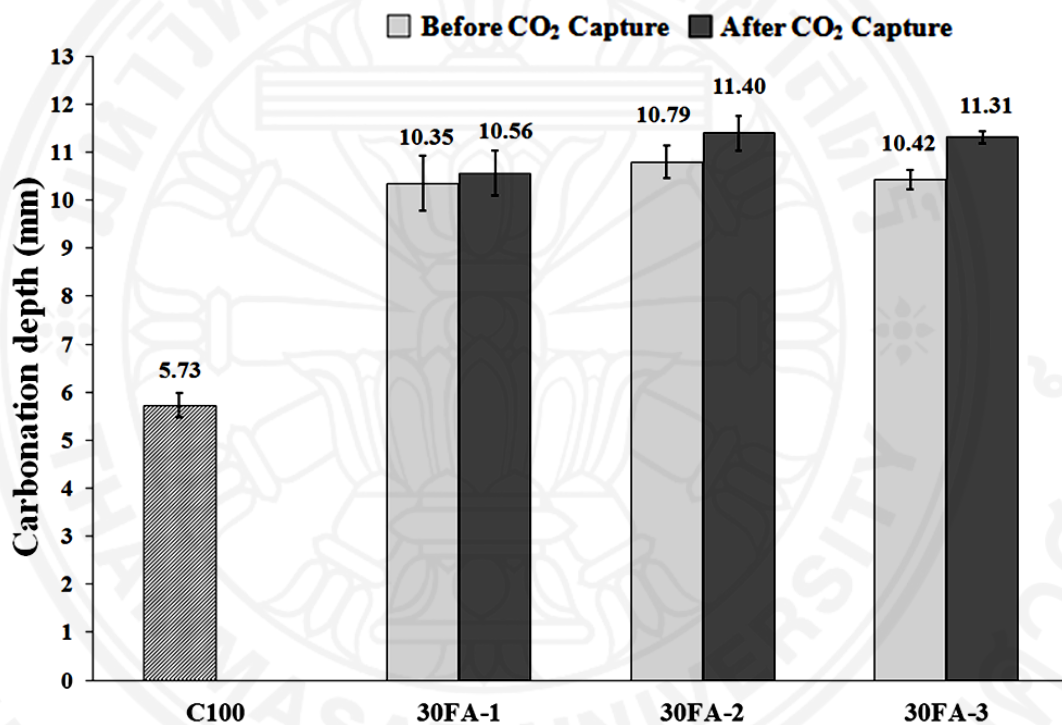


Figure 4.14 Carbonation depths of mortar specimens using 30 wt% of fly ash before and after CO₂ capture

Figure 4.14 shows the carbonation depth of mortar specimens with cement-only (C100) and mortar specimens using 30 wt % fly ash replacements before and after CO₂ capture. The specimens were prepared to study the effect of post CO₂ capture fly ash on the carbonation depth of specimens. Comparing to cement-only mortar, the carbonation depth of all mortar specimens using fly ash replacements are in the range of 10.35-11.40 mm which is deeper than that of cement-only mortar. The results also show that mortar specimens using fly ash after CO₂ capture have deeper carbonation depth than those using fresh fly ash in all batches of fly ash. The fly ash

after CO₂ capture can slightly decrease the carbonation resistance of mortar specimens. The CO₂ capture process consumes free CaO to form CaCO₃ instead of forming the Ca(OH)₂ for the carbonation resistance. However, the carbonation depth differences between mortar using fly ash before and after CO₂ capture are not so significant. Therefore, it is safe to conclude that the fly ash after CO₂ capture can be used as a mineral admixture in concrete.

Conclusions and Recommendations

The hydrogen production from methanol-steam reforming reaction and CO₂ capture process were studied and investigated. The Cu-Zn based catalyst for methanol-steam reforming at low temperature with low metal loading was developed in this work to overcome the sintering of catalyst and to reduce the cost of hydrogen production. Cu-Zn/ZrO₂ doped Al₂O₃ prepared by impregnation with urea exhibits a high hydrogen yield of 90.3% at a low temperature of 200°C. An addition of urea and ZrO₂ doped Al₂O₃ support can enhance the metal dispersion to overcome a low metal dispersion problem in a catalyst prepared by impregnation. A doping of ZrO₂ into Al₂O₃ support can alter the electronic property and interaction of Cu-Zn which provide a benefit in the activity of Cu-Zn catalyst for methanol-steam reforming. In addition, the activity in hydrogen production of Cu-Zn catalyst before and after sintering at 500°C was determined to evaluate the stability of the catalyst. The presence of ZrO₂ in Al₂O₃ support can also boost up the hydrogen production from methanol-steam reforming reaction even the specific copper surface area is decreased from sintering. Therefore, ZrO₂ doped Al₂O₃ could be a suitable support for the Cu-Zn based catalyst in a methanol-steam reforming reaction. The impregnation of Cu-Zn with urea over ZrO₂ doped Al₂O₃ could serve as a novel catalyst for methanol-steam reforming at low temperature.

The CO₂ capture using fly ash as solid sorbent and the use of fly ash after CO₂ capture as a mineral admixture in cement were evaluated in this study. A fly ash captures CO₂ by surface adsorption and carbonation reaction in the range of 304.7-870.1 μmol/g fly ash without any treatment. The adsorption temperature, pressure, and moisture content affect the CO₂ capture capacity via surface adsorption but does not significantly affect the CO₂ capture by carbonation reaction. However, the majority of CO₂ are captured by carbonation reaction which depends on the amount of free CaO content in fly ash. The capture capacities of fly ashes are comparable to the capacity of disposal solid sorbent (351 μmol/g of amine enriched solid sorbent) which requires chemical treatment and can be further used only for land filling. The properties of cement paste and mortar specimens using fly ash before and after CO₂ capture were also evaluated. There are no significant differences in the water requirement and

compressive strength in specimens using fly ash before and after CO₂ capture. The fly ash after CO₂ capture as the mineral admixture can slightly decrease the carbonation resistance in mortar specimens. The utilization of fly ash after CO₂ capture can greatly reduce the excessive expansion in specimens. This method can provide the solution to prevent the excessive expansion in concrete for fly ash with high free CaO content used as the mineral admixture. For the drawback of this material, the fly ash after CO₂ capture can increase the carbonation depth in mortar specimens which may cause the steel corrosion in reinforced concrete. However the depth increments are not much different from specimens using fresh fly ash. The results from this study can serve as an attractive technique for CO₂ reduction and the effective use of post CO₂ fly ash sorbent in concrete applications.

The recommendations for the future work can be separated into 2 parts; development of Cu-Zn based catalyst for hydrogen production and CO₂ capture by using fly ash.

For the development of Cu-Zn catalyst for hydrogen production from methanol-steam reforming, the recommendations for the future work can be listed as;

- ZrO₂ doped Al₂O₃ support should be analyzed using X-ray absorption spectroscopy (XAS) in the mode of X-ray absorption near edge structure (XANES) to investigate the electronic property and the adsorption edge of Zr. This result can be used to explain the role of Zr added in Al₂O₃ support to improve the activity of the catalyst.
- In this study, the amount of Zr is kept constant at 10 wt% of support. However, the amount of Zr doped in Al₂O₃ may affect the performance of Cu-Zn catalyst. Therefore, the proper ratio of Zr replacement of Al in Al₂O₃ should be investigated by varying the composition of Zr in Zr-Al₂O₃ support and tested in catalytic activity of the methanol-steam reforming.
- In this work, ZrO₂ doped Al₂O₃ provided a benefit to Cu-Zn based catalyst. Therefore, the future work should be further investigated in the replacement of Al atoms using other elements such as Sr, Y and Ce to produce a new supports and compare the catalytic activity of methanol-steam reforming with Zr-Al₂O₃

support. Sr, Y and Ce are the elements in the same period with di-, tri- and tetravalent elements. The replacement of these atoms may provide the electron transfer capability of the support which can alter the activity of catalyst. The result from this study could provide the useful information to understand the replacement role of elements to substitute Al in Al_2O_3 towards the catalytic activity of methanol-steam reforming reaction. The replacement of elements to substitute Al in Al_2O_3 can be simulated by using FEFF software which uses the information from X-ray absorption spectroscopy.

- The kinetics study of Cu-Zn based catalyst over various alumina based supports should be investigated by varying feed rate and reaction temperature in order to determine the activation energy of the catalysts.
- The deactivation rate of Cu-Zn based catalysts needs to be studied in order to precisely predict the lifetime of catalyst which can benefit in a process design for the methanol-steam reforming reaction.

For CO_2 capture by using fly ash, the recommendations for the future work can be listed as;

- Besides using fly ash to capture CO_2 from methanol-steam reforming process, the CO_2 capture by fly ash in this work can be used to capture CO_2 which releases from coal-fired power plant in Mae Moh. Therefore, CO_2 capture process using fly ash should be scaled up to be able to capture CO_2 in the real process from coal-fired power plant. The proper parameters such as temperature, pressure, flow rate and composition of flue gas before released from the exhaust stack should be investigated to evaluate feasibility in the application.
- The quality of coal and combustion conditions of coal in the furnace can influence the properties of fly ash such as a variation in composition, moisture content and the amount of free CaO. Thus, these properties of fly ash from coal-fired power need to be investigated in detail to evaluate the proper range of CO_2 capture conditions by fly ash which can be further used as an admixture in concrete.

Based on this work, NaOH treated over fly ash can improve the CO₂ capture capacity via adsorption, but a further application of fly ash treated with NaOH after CO₂ capture as other products besides using as a mineral admixture in concrete need to be investigated further.



References

- ASTM C33. (2003). Standard Specification for Concrete Aggregates. *American Society for Testing and Materials*, Philadelphia.
- ASTM C109/C109M. (1999). Standard Test Method for Compressive Strength of Hydraulic Cement Mortars (Using 2-in. or [50-mm] Cube Specimens). *American Society for Testing and Materials*, Philadelphia.
- ASTM C151. (2000). Standard Test Method for Autoclave Expansion of Portland Cement. *American Society for Testing and Materials*, Philadelphia.
- ASTM C188. (2003). Test Method for Density of Hydraulic Cement. *American Society for Testing and Materials*, Philadelphia.
- ASTM C204. (2007). Standard Test Methods for Fineness of Hydraulic Cement by Air-Permeability Apparatus. *American Society for Testing and Materials*, Philadelphia.
- ASTM C618. (2003). Standard Specification for Coal Fly Ash and Raw or Calcined Natural Pozzolan for Use in Concrete. *American Society for Testing and Materials*, Philadelphia.
- ASTM C1437. (1999). Standard Test Method for Flow of Hydraulic Cement Mortar. *American Society for Testing and Materials*, Philadelphia.
- Agrell, J., Birgersson, H., Boutonnet, M. (2002). Steam reforming of methanol over a Cu/ZnO/Al₂O₃ catalyst: a kinetic analysis and strategies for suppression of CO formation. *Journal of Power Sources* 106, 249-257.
- Agrell, J., Birgersson, H., Boutonnet, M., Melián-Cabrera, I., Navarro, R.M., Fierro, J.L.G. (2003). Production of hydrogen from methanol over Cu/ZnO catalysts promoted by ZrO₂ and Al₂O₃. *Journal of Catalysis* 219, 389-403.
- Ahmaruzzaman, M. (2010). A review on the utilization of fly ash. *Progress in Energy and Combustion Science* 36, 327-363.

Appleby, A.J. (1994). Fuel cells and hydrogen fuel. *International Journal of Hydrogen Energy* 19, 175-180.

Bachelor, T.T.N., Toochinda, P. (2012). Development of low-cost amine-enriched solid sorbent for CO₂ capture. *Environmental Technology* 33, 2645-2651.

BEL JAPAN, INC. (2012). *Operation manual of Catalyst Analyzer BELCAT-B*. JAPAN. Printed.

Bobicki, E.R., Liu, Q., Xu, Z., Zeng, H. (2012). Carbon capture and storage using alkaline industrial wastes. *Progress in Energy and Combustion Science* 38, 302-320.

Boycheva, S., Zgureva, D., Vassilev, V. (2013). Kinetic and thermodynamic studies on the thermal behaviour of fly ash from lignite coals. *Fuel* 108, 639-646.

Breen, J.P., Ross, J.R.H. (1999). Methanol reforming for fuel-cell applications: development of zirconia-containing Cu–Zn–Al catalysts. *Catalysis Today* 51, 521-533.

“Brunauer, Emmett and Teller (BET) Theory.” Particle Analytical. Retrieved Jan 2016, from <http://particle.dk/methods-analytical-laboratory/surface-area-bet/surface-area-bet-theory/>

Burghaus, U. (2014). Surface chemistry of CO₂ – Adsorption of carbon dioxide on clean surfaces at ultrahigh vacuum. *Progress in Surface Science* 89, 161-217.

Chang, C.-F., Chen, J.-W. (2006). The experimental investigation of concrete carbonation depth. *Cement and Concrete Research* 36, 1760-1767.

Cheng, W.-H., Chen, I., Liou, J.-s., Lin, S.-S. (2003). Supported Cu Catalysts with Yttria-Doped Ceria for Steam Reforming of Methanol. *Topics in Catalysis* 22, 225-233.

Chindaprasirt, P., Homwuttiwong, S., Sirivivatnanon, V. (2004). Influence of fly ash fineness on strength, drying shrinkage and sulfate resistance of blended cement mortar. *Cement and Concrete Research* 34, 1087-1092.

Chindaprasirt, P., Jaturapitakkul, C., Sinsiri, T. (2007). Effect of fly ash fineness on microstructure of blended cement paste. *Construction and Building Materials* 21, 1534-1541.

Choi, Y., Stenger, H.G. (2002). Fuel cell grade hydrogen from methanol on a commercial Cu/ZnO/Al₂O₃ catalyst. *Applied Catalysis B: Environmental* 38, 259-269.

Choi, Y., Stenger, H.G. (2005). Kinetics, simulation and optimization of methanol steam reformer for fuel cell applications. *Journal of Power Sources* 142, 81-91.

Chowdhury, M.B.I., Quddus, M.R., deLasa, H.I. (2013). CO₂ capture with a novel solid fluidizable sorbent: Thermodynamics and Temperature Programmed Carbonation–Decarbonation. *Chemical Engineering Journal* 232, 139-148.

Díaz, E., Muñoz, E., Vega, A., Ordóñez, S. (2008). Enhancement of the CO₂ retention capacity of X zeolites by Na- and Cs-treatments. *Chemosphere* 70, 1375-1382.

Dubina, E., Korat, L., Black, L., Strupi-Šuput, J., Plank, J. (2013). Influence of water vapour and carbon dioxide on free lime during storage at 80°C, studied by Raman spectroscopy. *Spectrochimica Acta Part A: Molecular and Biomolecular Spectroscopy* 111, 299-303.

Ertl, G., Knözinger, H., Weitkamp J. (1997). *Hand book of Heterogeneous catalysis*. Weinheim: VCH Verlagsgesellschaft mbH.

Esposito, S., Turco, M., Bagnasco, G., Cammarano, C., Pernice, P., Aronne, A. (2010). Highly dispersed sol–gel synthesized Cu–ZrO₂ materials as catalysts for oxidative steam reforming of methanol. *Applied Catalysis A: General* 372, 48-57.

Feio, L.S.F., Hori, C.E., Damyanova, S., Noronha, F.B., Cassinelli, W.H., Marques, C.M.P., Bueno, J.M.C. (2007). The effect of ceria content on the properties of Pd/CeO₂/Al₂O₃ catalysts for steam reforming of methane. *Applied Catalysis A: General* 316, 107-116.

Figuerola, J.D., Fout, T., Plasynski, S., McIlvried, H., Srivastava, R.D. (2008). Advances in CO₂ capture technology—The U.S. Department of Energy's Carbon Sequestration Program. *International Journal of Greenhouse Gas Control* 2, 9-20.

“Fly ash.” Wikipedia: The Free Encyclopedia. Wikimedia Foundation, Inc. (2015). Retrieved Jan 2016, from https://en.wikipedia.org/wiki/Fly_ash

Folger, P. (2013). *Carbon Capture and Sequestration (CCS): A Primer*. Retrieved Jan 2016, from: www.crs.gov

Fujitani, T., Nakamura, J. (2000). The chemical modification seen in the Cu/ZnO methanol synthesis catalysts. *Applied Catalysis A: General* 191, 111-129.

Garrabrants, A.C., Kosson, D.S., DeLapp, R., van der Sloot, H.A. (2014). Effect of coal combustion fly ash use in concrete on the mass transport release of constituents of potential concern. *Chemosphere* 103, 131-139.

Gray, M.L., Soong, Y., Champagne, K.J., Baltrus, J., Stevens Jr, R.W., Toochinda, P., Chuang, S.S.C. (2004). CO₂ capture by amine-enriched fly ash carbon sorbents. *Separation and Purification Technology* 35, 31-36.

Gray, M.L., Soong, Y., Champagne, K.J., Pennline, H., Baltrus, J.P., Stevens Jr, R.W., Khatri, R., Chuang, S.S.C., Filburn, T. (2005). Improved immobilized carbon dioxide capture sorbents. *Fuel Processing Technology* 86, 1449-1455.

Grove, W.R. (1845). On the Gas Voltaic Battery. Voltaic Action of Phosphorus, Sulphur and Hydrocarbons. *Philosophical Transactions of the Royal Society of London* 135, 351-361.

Günter, M.M., Ressler, T., Jentoft, R.E., Bems, B. (2001). Redox Behavior of Copper Oxide/Zinc Oxide Catalysts in the Steam Reforming of Methanol Studied by in Situ X-Ray Diffraction and Absorption Spectroscopy. *Journal of Catalysis* 203, 133-149.

Gurbani, A., Ayastuy, J.L., González-Marcos, M.P., Herrero, J.E., Guil, J.M., Gutiérrez-Ortiz, M.A. (2009). Comparative study of CuO–CeO₂ catalysts prepared by

wet impregnation and deposition–precipitation. *International Journal of Hydrogen Energy* 34, 547-553.

Hammoud, D., Gennequin, C., Aboukaïs, A., Aad, E.A. (2015). Steam reforming of methanol over x% Cu/Zn–Al 400 500 based catalysts for production of hydrogen: Preparation by adopting memory effect of hydrotalcite and behavior evaluation. *International Journal of Hydrogen Energy* 40, 1283-1297.

Hedin, N., Andersson, L., Bergström, L., Yan, J. (2013). Adsorbents for the post-combustion capture of CO₂ using rapid temperature swing or vacuum swing adsorption. *Applied Energy* 104, 418-433.

Holladay, J.D., Hu, J., King, D.L., Wang, Y. (2009). An overview of hydrogen production technologies. *Catalysis Today* 139, 244-260.

Huang, G., Liaw, B.-J., Jhang, C.-J., Chen, Y.-Z. (2009). Steam reforming of methanol over CuO/ZnO/CeO₂/ZrO₂/Al₂O₃ catalysts. *Applied Catalysis A: General* 358, 7-12.

HyGen Industries, Inc. (2016). *How a Hydrogen Fuel Cell Vehicle Works*. Retrieved Jan 2016, from <http://www.hygen.com/how-a-hydrogen-fuel-cell-vehicle-works/>

International Energy Agency. (2006). *Hydrogen Production and Storage*. Retrieved Jan 2016, from <https://www.iea.org/publications/freepublications/publication/hydrogen-production-and-storage.html>

Jeong, H., Kim, K.I., Kim, T.H., Ko, C.H., Park, H.C., Song, I.K. (2006). Hydrogen production by steam reforming of methanol in a micro-channel reactor coated with Cu/ZnO/ZrO₂/Al₂O₃ catalyst. *Journal of Power Sources* 159, 1296-1299.

Johnston, B., Mayo, M.C., Khare, A. (2005). Hydrogen: the energy source for the 21st century. *Technovation* 25, 569-585.

Jones, S.D., Hagelin-Weaver, H.E. (2009). Steam reforming of methanol over CeO₂- and ZrO₂-promoted Cu-ZnO catalysts supported on nanoparticle Al₂O₃. *Applied Catalysis B: Environmental* 90, 195-204.

Jones, S.D., Neal, L.M., Everett, M.L., Hoflund, G.B., Hagelin-Weaver, H.E. (2010). Characterization of ZrO₂-promoted Cu/ZnO/nano-Al₂O₃ methanol steam reforming catalysts. *Applied Surface Science* 256, 7345-7353.

Jones, S.D., Neal, L.M., Hagelin-Weaver, H.E. (2008). Steam reforming of methanol using Cu-ZnO catalysts supported on nanoparticle alumina. *Applied Catalysis B: Environmental* 84, 631-642.

Joseph, D., Basu, S., Jha, S.N., Bhattacharyya, D. (2012). Chemical shifts of K-X-ray absorption edges on copper in different compounds by X-ray absorption spectroscopy (XAS) with Synchrotron radiation. *Nuclear Instruments and Methods in Physics Research Section B: Beam Interactions with Materials and Atoms* 274, 126-128.

Kaewmanee, K., Krammart, P., Sumranwanich, T., Choktaweekarn, P., Tangtermsirikul, S. (2013). Effect of free lime content on properties of cement-fly ash mixtures. *Construction and Building Materials* 38, 829-836.

Kaithwas, A., Prasad, M., Kulshreshtha, A., Verma, S. (2012). Industrial wastes derived solid adsorbents for CO₂ capture: A mini review. *Chemical Engineering Research and Design* 90, 1632-1641.

Karim, A., Bravo, J., Datye, A. (2005a). Nonisothermality in packed bed reactors for steam reforming of methanol. *Applied Catalysis A: General* 282, 101-109.

Karim, A., Bravo, J., Gorm, D., Conant, T., Datye, A. (2005b). Comparison of wall-coated and packed-bed reactors for steam reforming of methanol. *Catalysis Today* 110, 86-91.

Khemthong, P., Photai, P., Grisdanurak, N. (2013). Structural properties of CuO/TiO₂ nanorod in relation to their catalytic activity for simultaneous hydrogen production under solar light. *International Journal of Hydrogen Energy* 38, 15992-16001.

Khunthongkeaw, J., Tangtermsirikul, S., Leelawat, T. (2006). A study on carbonation depth prediction for fly ash concrete. *Construction and Building Materials* 20, 744-753.

Kim, D.H., Woo, S.I., Yang, O.B. (2000). Effect of pH in a sol-gel synthesis on the physicochemical properties of Pd-alumina three-way catalyst. *Applied Catalysis B: Environmental* 26, 285-289.

Kniep, B.L., Girgsdies, F., Ressler, T. (2005). Effect of precipitate aging on the microstructural characteristics of Cu/ZnO catalysts for methanol steam reforming. *Journal of Catalysis* 236, 34-44.

Kocak, Y., Nas, S. (2014). The effect of using fly ash on the strength and hydration characteristics of blended cements. *Construction and Building Materials* 73, 25-32.

Larrubia Vargas, M.A., Busca, G., Costantino, U., Marmottini, F., Montanari, T., Patrono, P., Pinzari, F., Ramis, G. (2007). An IR study of methanol steam reforming over ex-hydrotalcite Cu-Zn-Al catalysts. *Journal of Molecular Catalysis A: Chemical* 266, 188-197.

Lattner, J.R., Harold, M.P. (2005). Comparison of methanol-based fuel processors for PEM fuel cell systems. *Applied Catalysis B: Environmental* 56, 149-169.

Lattner, J.R., Harold, M.P. (2007). Autothermal reforming of methanol: Experiments and modeling. *Catalysis Today* 120, 78-89.

Lee, M.-t., Greif, R., Grigoropoulos, C.P., Park, H.G., Hsu, F.K. (2007). Transport in packed-bed and wall-coated steam-methanol reformers. *Journal of Power Sources* 166, 194-201.

Lee, S.C., Chae, H.J., Lee, S.J., Park, Y.H., Ryu, C.K., Yi, C.K., Kim, J.C. (2009). Novel regenerable potassium-based dry sorbents for CO₂ capture at low temperatures. *Journal of Molecular Catalysis B: Enzymatic* 56, 179-184.

Li, B., Duan, Y., Luebke, D., Morreale, B. (2013). Advances in CO₂ capture technology: A patent review. *Applied Energy* 102, 1439-1447.

Lindström, B., Pettersson, L.J. (2001). Hydrogen generation by steam reforming of methanol over copper-based catalysts for fuel cell applications. *International Journal of Hydrogen Energy* 26, 923-933.

Liu, Y., Hayakawa, T., Suzuki, K., Hamakawa, S., Tsunoda, T., Ishii, T., Kumagai, M. (2002). Highly active copper/ceria catalysts for steam reforming of methanol. *Applied Catalysis A: General* 223, 137-145.

Lorenzut, B., Montini, T., De Rogatis, L., Canton, P., Benedetti, A., Fornasiero, P. (2011). Hydrogen production through alcohol steam reforming on Cu/ZnO-based catalysts. *Applied Catalysis B: Environmental* 101, 397-408.

Matsumura, Y., Ishibe, H. (2009). Selective steam reforming of methanol over silica-supported copper catalyst prepared by sol-gel method. *Applied Catalysis B: Environmental* 86, 114-120.

Matter, P.H., Ozkan, U.S. (2005). Effect of pretreatment conditions on Cu/Zn/Zr-based catalysts for the steam reforming of methanol to H₂. *Journal of Catalysis* 234, 463-475.

Meléndez-Ortiz, H.I., Perera-Mercado, Y., Mercado-Silva, J.A., Olivares-Maldonado, Y., Castruita, G., García-Cerda, L.A. (2014). Functionalization with amine-containing organosilane of mesoporous silica MCM-41 and MCM-48 obtained at room temperature. *Ceramics International* 40, 9701-9707.

Mercedes Maroto-Valer, M., Lu, Z., Zhang, Y., Tang, Z. (2008). Sorbents for CO₂ capture from high carbon fly ashes. *Waste Management* 28, 2320-2328.

Metha PK, Monteiro PJM. (2006). *Concrete, microstructure, properties and materials*. New York: McGraw-Hill.

Mondal, M.K., Balsora, H.K., Varshney, P. (2012). Progress and trends in CO₂ capture/separation technologies: A review. *Energy* 46, 431-441.

Montes-Hernandez, G., Pérez-López, R., Renard, F., Nieto, J.M., Charlet, L. (2009). Mineral sequestration of CO₂ by aqueous carbonation of coal combustion fly-ash. *Journal of Hazardous Materials* 161, 1347-1354.

Mrad, M., Gennequin, C., Aboukais, A., Abi-Aad, E. (2011). Cu/Zn-based catalysts for H₂ production via steam reforming of methanol. *Catalysis Today* 176, 88-92.

Nikulshina, V., Ayesa, N., Gálvez, M.E., Steinfeld, A. (2008). Feasibility of Na-based thermochemical cycles for the capture of CO₂ from air—Thermodynamic and thermogravimetric analyses. *Chemical Engineering Journal* 140, 62-70.

Oh, S.W., Bang, H.J., Bae, Y.C., Sun, Y.-K. (2007). Effect of calcination temperature on morphology, crystallinity and electrochemical properties of nano-crystalline metal oxides (Co₃O₄, CuO, and NiO) prepared via ultrasonic spray pyrolysis. *Journal of Power Sources* 173, 502-509.

Papadakis, V.G. (1999). Effect of fly ash on Portland cement systems: Part I. Low-calcium fly ash. *Cement and Concrete Research* 29, 1727-1736.

Papavasiliou, J., Avgouropoulos, G., Ioannides, T. (2004). Production of hydrogen via combined steam reforming of methanol over CuO–CeO₂ catalysts. *Catalysis Communications* 5, 231-235.

Papavasiliou, J., Avgouropoulos, G., Ioannides, T. (2007). Effect of dopants on the performance of CuO–CeO₂ catalysts in methanol steam reforming. *Applied Catalysis B: Environmental* 69, 226-234.

Patel, S., Pant, K.K. (2006) Activity and stability enhancement of copper–alumina catalysts using cerium and zinc promoters for the selective production of hydrogen via steam reforming of methanol. *Journal of Power Sources* 159, 139-143.

Patel, S., Pant, K.K. (2007). Selective production of hydrogen via oxidative steam reforming of methanol using Cu–Zn–Ce–Al oxide catalysts. *Chemical Engineering Science* 62, 5436-5443.

Patel, S., Pant, K.K. (2009). Kinetic modeling of oxidative steam reforming of methanol over Cu/ZnO/CeO₂/Al₂O₃ catalyst. *Applied Catalysis A: General* 356, 189-200.

Penner-Hahn J.E., n.d. *X-ray Absorption Spectroscopy*, University of Michigan, Ann Arbor, MI, USA. Retrieved Feb 2016, from http://www.umich.edu/~jphgroup/XAS_Course/Harbin/CCC2_XAS.pdf

Peppley, B.A., Amphlett, J.C., Kearns, L.M., Mann, R.F. (1999a). Methanol–steam reforming on Cu/ZnO/Al₂O₃ catalysts. Part 2. A comprehensive kinetic model. *Applied Catalysis A: General* 179, 31-49.

Peppley, B.A., Amphlett, J.C., Kearns, L.M., Mann, R.F. (1999b). Methanol–steam reforming on Cu/ZnO/Al₂O₃. Part 1: the reaction network. *Applied Catalysis A: General* 179, 21-29.

Perego, C., Villa, P. (1997). Catalyst preparation methods. *Catalysis Today* 34, 281-305.

Pevida, C., Plaza, M.G., Arias, B., Feroso, J., Rubiera, F., Pis, J.J. (2008). Surface modification of activated carbons for CO₂ capture. *Applied Surface Science* 254, 7165-7172.

Pillai, U.R., Deevi, S. (2006). Copper-zinc oxide and ceria promoted copper-zinc oxide as highly active catalysts for low temperature oxidation of carbon monoxide. *Applied Catalysis B: Environmental* 65, 110-117.

Pires, J., Bestilleiro, M., Pinto, M., Gil, A. (2008). Selective adsorption of carbon dioxide, methane and ethane by porous clays heterostructures. *Separation and Purification Technology* 61, 161-167.

Ribeiro, R.P.P.L., Grande, C.A., Rodrigues, A.E. (2013). Activated carbon honeycomb monolith – Zeolite 13X hybrid system to capture CO₂ from flue gases employing Electric Swing Adsorption. *Chemical Engineering Science* 104, 304-318.

Sá, S., Silva, H., Brandão, L., Sousa, J.M., Mendes, A. (2010). Catalysts for methanol steam reforming—A review. *Applied Catalysis B: Environmental* 99, 43-57.

Saeki, T., Monteiro, P.J.M. (2005). A model to predict the amount of calcium hydroxide in concrete containing mineral admixtures. *Cement and Concrete Research* 35, 1914-1921.

Sayari, A., Belmabkhout, Y., Serna-Guerrero, R. (2011). Flue gas treatment via CO₂ adsorption. *Chemical Engineering Journal* 171, 760-774.

Shafeeyan, M.S., Daud, W.M.A.W., Houshmand, A., Shamiri, A. (2010). A review on surface modification of activated carbon for carbon dioxide adsorption. *Journal of Analytical and Applied Pyrolysis* 89, 143-151.

Sear, L.K.A. (2001). *The Properties and Use of Coal Fly Ash*, Thomas Telford, London.

Shen, J.-P., Song, C. (2002). Influence of preparation method on performance of Cu/Zn-based catalysts for low-temperature steam reforming and oxidative steam reforming of methanol for H₂ production for fuel cells. *Catalysis Today* 77, 89-98.

Shi, L., Tao, K., Yang, R., Meng, F., Xing, C., Tsubaki, N. (2011). Study on the preparation of Cu/ZnO catalyst by sol-gel auto-combustion method and its application for low-temperature methanol synthesis. *Applied Catalysis A: General* 401, 46-55.

Shi, Y., Du, X., Yang, L., Sun, Y., Yang, Y. (2013). Experiments on hydrogen production from methanol steam reforming in fluidized bed reactor. *International Journal of Hydrogen Energy* 38, 13974-13981.

Shirai, H., Ikeda, M., Tanno, K. (2011). Factors Affecting the Density and Specific Surface Area (Blaine Value) of Fly Ash from Pulverized Coal Combustion. *Energy & Fuels* 25, 5700-5706.

Shishido, T., Yamamoto, Y., Morioka, H., Takaki, K., Takehira, K. (2004). Active Cu/ZnO and Cu/ZnO/Al₂O₃ catalysts prepared by homogeneous precipitation method in steam reforming of methanol. *Applied Catalysis A: General* 263, 249-253.

Shishido, T., Yamamoto, Y., Morioka, H., Takehira, K. (2007). Production of hydrogen from methanol over Cu/ZnO and Cu/ZnO/Al₂O₃ catalysts prepared by homogeneous precipitation: Steam reforming and oxidative steam reforming. *Journal of Molecular Catalysis A: Chemical* 268, 185-194.

Smaoui, N., Bérubé, M.A., Fournier, B., Bissonnette, B., Durand, B. (2005). Effects of alkali addition on the mechanical properties and durability of concrete. *Cement and Concrete Research* 35, 203-212.

Stanmore, B.R., Gilot, P. (2005). Review—calcination and carbonation of limestone during thermal cycling for CO₂ sequestration. *Fuel Processing Technology* 86, 1707-1743.

Szizybalski, A., Girgsdies, F., Rabis, A., Wang, Y., Niederberger, M., Ressler, T. (2005). In situ investigations of structure–activity relationships of a Cu/ZrO₂ catalyst for the steam reforming of methanol. *Journal of Catalysis* 233, 297-307.

Tangtermsirikul, S., Kaewkhluab, T., Jitvutikrai, P., (2004). A compressive strength model for roller-compacted concrete with fly ash, *Magazine of Concrete Research*, pp. 35-44.

TIS 2135. (2002). *Standard Specification for Coal Fly Ash*. Thai Industrial Standards, Bangkok.

Turco, M., Bagnasco, G., Cammarano, C., Senese, P., Costantino, U., Sisani, M. (2007). Cu/ZnO/Al₂O₃ catalysts for oxidative steam reforming of methanol: The role of Cu and the dispersing oxide matrix. *Applied Catalysis B: Environmental* 77, 46-57.

Valdés-Solís, T., Marbán, G., Fuertes, A.B. (2006). Nanosized catalysts for the production of hydrogen by methanol steam reforming. *Catalysis Today* 116, 354-360.

Velu, S., Suzuki, K., Kapoor, M.P., Ohashi, F., Osaki, T. (2001). Selective production of hydrogen for fuel cells via oxidative steam reforming of methanol over CuZnAl(Zr)-oxide catalysts. *Applied Catalysis A: General* 213, 47-63.

Velu, S., Suzuki, K., Okazaki, M., Kapoor, M.P., Osaki, T., Ohashi, F. (2000). Oxidative Steam Reforming of Methanol over CuZnAl(Zr)-Oxide Catalysts for the Selective Production of Hydrogen for Fuel Cells: Catalyst Characterization and Performance Evaluation. *Journal of Catalysis* 194, 373-384.

Wang, L., Ma, L., Wang, A., Liu, Q., Zhang, T. (2007). CO₂ Adsorption on SBA-15 Modified by Aminosilane. *Chinese Journal of Catalysis* 28, 805-810.

Wang, M., Lawal, A., Stephenson, P., Sidders, J., Ramshaw, C. (2011). Post-combustion CO₂ capture with chemical absorption: A state-of-the-art review. *Chemical Engineering Research and Design* 89, 1609-1624.

Wang, X.-Y. (2014). Effect of fly ash on properties evolution of cement based materials. *Construction and Building Materials* 69, 32-40.

Wang, Z., Xi, J., Wang, W., Lu, G. (2003). Selective production of hydrogen by partial oxidation of methanol over Cu/Cr catalysts. *Journal of Molecular Catalysis A: Chemical* 191, 123-134.

Wee, J.-H. (2013). A review on carbon dioxide capture and storage technology using coal fly ash. *Applied Energy* 106, 143-151.

Wirth, Karl and Barth, Andy. (n.d.). *X-Ray Fluorescence (XRF)*, Retrieved Feb 2016, from http://serc.carleton.edu/research_education/geochemsheets/techniques/XRF.html

Wu, K.H., Chang, Y.C., Wang, G.P. (2004). Preparation of NiZn ferrite/SiO₂ nanocomposite powders by sol-gel auto-combustion method. *Journal of Magnetism and Magnetic Materials* 269, 150-155.

“XAS: Theory.” Chemwiki, Retrieved Feb 2016, from http://chemwiki.ucdavis.edu/Physical_Chemistry/Spectroscopy/X-ray_Spectroscopy/XAS%3A_Theory

“X-ray absorption spectroscopy.” Wikipedia: The Free Encyclopedia. Wikimedia Foundation, Inc. (2016). Retrieved Feb 2016, from https://en.wikipedia.org/wiki/X-ray_absorption_spectroscopy

“X-ray fluorescence.” Wikipedia: The Free Encyclopedia. Wikimedia Foundation, Inc. (2015). Retrieved Jan 2016, from https://en.wikipedia.org/wiki/X-ray_fluorescence

Xu, J., Yeung, C.M.Y., Ni, J., Meunier, F., Acerbi, N., Fowles, M., Tsang, S.C. (2008). Methane steam reforming for hydrogen production using low water-ratios without carbon formation over ceria coated Ni catalysts. *Applied Catalysis A: General* 345, 119-127.

Yamei, Z., Wei, S., Lianfei, S., (1997). Mechanical properties of high performance concrete made with high calcium sulfate fly ash. *Cement and Concrete Research* 27 (7), 1093-1098.

Yang, H., Xu, Z., Fan, M., Gupta, R., Slimane, R.B., Bland, A.E., Wright, I. (2008). Progress in carbon dioxide separation and capture: A review. *Journal of Environmental Sciences* 20, 14-27.

Yang, J., Zheng, H.-Y., Zhu, Y.-L., Zhao, G.-W., Zhang, C.-H., Teng, B.-T., Xiang, H.-W., Li, Y. (2004). Effects of calcination temperature on performance of Cu–Zn–Al catalyst for synthesizing γ -butyrolactone and 2-methylfuran through the coupling of dehydrogenation and hydrogenation. *Catalysis Communications* 5, 505-510.

Yao, C.-Z., Wang, L.-C., Liu, Y.-M., Wu, G.-S., Cao, Y., Dai, W.-L., He, H.-Y., Fan, K.-N. (2006). Effect of preparation method on the hydrogen production from methanol steam reforming over binary Cu/ZrO₂ catalysts. *Applied Catalysis A: General* 297, 151-158.

Yong-Feng, L., Xin-Fa, D., Wei-Ming, L. (2004). Effects of ZrO₂-promoter on catalytic performance of CuZnAlO catalysts for production of hydrogen by steam reforming of methanol. *International Journal of Hydrogen Energy* 29, 1617-1621.

Yoon, H.C., Otero, J., Erickson, P.A. (2007). Reactor design limitations for the steam reforming of methanol. *Applied Catalysis B: Environmental* 75, 264-271.

Yue, M.B., Sun, L.B., Cao, Y., Wang, Z.J., Wang, Y., Yu, Q., Zhu, J.H. (2008). Promoting the CO₂ adsorption in the amine-containing SBA-15 by hydroxyl group. *Microporous and Mesoporous Materials* 114, 74-81.

Zeleňák, V., Badaničová, M., Halamová, D., Čejka, J., Zukal, A., Murafa, N., Goerigk, G. (2008). Amine-modified ordered mesoporous silica: Effect of pore size on carbon dioxide capture. *Chemical Engineering Journal* 144, 336-342.

Zelenak, V., Halamova, D., Gaberova, L., Bloch, E., Llewellyn, P. (2008). Amine-modified SBA-12 mesoporous silica for carbon dioxide capture: Effect of amine basicity on sorption properties. *Microporous and Mesoporous Materials* 116, 358-364.

Zhang, J., Singh, R., Webley, P.A. (2008). Alkali and alkaline-earth cation exchanged chabazite zeolites for adsorption based CO₂ capture. *Microporous and Mesoporous Materials* 111, 478-487.

Zhao, H., Hu, J., Wang, J., Zhou, L., Liu, H. (2007a). CO₂ Capture by the Amine-modified Mesoporous Materials. *Acta Physico-Chimica Sinica* 23, 801-806.

Zhao, Z., Cui, X., Ma, J., Li, R. (2007b). Adsorption of carbon dioxide on alkali-modified zeolite 13X adsorbents. *International Journal of Greenhouse Gas Control* 1, 355-359.



Appendix A

Analytical methods

A.1 Gas chromatography (GC)

A gas chromatograph is a chemical analysis instrument for separating chemicals in a complex sample. A gas chromatograph uses a flow-through narrow tube known as the column, through which different chemical constituents of a sample pass in a gas stream (carrier gas, mobile phase) at different rates depending on their various chemical and physical properties and their interaction with a specific column filling, called the stationary phase. As the chemicals exit the end of the column, they are detected and identified electronically. The function of the stationary phase in the column is to separate different components, causing each one to exit the column at a different time (retention time). Other parameters that can be used to alter the order or time of retention are the carrier gas flow rate, and the temperature.

In a GC analysis, a known volume of gas is injected into the entrance of the column, usually using a micro-syringe. As the carrier gas sweeps the gas sample molecules through the column, this motion is inhibited by the adsorption of the gas molecules either onto the column walls or onto packing materials in the column. The rate at which the molecules progress along the column depends on the strength of adsorption, which in turn depends on the type of molecule and on the stationary phase materials. Since each type of molecule has a different rate of progression, the various components of the gas mixture are separated as they progress along the column and reach the end of the column at different times (retention time). A detector is used to monitor the outlet stream from the column; thus, the time at which each component reaches the outlet and the amount of that component can be determined. Generally, substances are identified (qualitatively) by the order in which they emerge from the column and by the retention time of the gas sample in the column. The area under a peak is proportional to the amount of analyzed present in the chromatogram. The area of the peak can be calculated using the mathematical function of integration. The Concentration of the gas sample can be calculated using a calibration curve created from a standard gas.

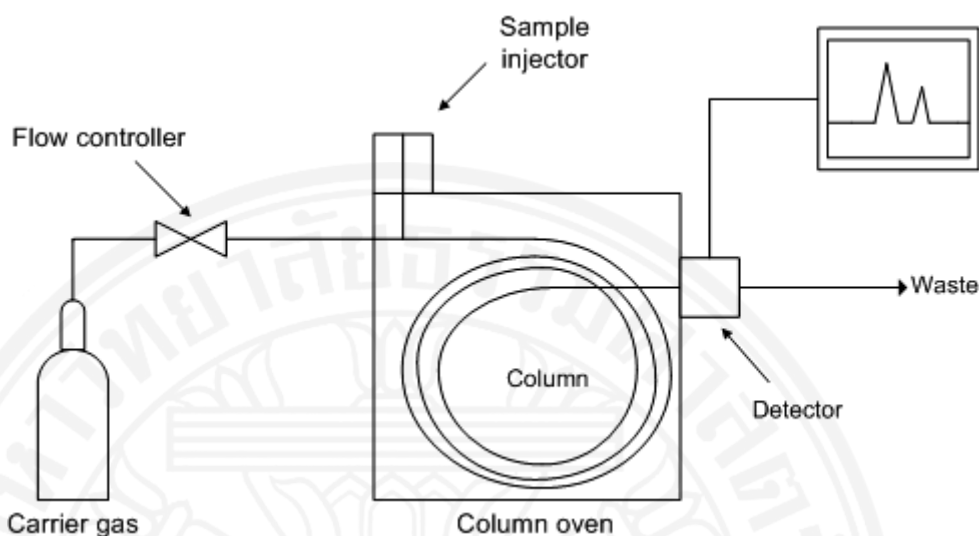


Figure A.1-1 Schematic of gas chromatograph



Figure A.1-2 Gas chromatograph (Perkin Elmer- Autosystem XL)

A Perkin Elmer (Waltham, Mass., USA) Autosystem XL gas chromatograph with Porapak Q column (Supleco, Bellefonte, PA, USA) coupled with a thermal conductivity detector (TCD) was used to determine the amount of hydrogen production. The GC was linked to a computer for automatic determination of peak areas, which could be converted to concentration.

A.2 Brunauer-Emmett-Teller (BET) surface area

The specific surface area of a powder is determined by physical adsorption of a gas on the surface of the solid and by calculating the amount of adsorbate gas corresponding to a monomolecular layer on the surface. Physical adsorption results from relatively weak forces (van der Waals forces) between the adsorbate gas molecules and the adsorbent surface area of the test powder. The determination is usually carried out at the temperature of liquid nitrogen. The amount of gas adsorbed can be measured by a volumetric or continuous flow procedure (Brunauer, Emmett and Teller (BET) Theory, 2016).

The concept of the theory is an extension of the Langmuir theory, which is a theory for monolayer molecular adsorption, to multilayer adsorption with the following hypotheses: (a) gas molecules physically adsorb on a solid in layers infinitely; (b) there is no interaction between each adsorption layer; and (c) the Langmuir theory can be applied to each layer. The resulting BET equation is expressed by:

$$\frac{1}{V_a \left(\frac{P_o}{P} - 1 \right)} = \frac{C - 1}{V_m C} \times \frac{P}{P_o} + \frac{1}{V_m C} \quad (\text{A.2-1})$$

P = partial vapour pressure of adsorbate gas in equilibrium with the surface at 77.4 K (b.p. of liquid nitrogen), in pascals,

P_o = saturated pressure of adsorbate gas, in pascals,

V_a = volume of gas adsorbed at standard temperature and pressure (STP) [273.15 K and atmospheric pressure (1.013×10^5 Pa)], in millilitres,

V_m = volume of gas adsorbed at STP to produce an apparent monolayer on the sample surface, in millilitres,

C = dimensionless constant that is related to the enthalpy of adsorption of the adsorbate gas on the powder sample.

A value of V_a is measured at each of not less than 3 values of P/P_o . Then the BET value is plotted against P/P_o according to equation A2-1. This plot should yield a straight line usually in the approximate relative pressure range 0.05 to 0.3. The data

are considered acceptable if the correlation coefficient, r , of the linear regression is not less than 0.9975; that is, r^2 is not less than 0.995. From the resulting linear plot, the slope, which is equal to $(C - 1)/V_m C$, and the intercept, which is equal to $1/V_m C$, are evaluated by linear regression analysis. From these values, V_m is calculated as $1/(\text{slope} + \text{intercept})$, while C is calculated as $(\text{slope}/\text{intercept}) + 1$. From the value of V_m so determined, the specific surface area, S , in $\text{m}^2 \cdot \text{g}^{-1}$, is calculated by the equation:

$$S_{total} = \frac{V_m N s}{V} \quad (\text{A.2-2})$$

$$S = \frac{S_{total}}{a} \quad (\text{A.2-3})$$

N = Avogadro constant ($6.022 \times 10^{23} \text{ mol}^{-1}$),

s = adsorbate cross section

a = mass of test powder, in grams,

V = volume occupied by 1 mole of the adsorbate gas at STP allowing for minor departures from the ideal, in millilitres.

A.3 Scanning Electron Microscope (SEM)

Electron microscopy can be used for direct observation of catalyst morphology with a magnification tunable in the range of 10^4 - 10^{10} m. The image of SEM can show the information of shape and size of the catalyst including a distribution of active metal over catalyst supports.

In general principles of SEM, an electron beam is focused by lenses placed before the specimen to obtain a very small electron probe directed onto the specimen. The electron beam has an energy ranging from a few hundred electron volts (eV) to 40 keV, is focused by one or two condenser lenses to a spot about 0.4 nm to 5 nm in diameter. The beam passes through pairs of scanning coils or pairs of deflector plates in the electron column, typically in the final lens, which deflect the beam in the x and y axes so that it scans over a rectangular area of the sample surface.

The interaction between the electron probe and the atoms in the small irradiated volume of specimen gives rise to different types of signals which are recorded by specific detectors and which can be used for imaging or for analytical purposes.

The energy exchange between the electron beam and the sample results in the reflection of high-energy electrons by elastic scattering, emission of secondary electrons by inelastic scattering and the emission of electromagnetic radiation, each of which can be detected by specialized detectors. The beam current absorbed by the specimen can also be detected and used to create images of the distribution of specimen current. Electronic amplifiers of various types are used to amplify the signals which are displayed as variations in brightness on a cathode ray tube (CRT). The raster scanning of the CRT display is synchronized with that of the beam on the specimen in the microscope, and the resulting image is therefore a distribution map of the intensity of the signal being emitted from the scanned area of the specimen. The image can be digitally captured and displayed on a computer monitor and saved to a computer's hard disc. X-rays, which are also produced by the interaction of electrons with the sample, may also be detected in an SEM equipped with energy dispersive spectroscopy.

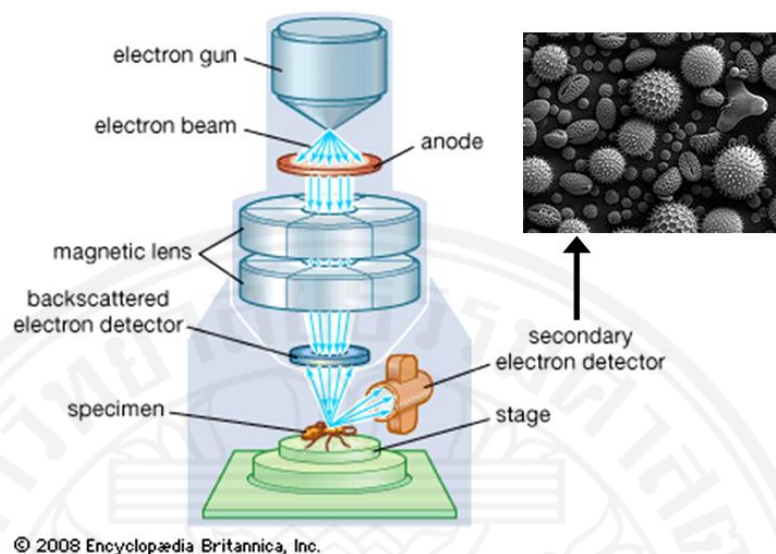


Figure A.3-1 Schematic of scanning electron microscope



Figure A.3-2 Scanning electron microscope (JEOL JSM-5410)

The surfaces of the catalysts were inspected by a scanning electron microscope (SEM) from JEOL JSM-5410, Jeol Inc., Tokyo, Japan. The elemental composition of the catalyst surface was determined by energy dispersive spectrometry (EDS, Oxford) which the SEM was equipped with.

A.4 N₂O Chemisorption

Pulse injection adsorption method (chemisorption) is the widely known qualitative method to evaluate catalyst, there is metal dispersion measurement by chemisorption with the use of adsorbed gas. Metal dispersion measurement by pulse injection is to introduce adsorbed gas to the sample until the saturated chemisorption, and measure the metal surface area of the sample from the total gas chemisorption. Metal dispersion and size of metal particles can be calculated from the metal surface area and the weight.

There are various measurement instruments and measurement methods, but in case of using the automated flow-type instrument, you can first oxidize or reduce the sample by heating in order to expose the clean surface of the rare metal. Then introduce certain volume of chemisorption gas by using 6-way valve. Normally, introduce enough volume and concentration of chemisorption gas to achieve the saturated chemisorption by the second or third time. You can calculate the volume of chemisorption from the difference in the volume of gas you introduced and volume of gas remaining in the sample cell (BEL JAPAN, INC, 2012).

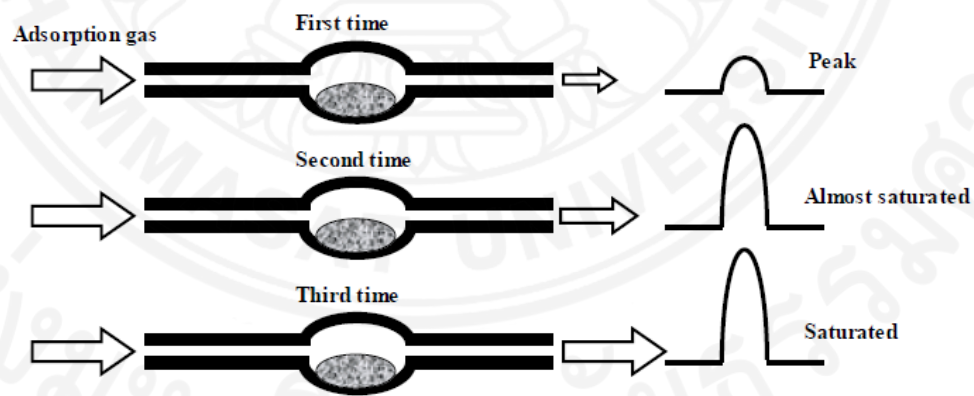


Figure A.4-1 Pulse injection measurement

Amount of adsorption per unit [amount of adsorption per 1g of sample], V_m (cm^3/g)

$$V_m = \frac{V_{Chem}}{m} \quad (\text{A.4-1})$$

where, V_{Chem} is amount of adsorption (cm^3), m is sample weight (g).

Metal dispersion [percentage of metal surface exposure], D_m (%)

$$D_m = \frac{V_{Chem}}{c \times 22414 \times SF \times MW} \times 100 \quad (\text{A.4-2})$$

where, V_{Chem} is amount of adsorption (cm^3), MW is atomic weight of metal (g/mol), m is sample weight, SF is stoichiometry factor and c is metal weight (g)

$$c = \frac{m \times p}{100} \quad (\text{A.4.3})$$

where, p is weight percentage of supported metal content (wt%)

Surface area of metal [surface area of metal per 1 g of sample], A_m (m^2/g)

$$A_m = \frac{V_{Chem}}{m \times 22414 \times SF \times 6.02 \times 10^{23} \times \sigma_m \times 10^{-18}} \quad (\text{A.4-4})$$

Size of metal particle [diameter assuming metal particle is spherical] d (nm)

$$d = \frac{6000}{A_m(\text{metal}) \times \rho} \quad (\text{A.4.5})$$

where, ρ is density of metal (g/cm^3), A_m (metal) is surface area of metal per 1 g of supported metal.

$$A_m(\text{metal}) = \frac{V_{Chem}}{c \times 22414 \times SF \times 6.02 \times 10^{23} \times \sigma_m \times 10^{-18}} \quad (\text{A.4.6})$$

In this work, Cu metal was used as catalyst and N_2O was used as an adsorption gas for chemisorption with SF equal 2. The molecular weight of Cu is 63.546 mol/g, density is $8.960 \text{ g}/\text{cm}^3$ and surface area is $0.0680 \text{ nm}^2/\text{atom}$.

A.5 X-ray Diffraction (XRD)

X-ray diffraction (XRD) has been generally used for characterization of supported catalyst crystallites. XRD is also used to estimate of the crystallite size of the catalysts. The diffraction pattern is the fingerprint of a crystalline phase and powder diffraction is used to identify the mixture of the phases on the catalysts.

X-ray diffraction is commonly used to identify unknown crystalline substances, by comparing diffraction data against a database maintained by the International Centre for Diffraction Data. The peaks in an x-ray diffraction pattern are directly related to the atomic distances as described in the Bragg's equation.

$$2d\sin\theta = n\lambda \quad (\text{A.5-1})$$

In the equation, d is the distance between atomic planes in crystalline materials; θ is the scattering angle; n is an integer representing the order of the diffraction peak and λ is the x-ray wavelength. The x-ray diffraction can also be used for determining crystalline size in crystalline materials. An effect of the finite crystallite size can be seen as a broadening of the peaks in an x-ray diffraction as is explained by the Scherrer's equation.

$$\tau = \frac{K\lambda}{\beta\cos\theta} \quad (\text{A.5-2})$$

where τ is the mean crystallite dimension, K is the shape factor, λ is the x-ray wavelength, typically 1.54 Å, β is the line broadening at half the maximum intensity (FWHM) in radians, and θ is the scattering angle. The dimensionless shape factor has a typical value of about 0.9, but varies with the actual shape of the crystallite. The Scherrer equation is limited to nano-scale particles. It is not applicable to crystals larger than about 100 nm.

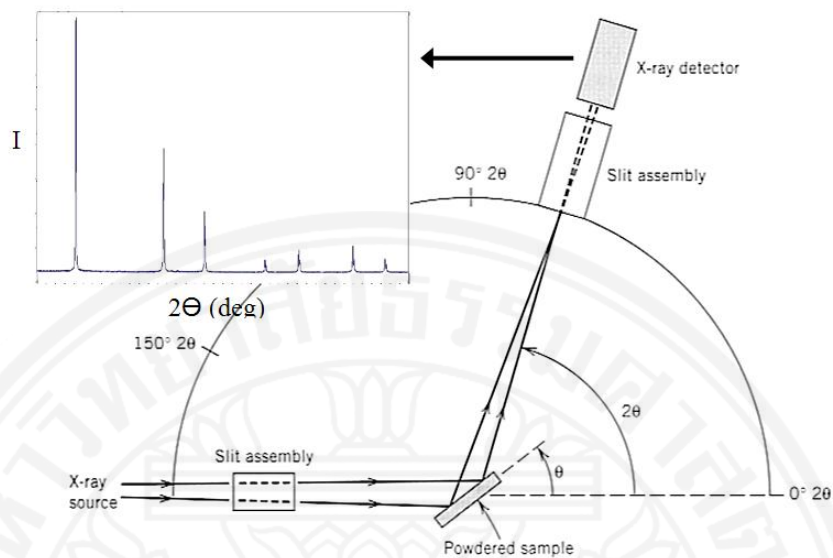


Figure A.5-1 Schematic of x-ray diffractometer

The catalyst supports (α - Al_2O_3 , γ - Al_2O_3 and ZrO_2 doped Al_2O_3 .) were characterized using an X-ray diffraction (X'Pert PRO diffractometer, Panalytical, Almelo,) using $\text{Cu K}\alpha_1$ radiation, 2θ between 20° - 75° , 0.02° step size, and 0.5 sec step time. Phase identification of the supports was determined by using JADE software (Jade Software Corporation Ltd., Christchurch, New Zealand) which compares to references of XRD databases from the International Centre for Diffraction Data (Newtown Square, PA, USA). The XRD pattern references of α - Al_2O_3 , γ - Al_2O_3 and ZrO_2 are JCPDS NO.: 46-1212, JCPDS No.: 04-0880, and JCPDS No.: 50-1089, respectively.

A.6 X-ray fluorescence (XRF)

X-ray fluorescence (XRF) is the emission of characteristic "secondary" (or fluorescent) X-rays from a material that has been excited by bombarding with high-energy X-rays or gamma rays. The phenomenon is widely used for elemental analysis and chemical analysis, particularly in the investigation of metals, glass, ceramics and building materials, and for research in geochemistry, forensic science, archaeology and art objects such as paintings and murals.

When materials are exposed to short-wavelength X-rays or to gamma rays, ionization of their component atoms may take place. Ionization consists of the ejection of one or more electrons from the atom, and may occur if the atom is exposed to radiation with energy greater than its ionization potential. X-rays and gamma rays can be energetic enough to expel tightly held electrons from the inner orbitals of the atom. The removal of an electron in this way makes the electronic structure of the atom unstable, and electrons in higher orbitals "fall" into the lower orbital to fill the hole left behind. In falling, energy is released in the form of a photon, the energy of which is equal to the energy difference of the two orbitals involved. Thus, the material emits radiation, which has energy characteristic of the atoms present. The term fluorescence is applied to phenomena in which the absorption of radiation of a specific energy results in the re-emission of radiation of a different energy (generally lower) (X-ray fluorescence, 2015).

X-Ray fluorescence is particularly well-suited for investigations that involve

- bulk chemical analyses of major elements (Si, Ti, Al, Fe, Mn, Mg, Ca, Na, K, P) in rock and sediment
- bulk chemical analyses of trace elements (in abundances >1 ppm; Ba, Ce, Co, Cr, Cu, Ga, La, Nb, Ni, Rb, Sc, Sr, Rh, U, V, Y, Zr, Zn) in rock and sediment - detection limits for trace elements are typically on the order of a few parts per million

X-ray fluorescence is limited to analysis of

- relatively large samples, typically > 1 gram
- materials that can be prepared in powder form and effectively homogenized

- materials for which compositionally similar, well-characterized standards are available
- materials containing high abundances of elements for which absorption and fluorescence effects are reasonably well understood

In most cases for rocks, ores, sediments and minerals, the sample is ground to a fine powder. At this point it may be analyzed directly, especially in the case of trace element analyses. However, the very wide range in abundances of different elements, especially iron, and the wide range of sizes of grains in a powdered sample, makes the proportionality comparison to the standards particularly troublesome. For this reason, it is common practice to mix the powdered sample with a chemical flux and use a furnace or gas burner to melt the powdered sample. Melting creates a homogenous glass that can be analyzed and the abundances of the elements calculated (Wirth and Barth, n.d.).

A.7 X-ray Absorption Spectroscopy (XAS)

X-ray Absorption Spectroscopy (XAS) is a broadly used method to investigate atomic local structure as well as electronic states. An X-ray strikes an atom and excites a core electron that can either be promoted to an unoccupied level, or ejected from the atom. Both of these processes will create a core hole.

The electrons that are excited are typically from the 1s or 2p shell, so the energies are on the order of thousands of electron volts. XAS therefore requires high-energy X-ray excitation, which occurs at synchrotron facilities. X-ray energy is about 10^4 eV (where "soft x-rays" are between 100 eV- 3 keV and "hard x-rays" are above 3 keV) corresponding to wavelengths around 1 Angstrom. This wavelength is on the same order of magnitude as atom-atom separation in molecular structures, so XAS is a useful tool to deduce local structure of atoms. XAS is also utilized in analyzing materials based on their characteristic X-ray absorption "fingerprints." It is possible to deduce local atomic environments of each separate type of atom in a compound. XAS is particularly convenient because it is a non-destructive method to examine samples directly. Structures can be determined from samples that are both heterogeneous and amorphous.

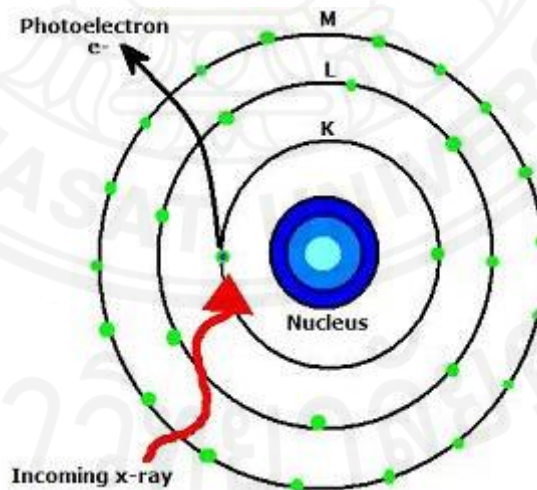


Figure A.7-1 Atom absorbing X-ray with subsequent core-electron ejection (XAS: Theory, n.d.)

X-ray Absorption Edges

Figure A.7-2 illustrated the absorption edge from XAS spectrum. The absorption edge is not simply a discontinuous increase in absorption, but in fact shows significant structure both in the immediate vicinity of the edge jump and well above the edge. The structure in the vicinity of the edge is sometimes referred to as X-ray absorption near-edge structure (XANES). The oscillations above the edge, which can extend for 1,000 eV or more, are often referred to as extended X-ray absorption fine structure (EXAFS). The distinction between XANES and EXAFS is arbitrary, since the same fundamental physical principles govern photo absorption over the entire XAS region and there is no unambiguous definition that distinguishes between “near-edge” and “extended” structure. In an attempt to emphasize the essential similarity of these regions, the term XAFS (X-ray absorption fine structure) has gained some currency as a reference to the entire structured absorption region. Nevertheless, the terms EXAFS and XANES remain the most widely used, with some justification, since the XANES and EXAFS regions are generally analyzed differently. As described in detail below, the XANES region is sensitive to oxidation state and geometry, but is not, in most cases, analyzed quantitatively. The EXAFS region is sensitive to the radial distribution of electron density around the absorbing atom and is used for quantitative determination of bond length and coordination number.

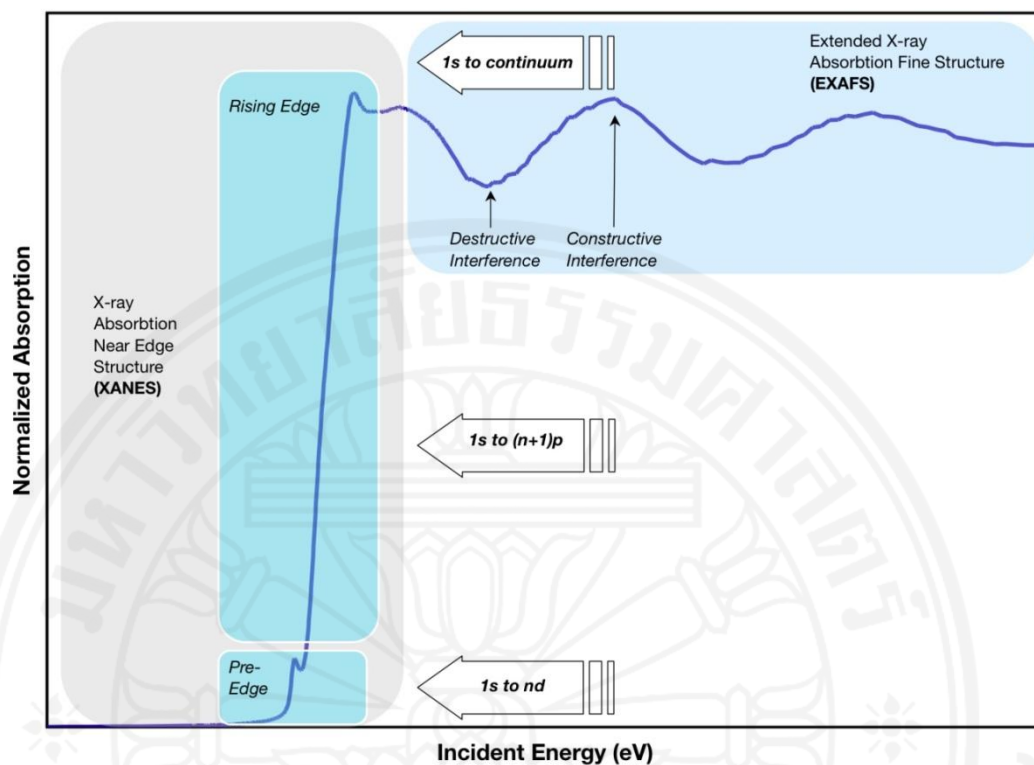


Figure A.7-2 XANES and EXAFS regions of XAS data (X-ray absorption spectroscopy, 2016)

X-Ray Absorption Near Edge Structure (XANES)

It is clear that the region is more complex than simply an abrupt increase in absorption cross-section. There are several weak transitions below the edge (pre-edge transitions) together with structured absorption on the high energy side of the edge. Some XANES spectra show intense narrow transitions on the rising edge (these can be much more intense than the transition at the edge in Figure A.7-2). These are often referred to as “white lines” in reference to the fact that when film was used to record X-ray absorption spectra, an intense transition would absorb all of the incident X rays, thus preventing the film from being exposed and leaving a white line on the film. Above the edge, there are a variety of structures that show generally oscillatory behavior, ultimately becoming the EXAFS oscillations.

The same physical principles govern both the EXAFS region and the XANES region. However, in the near edge region the photoelectron has low kinetic energy, giving it a long mean-free path. These effects combine to make the XANES region

sensitive to longer distance absorber-scatterer interactions than are typically sampled by EXAFS. This greatly complicates simulation of XANES structure, since many interactions and a large number of multiple scattering path ways need to be included. However, the sensitivity to multiple scattering is, at least in principle, an advantage since it provides the possibility of extracting information about the three-dimensional structure from XANES spectra. Although much progress has been made recently in the theoretical modeling of XANES, most simulations of XANES structure remain qualitative. Nevertheless, the ability to make even qualitative fingerprint-like comparisons of XANES spectra can be important. If a representative library of reference spectra is available, spectral matching can be used to identify an unknown. Beyond this qualitative application, there are three main ways in which XANES spectra are used: to determine oxidation state, to deduce three-dimensional structure, and as a probe of electronic structure (Penner-Hahn J.E., n.d.).

Appendix B

Chemical properties

B.1 α -alumina

Product Name:	Aluminum oxide
Company Name:	Sigma-Aldrich
CAS-No:	1344-28-1 (Product No. 11028)
Formula:	Al_2O_3
Appearance	Form: solid
Odor:	Odorless
Melting Point:	Melting point/range: 2.040 °C - lit
Boiling Point:	Boiling range 2.980 °C
Solubility in Water:	Insoluble
Specific Gravity:	4.000
Molecular Weight:	101.96 g/mol

B.2 γ -alumina

Product Name:	Alumina
Company Name:	Sigma-Aldrich
CAS-No:	1344-28-1 (Product No. 199974)
Formula:	Al_2O_3
Appearance	Form: solid
Odor:	Odorless
Melting Point:	Melting point/range: 2.040 °C - lit
Boiling Point:	Boiling range 2.980 °C
Solubility in Water:	Insoluble
Specific Gravity:	4.000
Molecular Weight:	101.96 g/mol

B.3 Ammonium chloride

Product Name:	Ammonium chloride
Company Name:	Ajax Finechem
CAS-No:	12125-02-9
Formula:	NH ₄ Cl
Appearance	Colorless crystals or crystal masses; or white, granular powder; hygroscopic (absorbs moisture from the air)
Odor:	Odorless
Melting Point:	Sublimes at 340 °C
Boiling Point:	520 °C
Solubility in Water:	Very soluble. (374 g/L at 20 °C)
Solubility in Organic Solvents:	Soluble in liquid ammonia, methanol, ethanol, almost insoluble in acetone, ether, ethyl acetate
Specific Gravity:	1.5274 (25 °C)
pH Value	5.5 (1% aqueous solution at 25 °C)
Vapor Pressure:	1 mmHg (0.133 kPa at 160.4 °C)
Vapor Density (Air=1):	1.9
Molecular Weight:	53.49 g/mol
Other Information:	Conversion factor 1 ppm = 2.183 mg/m ³ ; 1 mg/m ³ = 0.458 ppm at 25°C

B.4 Ammonium hydroxide solution

Product Name:	Ammonium hydroxide solution
Company Name:	Sigma-Aldrich
CAS-No:	1336-21-6
Formula:	H_5NO
Appearance	Liquid, colorless
Melting Point:	-60 °C
Boiling Point:	38°C at 1.013 hPa
Specific Gravity:	1.5274 (25°C)
pH Value	5.5 (1% aqueous solution at 25°C)
Vapor Pressure:	153 hPa at 20 °C
Vapor Density (Air=1):	1.21
Flammable Limits-Lower:	16 %(V)
Flammable Limits-Upper:	27 %(V)
Molecular Weight:	35.05 g/mol

B.5 Aluminium nitrate

Product Name:	Aluminum nitrate nonahydrate
Company Name:	Sigma-Aldrich
CAS-No:	7784-27-2
Formula:	$\text{AlN}_3\text{O}_9 \cdot 9\text{H}_2\text{O}$
Appearance	Form: solid, Color: colorless
Melting Point:	Melting point/range: 73 °C - lit.
pH Value	2.5 – 3.5 at 50 g/l at 25 °C
Molecular Weight:	375.13 g/mol

B.6 Citric acid

Product Name:	Citric acid monohydrate
Company Name:	Ajax Finechem
CAS-No:	5949-29-1
Formula:	$\text{HOC}(\text{COOH})(\text{CH}_2\text{COOH})_2 \cdot \text{H}_2\text{O}$
Appearance	Solid
Odor:	Colorless, translucent crystals, or white, crystalline powder
Melting Point:	153°C
Boiling Point:	Decomposes
Solubility in Water:	Soluble
Solubility in Organic Solvents:	Very soluble in ethyl alcohol, methyl alcohol, propyl alcohol;
Specific Gravity:	1.665 (18 °C)
pH Value	2.2 (0.1 N)
Auto-Ignition Temperature:	1010 °C
Molecular Weight:	210.14 g/mol
Other Information:	pKa1 = 3.14, pKa2 = 4.77, pKa3 = 6.39

B.7 Copper nitrate trihydrate

Product Name:	Copper (II) nitrate trihydrate
Company Name:	Fluka
CAS-No:	10031-43-3
Formula:	$\text{CuN}_2\text{O}_6 \cdot 3\text{H}_2\text{O}$
Appearance	Form: crystalline, Color: dark blue
Molecular Weight:	241.60 g/mol

B.8 EDTA di-sodium salt

Product Name:	EDTA Disodium Salt
Company Name:	LOMB SCIENTIFIC PTY LTD
CAS-No:	139-33-3
Formula:	$C_{10}H_{14}N_2Na_2O_8 \cdot 2H_2O$
Appearance	White powder at 25°C
Odor:	Odorless
Melting Point:	Decomposes prior to melting
Boiling Point:	Not applicable
Solubility in Water:	100 g/l (approximate)
Solubility in Organic Solvents:	No data available
Specific Gravity:	Bulk density: 600 kg/m ³ (approximate)
pH Value	4-5 (1% solution)
Flammability:	Combustible solid
Auto-Ignition Temperature:	>200 °C (glowing temperature of 5 mm product layer)
Flammable Limits-Lower:	40 g/m ³
Flammable Limits-Upper:	Not available
Molecular Weight:	372.24 g/mol

B.9 Ethanol

Product Name:	Ethanol
Company Name:	Merck
CAS-No:	64-17-5
Formula:	C ₂ H ₅ OH
Appearance	Liquid (colourless)
Odor:	Alcohol-like
Melting Point:	-114.5°C
Boiling Point:	78.3 °C
Solubility in Water:	At 20 °C, completely miscible
Specific Gravity:	0.790-0.793
pH Value	7.0
Vapor Pressure:	59 hPa at 20 °C
Vapor Density (Air=1):	1.6
Flash Point:	12 °C
Flammable Limits-Lower:	3.5% (V)
Flammable Limits-Upper:	15% (V)
Molecular Weight:	46.07 g/mol
Other Information:	Ignition temperature 425 °C (DIN 51794) Conductivity < 1µS/cm

B.10 Ethanolamine

Product Name:	Monoethanolamine
Company Name:	UNILAB Reagent
CAS-No:	141-43-5
Formula:	C ₂ H ₇ NO
Appearance	Transparent, colorless, liquid
Odor:	Mild ammoniacal odor
Melting Point:	Not available
Boiling Point:	170.4°C @ 1013 hPa
Solubility in Water:	100 at 20°C
Specific Gravity:	1.018 at 20°C
pH Value	No data available
Vapor Pressure:	0.27 hPa @ 20°C
Vapor Density (Air=1):	2.1
Evaporation Rate:	No data available
Flash Point:	96.1°C Method: Pensky-Martens Closed Cup ASTM D 93. 104.4°C Method: Cleveland Open Cup ASTM D 92.
Molecular Weight:	61.08 g/mol
Other Information:	Evaporation rate (Butyl acetate = 1): 0.02. Freezing Point 10.5°C.

B.11 Eriochrome black T

Product Name:	Eriochrome Black T
Company Name:	PANREAC QUIMICA S.L.U.
CAS-No:	1787-61-7
Formula:	$C_{20}H_{12}N_3NaO_7S$
Appearance	Solid
Odor:	Odorless
Solubility in Water:	80 g/l in water 20°C
Solubility in Organic Solvents:	10 g/l in alcohol
Specific Gravity:	3.7
Molecular Weight:	461.38 g/mol

B.12 Methanol

Product Name:	Methanol
Company Name:	Merck
CAS-No:	67-56-1
Formula:	CH ₃ OH
Appearance	liquid
Odor:	characteristic
Melting Point:	-98 °C
Boiling Point:	64.5 °C
Solubility in Water:	at 20 °C soluble
Specific Gravity:	0.792 g/cm ³ at 20 °C
Vapor Pressure:	128 hPa at 20 °C
Vapor Density (Air=1):	1.11
Evaporation Rate:	6.3 Reference substance: Diethylether
Flash Point:	10 °C Method: c.c.
Auto-Ignition Temperature:	455 °C
Flammable Limits-Lower:	5.5 %(V)
Flammable Limits-Upper:	44 %(V)
Molecular Weight:	32.04 g/mol

B.13 Urea

Product Name:	Urea
Company Name:	Carlo Erba
CAS-No:	57-13-6
Formula:	CH ₄ N ₂ O
Appearance	Solid (white)
Odor:	Ammonia-like
Melting Point:	135°C
Boiling Point:	Underdetermined
Solubility in Water:	1080 g/l
Solubility in Organic Solvents:	Soluble in alcohols
Specific Gravity:	1.323
pH Value	9.2-9.5
Vapor Pressure:	2 hPa
Flammability:	Product is not flammable
Molecular Weight:	60.06 g/mol
Other Information:	No data available

B.14 Zinc nitrate hexahydrate

Product Name:	Zinc nitrate hexahydrate
Company Name:	Fluka
CAS-No:	10196-18-6
Formula:	N ₂ O ₆ Zn · 6H ₂ O
Appearance	Form: crystalline, Color: colorless
Melting Point:	Melting point/range: 36 °C
Molecular Weight:	297.49 g/mol

B.15 Zirconium dinitrate oxide hydrate

Product Name:	Zirconium dinitrate oxide hydrate
Company Name:	Fluka
CAS-No:	14985-18-3
Formula:	$\text{ZrO}(\text{NO}_3)_2 \cdot 6\text{H}_2\text{O}$
Appearance	Powder (white)
Molecular Weight:	231.23 g/mol

Appendix C

SEM of Catalysts

C.1 SEM of Cu-Zn/ α -Al₂O₃ without urea

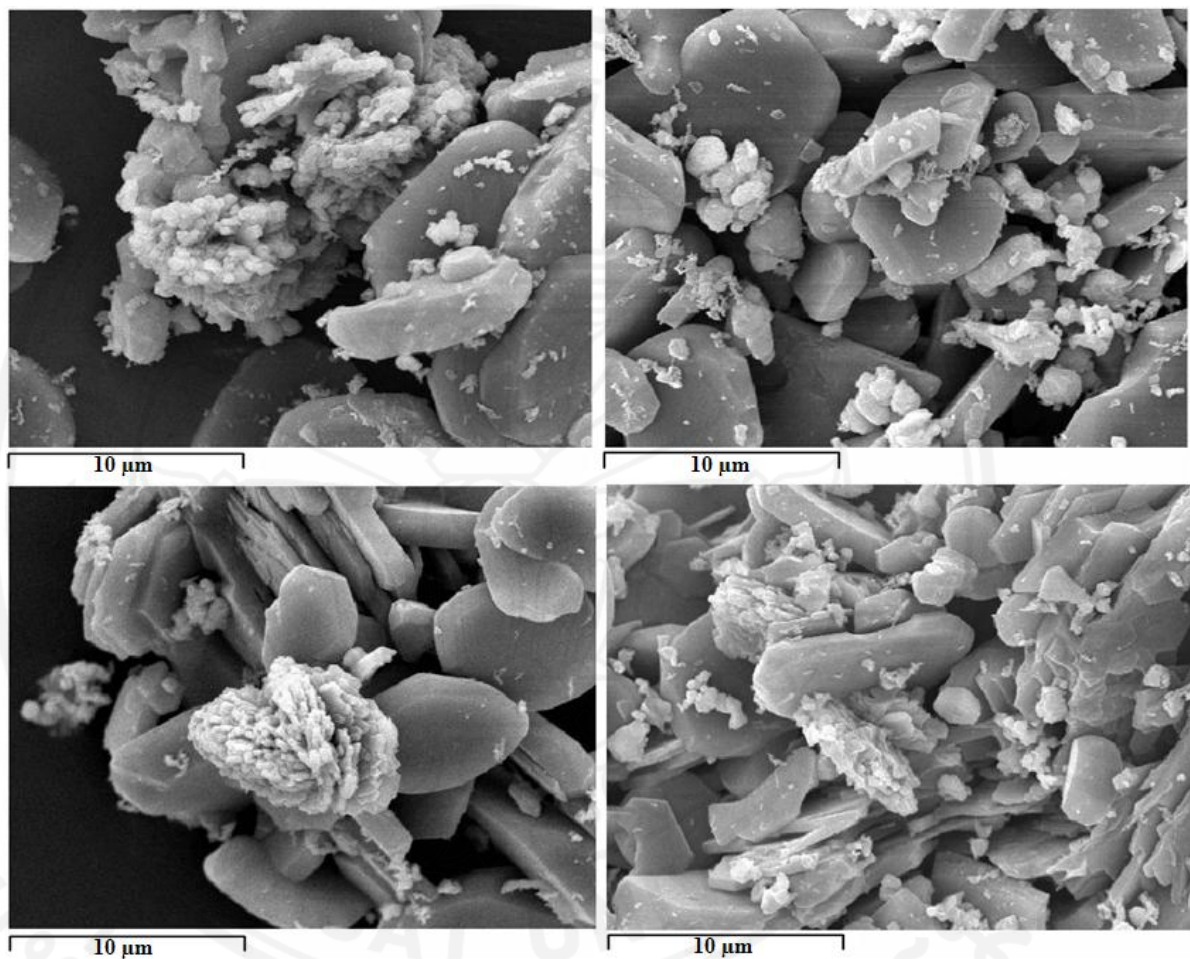


Figure C.1-1 SEM of Cu-Zn/ α -Al₂O₃ without urea (Fresh catalysts)

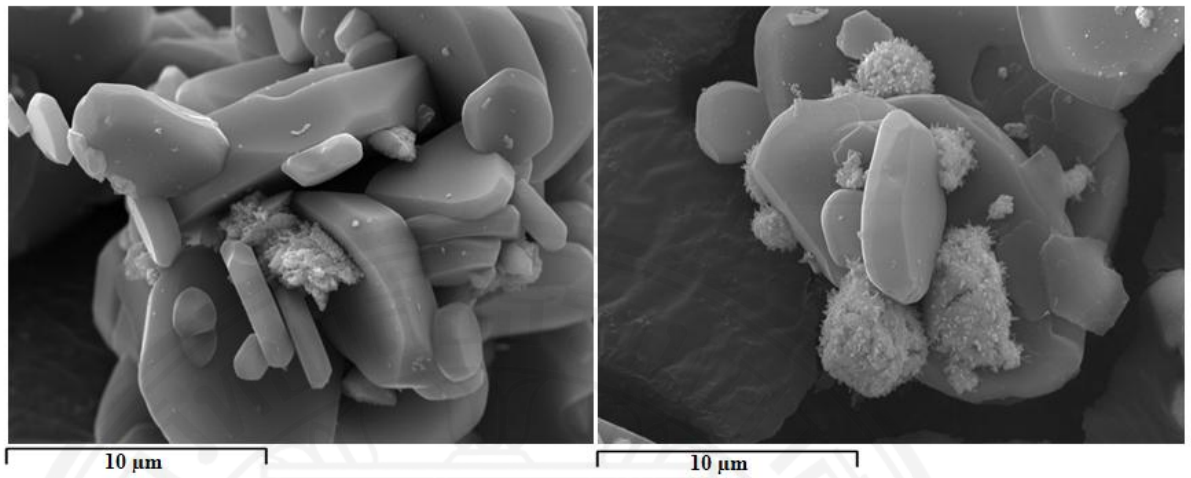


Figure C.1-2 SEM of Cu-Zn/ α -Al₂O₃ without urea (After reaction 300°C)

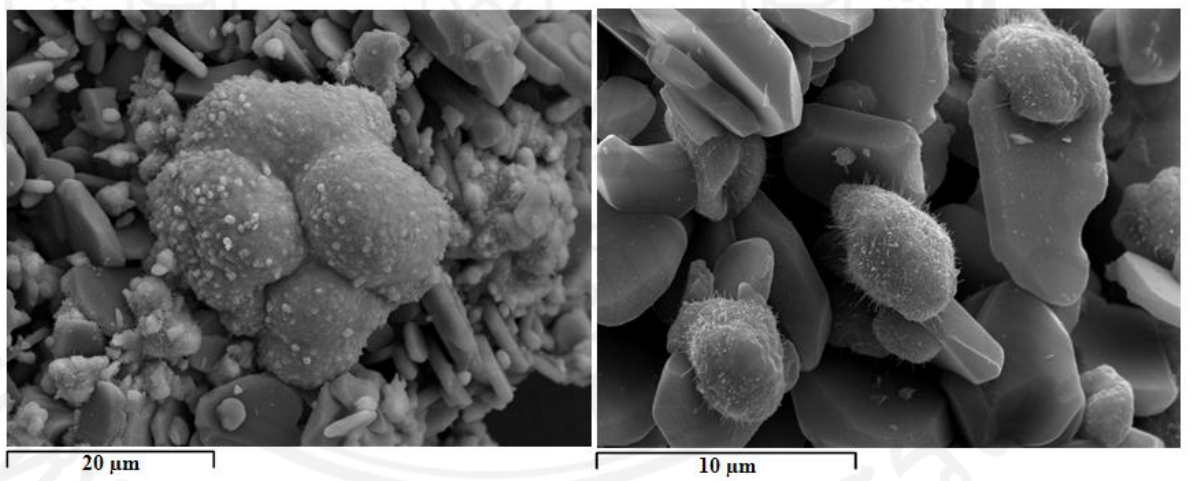


Figure C.1-3 SEM of Cu-Zn/ α -Al₂O₃ without urea (After sintering 500°C)

C.2 SEM of Cu-Zn/ α -Al₂O₃ with urea

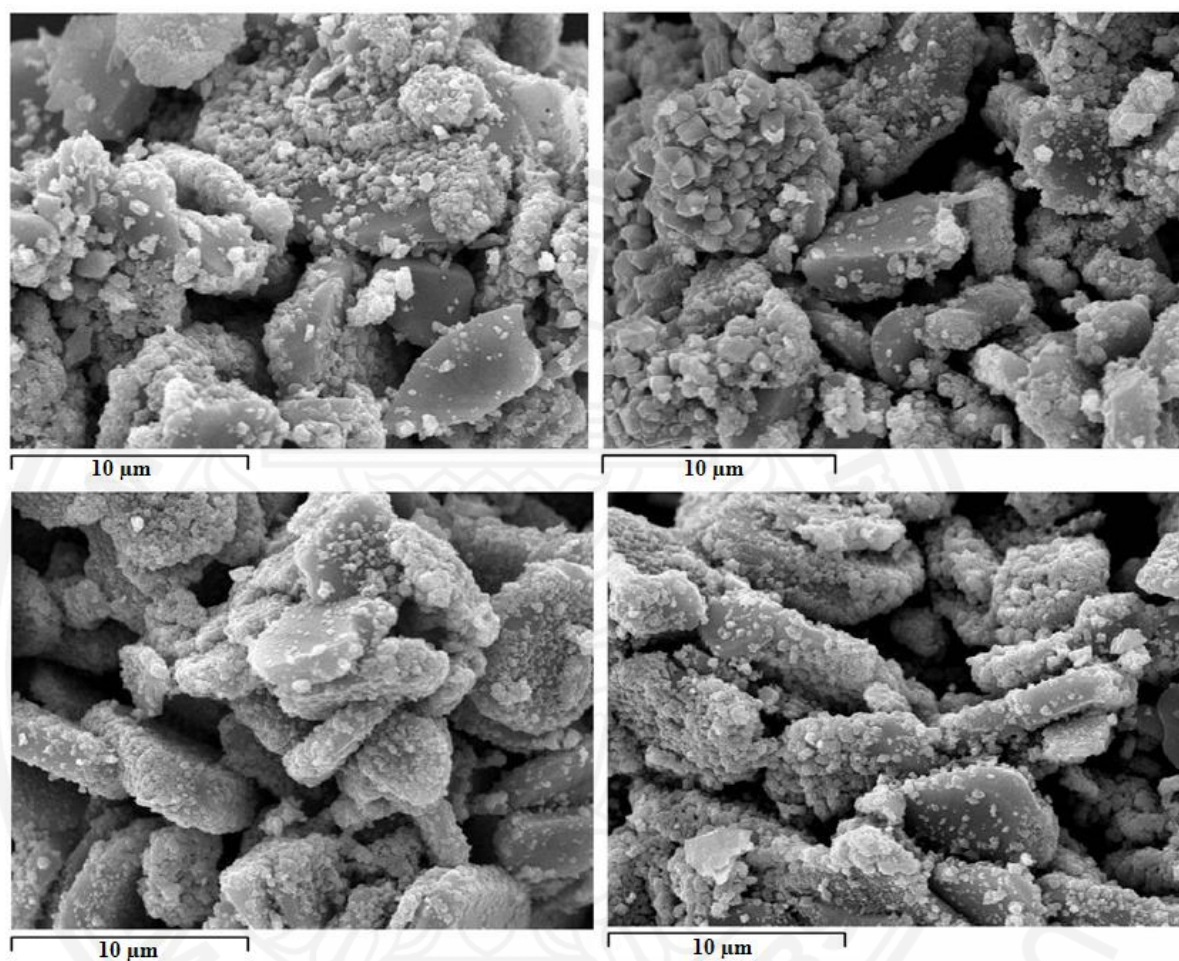


Figure C.2-1 SEM of Cu-Zn/ α -Al₂O₃ with urea (Fresh catalysts)

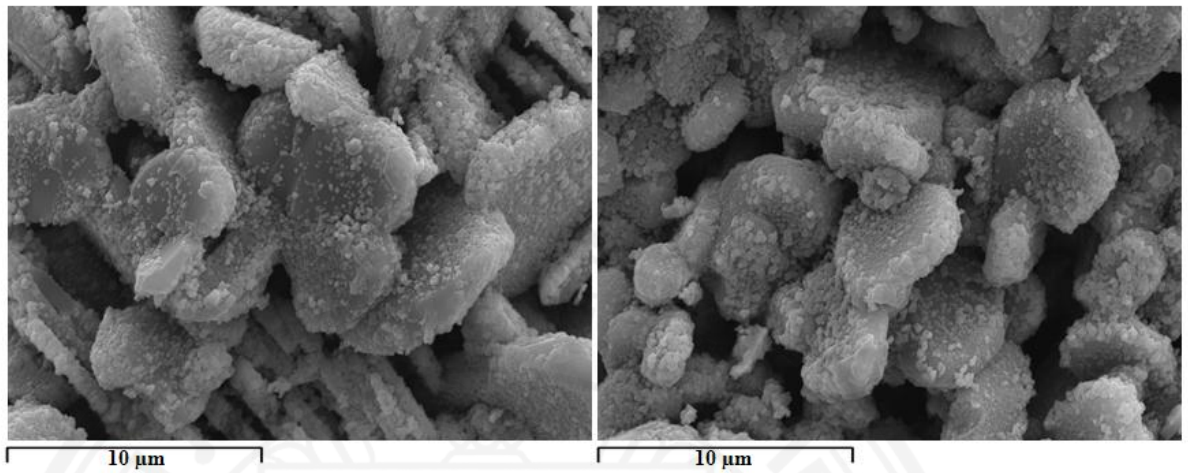


Figure C.2-2 SEM of Cu-Zn/ α -Al₂O₃ with urea (After reaction 300°C)

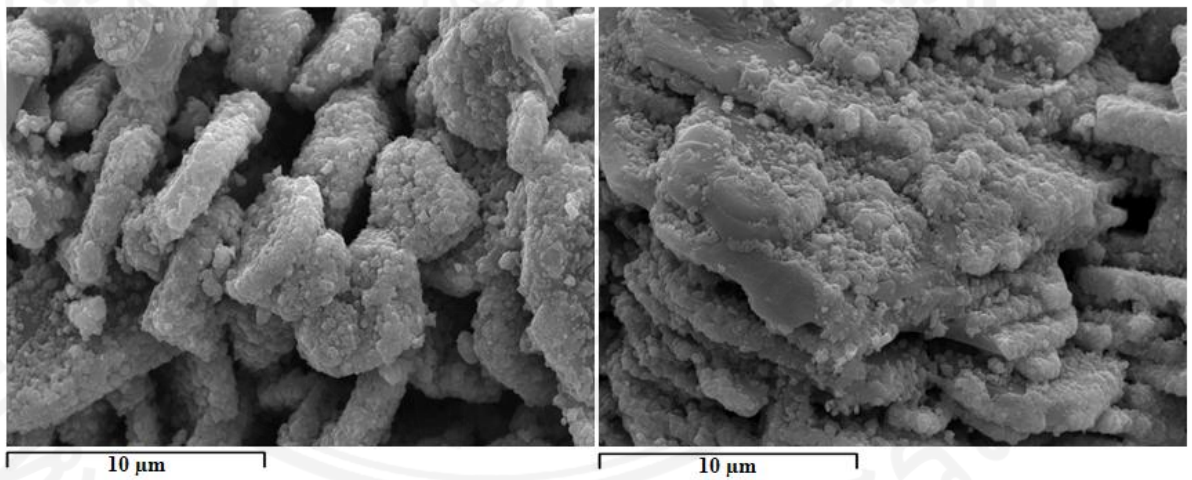
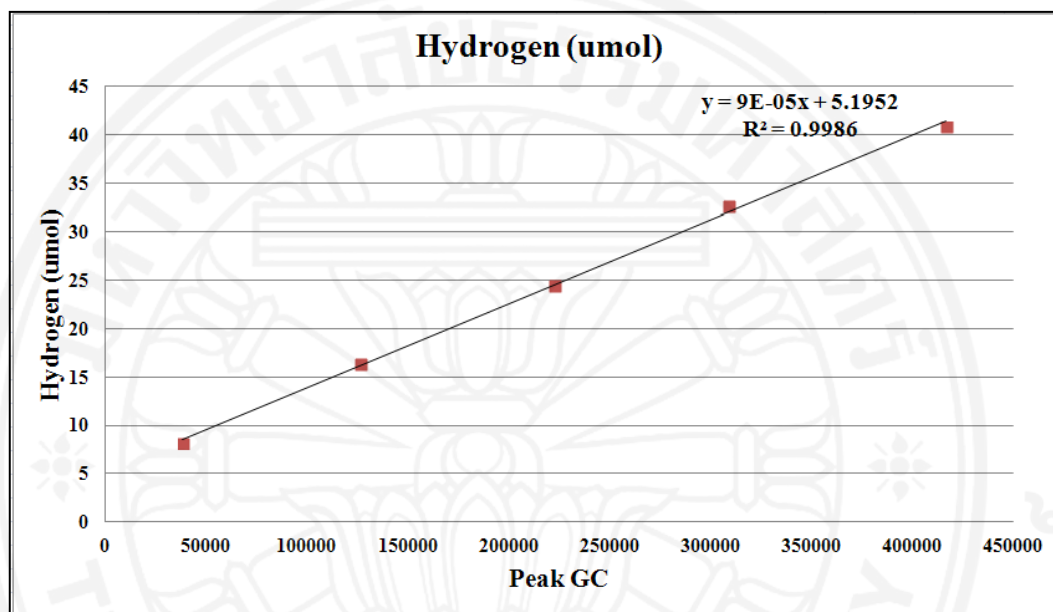


Figure C.2-3 SEM of Cu-Zn/ α -Al₂O₃ with urea (After sintering 500°C)

Appendix D

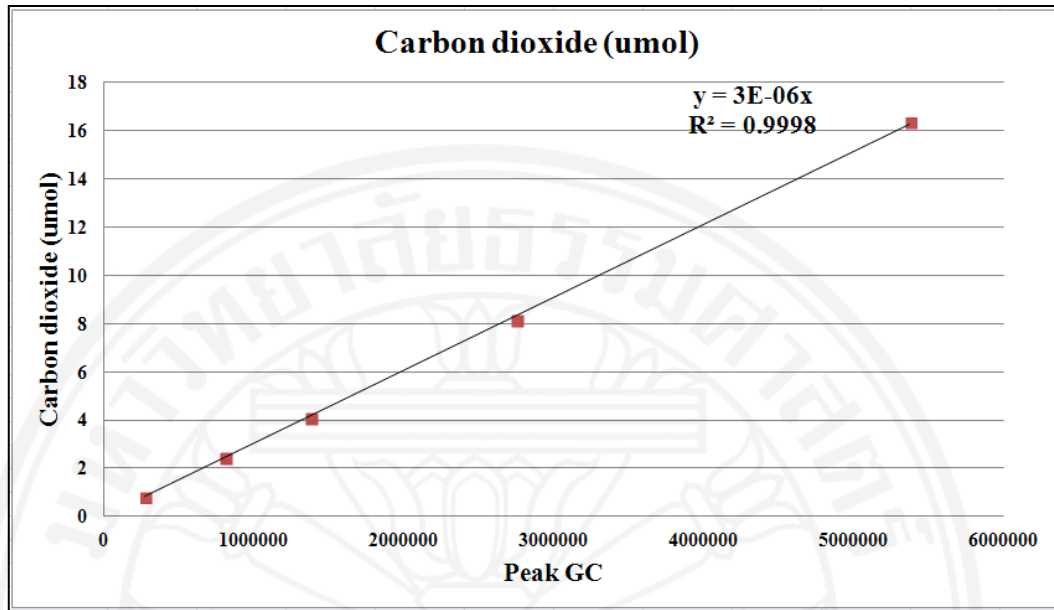
Calibration curve

D.1 Calibration curve of H₂



Peak GC	Avg Peak GC	H ₂ Volume (mL)	H ₂ (μmol)
37,155	38,237±887	0.2	8.2
37,809			
39,261			
39,008			
37,953			
129,075	126,135±2,494	0.4	16.3
125,643			
127,616			
122,427			
125,917			
238,826	222,424±11,816	0.6	24.5
229,879			
209,608			
218,989			
214,820			
308,856	308,580±7,548	0.8	32.7
296,891			
315,383			
306,743			
315,026			
415,863	416,812±10,564	1.0	40.9
405,105			
420,949			
409,780			
432,364			

D.1 Calibration curve of CO₂



Peak GC	Avg Peak GC	CO ₂ Volume (mL)	CO ₂ (umol)
269,082	270,662±8,240	0.02	0.82
269,282			
278,880			
258,395			
277,672			
794,646	801,068±11,742	0.06	2.45
809,174			
808,525			
783,322			
809,671			
1,376,583	1,375,405±9,030	0.10	4.09
1,367,453			
1,368,227			
1,389,887			
1,374,874			
2,688,593	2,744,478±81,300	0.20	8.17
2,887,627			
2,714,944			
2,703,675			
2,727,549			
5,378,302	5,376,679±22,013	0.40	16.34
5,368,437			
5,399,749			
5,343,957			
5,392,950			

Appendix E

Testing and Material Standards

ASTM standards test methods and specifications

ASTM	Significance and Use	Specification
ASTM C 1437 Standard Test Method for Flow of Hydraulic Cement Mortar	This test method is intended to be used to determine the flow of hydraulic cement mortars, and of mortars containing cementitious materials other than hydraulic cements.	N/A
ASTM C 151 Standard Test Method for Autoclave Expansion of Portland Cement	The autoclave expansion test provides an index of potential delayed expansion caused by the hydration of CaO, or MgO, or both, when present in portland cement.	N/A
ASTM C 33 Standard Specification for Concrete Aggregates	This specification defines the requirements for grading and quality of fine and coarse aggregate (other than lightweight or heavyweight aggregate) for use in concrete.	Sand fineness $\leq 75\text{-}\mu\text{m}$ (Mesh No.200)
ASTM C 618 Standard Specification for Coal Fly Ash and Raw or Calcined Natural	This specification covers coal fly ash and raw or calcined natural pozzolan for use in concrete where cementitious or pozzolanic action, or both, is desired, or where other properties normally attributed to fly	Strength activity index With portland cement, at 7 days $\geq 75\%$ With portland cement, at 28 days $\geq 75\%$

ASTM	Significance and Use	Specification
Pozzolan for Use in Concrete	ash or pozzolans may be desired, or where both objectives are to be achieved.	Water requirement \geq 105% Autoclave expansion or contraction \leq 0.8 %
ASTM C 188 Standard Test Method for Density of Hydraulic Cement	This test method covers the determination of the density of hydraulic cement. Its particular usefulness is in connection with the design and control of concrete mixtures.	N/A
ASTM C 109/C 109M Standard Test Method for Compressive Strength of Hydraulic Cement Mortars (Using 2-in. or [50-mm] Cube Specimens)	This test method provides a means of determining the compressive strength of hydraulic cement and other mortars and results may be used to determine compliance with specifications. Further, this test method is referenced by numerous other specifications and test methods. Caution must be exercised in using the results of this test method to predict the strength of concretes.	N/A